

LIGHT HARVESTING AND EFFICIENT ENERGY TRANSFER IN
BORON DIPYRRIN DYADS AND
DERIVATIZATION FOR POTENTIAL UTILITY IN
DYE-SENSITIZED SOLAR CELLS

A THESIS

SUBMITTED TO THE MATERIALS SCIENCE AND NANOTECHNOLOGY
PROGRAM OF THE INSTITUTE OF ENGINEERING AND SCIENCES

OF BİLKENT UNIVERSITY

IN PARTIAL FULFILLMENT OF THE REQUIREMENTS

FOR THE DEGREE OF

MASTER OF SCIENCE

By

GÖKHAN BARIN

July 2008

I certify that I have read this thesis and that in my opinion it is fully adequate, in scope and in quality, as a thesis of the degree of Master of Science.

.....
Prof. Dr. Engin U. Akkaya (Principal Advisor)

I certify that I have read this thesis and that in my opinion it is fully adequate, in scope and in quality, as a thesis of the degree of Master of Science.

.....
Assist. Prof. Dr. Mehmet Bayındır

I certify that I have read this thesis and that in my opinion it is fully adequate, in scope and in quality, as a thesis of the degree of Master of Science.

.....
Assist. Prof. Dr. Emrah Özensoy

Approved for the Institute of Engineering and Science:

.....
Prof. Dr. Mehmet Baray
Director of the Institute of Engineering and Science

ABSTRACT

LIGHT HARVESTING AND EFFICIENT ENERGY TRANSFER IN BORON DIPYRRIN DYADS AND DERIVATIZATION FOR POTENTIAL UTILITY IN DYE-SENSITIZED SOLAR CELLS

Gökhan Barın

M.S. in Materials Science and Nanotechnology

Supervisor: Prof. Dr. Engin U. Akkaya

July, 2008

In bichromophoric supramolecular systems light is harvested by antenna components and excitation energy is channeled into an acceptor component. We have designed and synthesized novel energy transfer cassettes which are based on boradiazaindacene (BODIPY) units. Facile synthesis of long wavelength absorbing distyryl BODIPY dyes has been applied successfully in this study. In the first part of the thesis, efficient energy transfer from energy donor BODIPYs to long wavelength absorbing distyryl BODIPY core was demonstrated. To observe the antenna effect quantitatively, we have designed the cassettes with an increasing number of energy donor components. Based on these observations, in the second part of the thesis, we have introduced a light-harvesting photosensitizer for dye-sensitized solar cell (DSSC) purposes. The target molecule absorbs in visible and near-IR region and energy transfer is demonstrated successfully. Our design appears to be highly promising for DSSC.

Keywords: Boradiazaindacene, light harvesting, energy transfer, dye-sensitized solar cells

ÖZET

BORON DİPİRİN TÜREVLERİNDE IŞIK HASATI VE ETKİN ENERJİ TRANSFERİ VE BOYAR MADDE UYARIMLI GÜNEŞ PİLLERİNDE POTANSİYEL KULLANIMA YÖNELİK TÜREVLENDİRME

Gökhan Barın

Malzeme Bilimi ve Nanoteknoloji Programı, Yüksek Lisans

Tez Yöneticisi: Prof. Dr. Engin U. Akkaya

Temmuz, 2008

Bikromoforik supramoleküler sistemlerde ışık anten bileşenleri tarafından toplanır ve uyarılma enerjisi akseptör bileşenine aktarılır. Bu çalışmada boradiazaindasen (BODIPY) kromoforundan oluşan yeni enerji transfer kasetleri tasarlanıp sentezlenmiştir. Uzun dalga boyunda absorplayan distiril BODIPY türevinin kolay sentezi akseptör bileşenlerinin sentezinde başarıyla uygulanmıştır. Çalışmanın birinci kısmında, anten görevi gören enerji donör BODIPY bileşenlerinden distiril BODIPY akseptörüne etkin enerji transferi gösterilmiştir. Anten etkisini göstermek için enerji transfer kasetleri artan enerji donör bileşen sayısına göre tasarlanmıştır. Bu gözlemlere dayanarak çalışmanın ikinci kısmında, boyar madde uyarımlı güneş pillerinde (DSSC) kullanılmak üzere ışığı toplayabilen fotosensitizer bir madde elde edilmiştir. Elde edilen molekül ışığın görünür ve yakın-IR bölgesinde absorpladığı ve etkin enerji transferinin gerçekleştiği gösterilmiştir. Yapının boyar madde uyarımlı güneş pillerinde yüksek bir verim göstereceği öngörülmektedir.

Anahtar Kelimeler: Boradiazaindasen, ışık hasatı, enerji transferi, boyar madde uyarımlı güneş pilleri

ACKNOWLEDGEMENT

I would like to express my sincere thanks to my supervisor Prof. Dr. Engin U. Akkaya for his guidance, support, and patience during the course of this research. I am also grateful to him for teaching us how to become a good mentor. I will never forget his support throughout my life.

I owe a special thank to Dr. Ö. Altan Bozdemir, M. Deniz Yılmaz, and Dr. Ali Coşkun for their support and guidance to improve my skills in the field of supramolecular chemistry.

I want to thank to our group members Yusuf Çakmak, Ruslan Guliyev, İlker Kütük, Tuğba Özdemir, Serdar Atılgan, Bora Bilgiç, Suriye Özlem, Onur Büyükçakır, and rest of the SCL (Supramolecular Chemistry Laboratory) members. It was wonderful to work with them.

I would like to thank to TÜBİTAK (The Scientific and Technological Research Council of Turkey) for financial support.

Finally, I want to express my gratitude to my family for their love, support, and understanding. I owe them a lot. I dedicate this dissertation to them.

TABLE OF CONTENTS

1. INTRODUCTION	1
1.1 Supramolecular Chemistry	1
1.2 Fundamentals of Fluorescence.....	2
1.3 BODIPY [®] Dyes	5
1.3.1 Applications of BODIPY Dyes	6
1.4 Light Harvesting and Energy Transfer	11
1.4.1 Energy Transfer Mechanisms.....	12
1.4.1.1 Dexter-type Energy Transfer	13
1.4.1.2 Förster-type Energy Transfer	15
1.4.2 Light Frequency Conversion	17
1.4.3 Cascade Systems	19
1.4.4 Artificial Photosynthetic Antenna	20
1.4.5 FRET for Biological Purposes and Fluorescent Signaling Systems ..	21
1.4.6 BODIPY dyes as Light Harvesters.....	23
1.5 Dye-sensitized Solar Cells	25
1.5.1 Working Principle of DSSCs.....	25
1.5.2 Photosensitizers for DSSCs.....	28
2. EXPERIMENTAL	32
2.1 Instrumentation	32
2.2 PART I.....	33
2.2.1 Synthesis of 4,4-difluoro-8-{4-(1,3-dioxolan-2-yl)}phenyl- 1,3,5,7- tetramethyl-2,6-diethyl-4-bora-3a,4a-diaza-s-indacene (41).....	33
2.2.2 Synthesis of 4-[3,5-di{2-(4-methylphenyl)ethenyl}-4,4-difluoro- 1,3,5,7-tetramethyl-2,6-diethyl-4-bora-3a,4a-diaza-s-indacen-8-yl]- benzaldehyde (42)	34

2.2.3	Synthesis of 1-{4,4-difluoro-1,3,5,7-tetramethyl-2,6-diethyl-4-bora-3a,4a-diaza-s-indacen-8-yl}-4-[3,5-di{2-(4-methylphenyl)ethenyl}-4,4-difluoro-1,3,5,7-tetramethyl-2,6-diethyl-4-bora-3a,4a-diaza-s-indacen-8-yl]-benzene (43)	35
2.2.4	Synthesis of 4,4-difluoro-8-phenyl-1,3,5,7-tetramethyl-2,6-diethyl-4-bora-3a,4a-diaza-s-indacene (44)	36
2.2.5	Synthesis of 3,5-di{2-(4-methanoylphenyl)ethenyl}-4,4-difluoro-8-phenyl-1,3,5,7-tetramethyl-2,6-diethyl-4-bora-3a,4a-diaza-s-indacene (45)	37
2.2.6	Synthesis of 3,5-di[2-{4-(4,4-difluoro-1,3,5,7-tetramethyl-2,6-diethyl-4-bora-3a,4a-diaza-s-indacen-8-yl)phenyl}ethenyl]-4,4-difluoro-8-phenyl-1,3,5,7-tetramethyl-2,6-diethyl-4-bora-3a,4a-diaza-s-indacene (46)	38
2.2.7	Synthesis of 4-[3,5-di{2-(4-methanoylphenyl)ethenyl}-4,4-difluoro-1,3,5,7-tetramethyl-2,6-diethyl-4-bora-3a,4a-diaza-s-indacen-8-yl]-benzaldehyde (47)	39
2.2.8	Synthesis of 1-[3,5-di{2-(4-(4,4-difluoro-1,3,5,7-tetramethyl-2,6-diethyl-4-bora-3a,4a-diaza-s-indacen-8-yl)phenyl)ethenyl}-4,4-difluoro-1,3,5,7-tetramethyl-2,6-diethyl-4-bora-3a,4a-diaza-s-indacen-8-yl]-4-(4,4-difluoro-1,3,5,7-tetramethyl-2,6-diethyl-4-bora-3a,4a-diaza-s-indacen-8-yl)-benzene (48)	40
2.3	PART II.....	42
2.3.1	Synthesis of 4,4-difluoro-8-(4-carboxy)phenyl-1,3,5,7-tetramethyl-4-bora-3a,4a-diaza-s-indacene (49)	42
2.3.2	Synthesis of 4,4-difluoro-8-(4-carboxy)phenyl -2,6-diiodo-1,3,5,7-tetramethyl-4-bora-3a,4a-diaza-s-indacene (50)	43
2.3.3	Synthesis of 4-[3,5-bis{4-(diphenylamino)styryl}-4,4-difluoro-1,3,5,7-tetramethyl-2,6-diiodo-4-bora-3a,4a-diaza-s-indacen-8-yl]-benzoic acid (52)	43
2.3.4	Synthesis of 4,4-difluoro-8-{4-(prop-2-ynyloxy)phenyl}-2,6-diethyl-1,3,5,7-tetramethyl-4-bora-3a,4a-diaza-s-indacene (54).....	44

2.3.5	Synthesis of compound 55.....	45
3.	RESULTS AND DISCUSSIONS.....	47
3.1	Synthesis and Spectroscopic Properties of Light-Harvesting Cassettes 43, 46, and 48	47
3.2	Novel Light-Harvesting Photosensitizer.....	53
4.	CONCLUSION	57
	REFERENCES	58
	APPENDIX A.....	64
	APPENDIX B.....	88

LIST OF FIGURES

Figure 1. Comparison between molecular and supramolecular chemistry.....	1
Figure 2. Structures of typical fluorescent substances	3
Figure 3. Jablonski Diagram.....	4
Figure 4. Stokes' shift.....	4
Figure 5. Applications and chemistry of BODIPY	7
Figure 6. Selective BODIPY-based chemosensors	8
Figure 7. Photosensitizers for photodynamic therapy	9
Figure 8. BODIPY dyes with ancillary light absorbers.....	9
Figure 9. BODIPY as logic gate operator and liquid crystal, and water-soluble derivatives.....	10
Figure 10. Schematic representation of a light-harvesting antenna system	11
Figure 11. Schematic representation of the overall light-harvesting process by LH2 and LH1	12
Figure 12. Pictorial representation of exchange energy transfer mechanism.....	13
Figure 13. Through-bond energy transfer	13
Figure 14. Through-bond energy transfer cassettes	14
Figure 15. Porphyrin containing Dexter-type cassettes.....	15
Figure 16. Pictorial representation of coulombic energy transfer mechanism.....	16
Figure 17. Through-space energy transfer.....	17
Figure 18. Chemical structure of compound 17	18
Figure 19. Chemical structure of compound 18	19
Figure 20. The structure of cascade system 19.....	20
Figure 21. Artificial photosynthetic antenna systems	21
Figure 22. Singlet oxygen generation via FRET	22
Figure 23. Electron and energy transfers in compound 23.....	22
Figure 24. Light-harvesting dendrimer 24.....	23
Figure 25. Light-harvesting arrays with BODIPY energy donors	24
Figure 26. Light-harvesting cassette with BODIPY donors and acceptor	24
Figure 27. Principle of operation of DSSC	26
Figure 28. The structures of N3, N719, and black dye.....	28

Figure 29. Ruthenium complexes with electron donor groups.....	29
Figure 30. Organic dyes as DSSC	30
Figure 31. Effect of COOH position on cell efficiency.....	31
Figure 32. BODIPY photosensitizers	31
Figure 33. Synthesis of compound 41	34
Figure 34. Synthesis of compound 42	35
Figure 35. Synthesis of energy transfer cassette 43	36
Figure 36. Synthesis of compound 44	37
Figure 37. Synthesis of compound 45	38
Figure 38. Synthesis of energy transfer cassette 46	39
Figure 39. Synthesis of compound 47	40
Figure 40. Synthesis of energy transfer cassette 48	41
Figure 41. Synthesis of compound 49	42
Figure 42. Synthesis of compound 50	43
Figure 43. Synthesis of compound 52	44
Figure 44. Synthesis of compound 54	45
Figure 45. Synthesis of compound 55	46
Figure 46. The structures of cassettes 43, 46, and 48.....	48
Figure 47. Schematic representation of energy transfer in cassette 48	49
Figure 48. Absorbance spectra of compounds 43, 46, and 48 at equal absorbances at 650 nm in CHCl ₃	50
Figure 49. The emission spectra of compounds in CHCl ₃ ($\lambda_{exc} = 525$ nm).....	51
Figure 50. Excitation spectra of compounds 43, 46, and 48 in CHCl ₃	52
Figure 51. The structure of light-harvesting photosensitizer 55.....	54
Figure 52. Absorption spectra of compounds 52, 54, and 55 in CHCl ₃	55
Figure 53. The emission spectra of compounds 52, 54, and 55 in CHCl ₃ . Inset: expanded spectrum in the region of core emission	56
Figure 54. ¹ H NMR spectrum of compound 41	64
Figure 55. ¹³ C NMR spectrum of compound 41	65
Figure 56. ¹ H NMR spectrum of compound 42	66
Figure 57. ¹³ C NMR spectrum of compound 42	67
Figure 58. ¹ H NMR spectrum of compound 43	68
Figure 59. ¹³ C NMR spectrum of compound 43	69

Figure 60. ^1H NMR spectrum of compound 44	70
Figure 61. ^{13}C NMR spectrum of compound 44	71
Figure 62. ^1H NMR spectrum of compound 45	72
Figure 63. ^{13}C NMR spectrum of compound 45	73
Figure 64. ^1H NMR spectrum of compound 46	74
Figure 65. ^{13}C NMR spectrum of compound 46	75
Figure 66. ^1H NMR spectrum of compound 47	76
Figure 67. ^{13}C NMR spectrum of compound 47	77
Figure 68. ^1H NMR spectrum of compound 48	78
Figure 69. ^{13}C NMR spectrum of compound 48	79
Figure 70. ^1H NMR spectrum of compound 49	80
Figure 71. ^{13}C NMR spectrum of compound 49	81
Figure 72. ^1H NMR spectrum of compound 52	82
Figure 73. ^{13}C NMR spectrum of compound 52	83
Figure 74. ^1H NMR spectrum of compound 54	84
Figure 75. ^{13}C NMR spectrum of compound 54	85
Figure 76. ^1H NMR spectrum of compound 55	86
Figure 77. ^{13}C NMR spectrum of compound 55	87
Figure 78. ESI-HRMS of compound 41	88
Figure 79. ESI-HRMS of compound 42	89
Figure 80. ESI-HRMS of compound 43	90
Figure 81. ESI-HRMS of compound 45	91
Figure 82. MALDI-MS of compound 46	92
Figure 83. ESI-HRMS of compound 47	93
Figure 84. ESI-HRMS of compound 48	94
Figure 85. ESI-HRMS of compound 50	95
Figure 86. ESI-HRMS of compound 52	96
Figure 87. ESI-HRMS of compound 54	97
Figure 88. MALDI-MS of compound 55	98

LIST OF TABLES

Table 1. Photophysical Properties of Compounds in CHCl_3	52
Table 2. Photophysical Properties of Compounds 52, 54, and 55 in CHCl_3	56

LIST OF ABBREVIATIONS

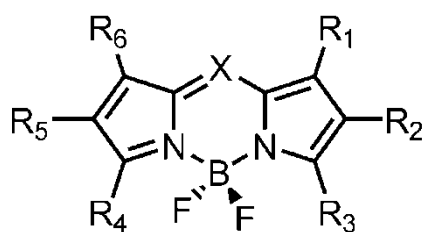
FRET: Fluorescence Resonance Energy Transfer

TFA: Trifluoroacetic acid

DDQ: 2,3-dichloro-5,6-dicyanobenzoquinone

TEA: Triethylamine

BODIPY: Boradiazaindacene



R = H or any group
X = C or N

CHAPTER 1

INTRODUCTION

1.1 Supramolecular Chemistry

Supramolecular chemistry is a new branch of chemistry which has attracted many scientists in the last two decades.¹⁻⁴ Paul Ehrlich's receptor idea, Alfred Werner's coordination chemistry, and Emil Fischer's lock-and-key image play a significant role in the development of supramolecular chemistry.⁵ The most widely accepted definition for supramolecular chemistry is "the chemistry beyond the molecule", as J.-M. Lehn stated.⁶ It is a highly interdisciplinary field by means of synthetic methodology and application fields. Organic and inorganic chemistry are the primary tools for the synthesis of desired molecules and physical chemistry is used in order to characterize and investigate the properties of supramolecular systems.

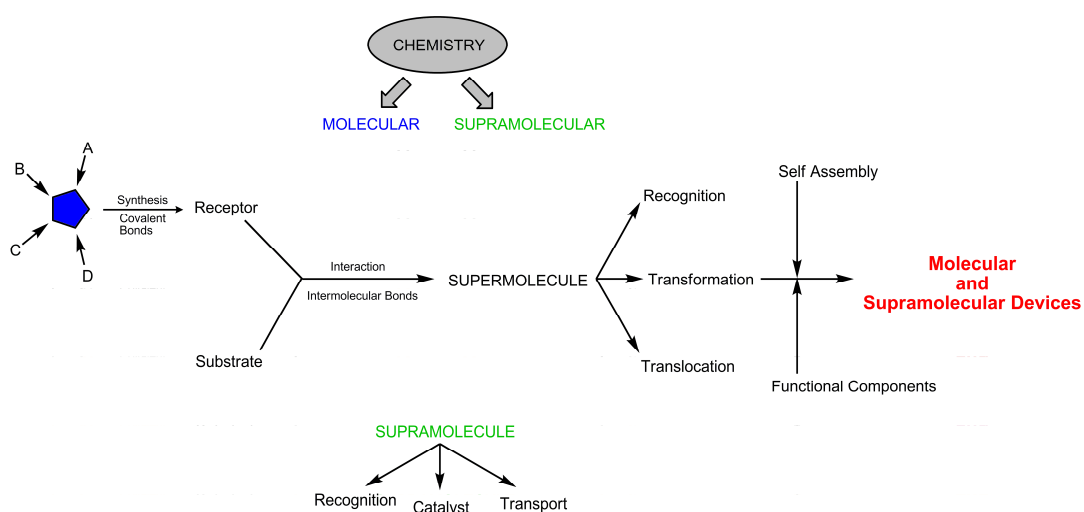


Figure 1. Comparison between molecular and supramolecular chemistry¹

There are many applications of supramolecular chemistry in the fields of chemical synthesis, catalysis, materials science and nanotechnology, and life sciences. In chemical synthesis and catalysis, the idea of noncovalent synthesis was developed.^{7,8} That has given rise in molecular recognition and catalysis with the help of self-assembly and biomimetic design.^{9,10} Additionally, molecular level devices were successfully synthesized with certain functions.^{11,12} In materials science and nanotechnology, there are great developments in surface studies with the assistance of supramolecular concepts.^{13,14} Design and synthesis of macromolecules, which can function as light-harvesting agents,^{15,16} sensitizers for solar cell applications^{17,18} and operate as logic gates,^{19,20} are hot applications of supramolecular chemistry. Finally supramolecular concepts are used to synthesize artificial biological agents^{21,22} such as enzymes, DNA and to develop new therapeutic agents^{23,24} for many diseases.

Nature is the main source of inspiration for the design of new supramolecular species. Mimicking the functions of biological systems and achieving macroscopic functions at molecular level are the great interest of scientists in supramolecular chemistry and nanotechnology.

1.2 Fundamentals of Fluorescence

Absorption is a process in which the intensity of light is decreased at certain frequencies by a chemical species, so that valence electrons in an atom make a transition between two electronic energy levels. Most elementary particles are in their ground state at room temperature. When these particles are irradiated by photons with proper energies, the electrons move to a higher energy state, which can also be termed as excited state.



The excited species relaxes to its ground state and it is called luminescence if emission of light occurs during relaxation. Luminescence is formally divided into two categories, fluorescence and phosphorescence. In fluorescence return of the

excited electron to the ground state is spin-allowed and emission rates of fluorescence are typically 10^8 s^{-1} , in other words fluorescence lifetime is 10 ns. Lifetime (τ) of a fluorophore is the average time between its excitation and its return to ground state.

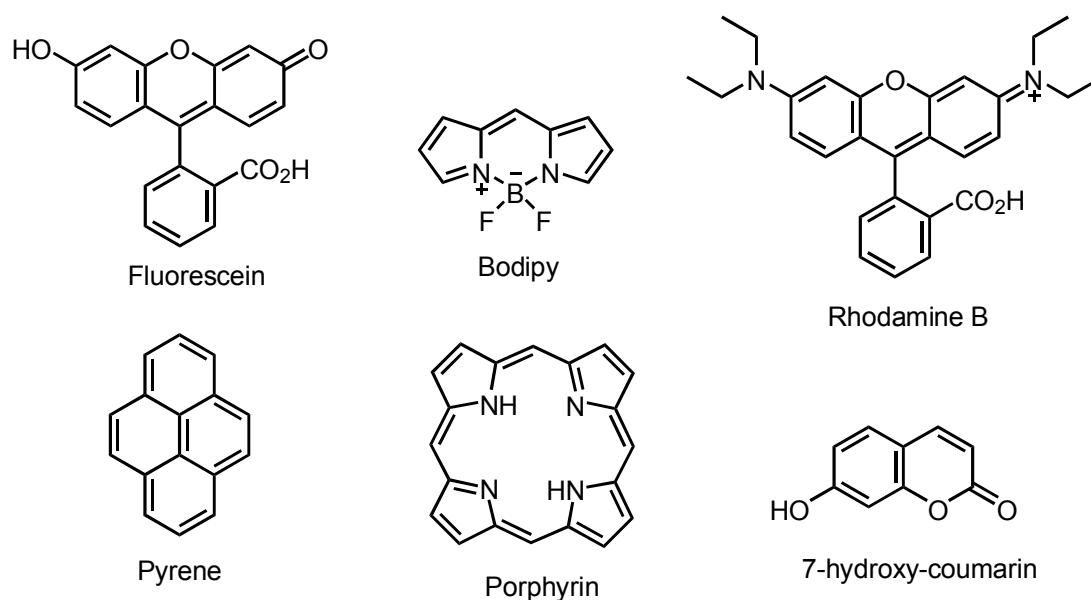


Figure 2. Structures of typical fluorescent substances

Following light absorption, fluorophore is excited to some higher vibrational levels of S_1 or S_2 states. All of these states relax to the lowest vibrational level of S_1 , a process which is called internal conversion. Internal conversion is generally complete (10^{-12} s) before emission takes place. Phosphorescence is emission of light from triplet excited states. In that process transitions to the ground state is spin-forbidden and as a consequence the phosphorescence lifetimes vary from milliseconds to seconds. Heavy atoms such as bromine and iodine make the molecule phosphorescent. Transition of electron from singlet excited state to the triplet excited state is called intersystem crossing. Figure 3 summarizes the processes mentioned here, which is also known as Jablonski Diagram.

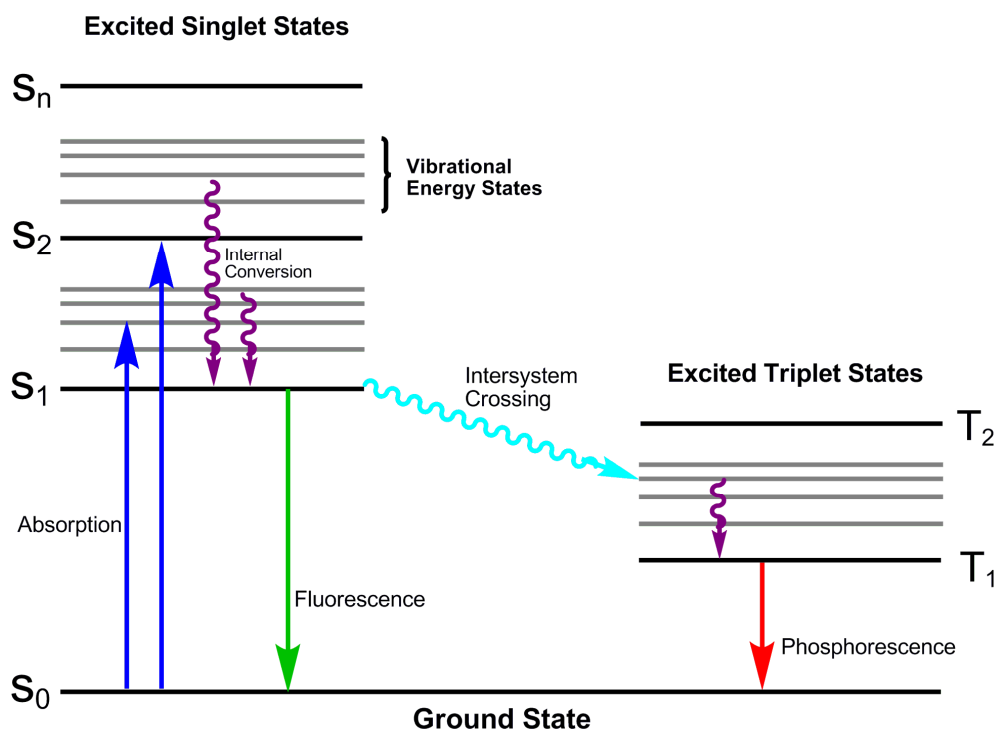


Figure 3. Jablonski Diagram

It can be concluded from Jablonski diagram that the energy of the emission is less than the energy of absorption. Therefore fluorescence occurs at longer wavelengths (Stokes' shift, Figure 4).²⁵ One of the reasons for Stokes' shift is the rapid decay to the lowest vibrational level of S_1 . Further loss of excitation energy occurs due to the decay to higher vibrational levels of S_0 , where excess vibrational energy is lost. Stokes' shift is also observed due to solvent effects, complex formation, and energy transfer. A general property of fluorescence is that same fluorescence emission spectrum is observed irrespective of excitation wavelength. This is known as Kasha's rule.²⁶

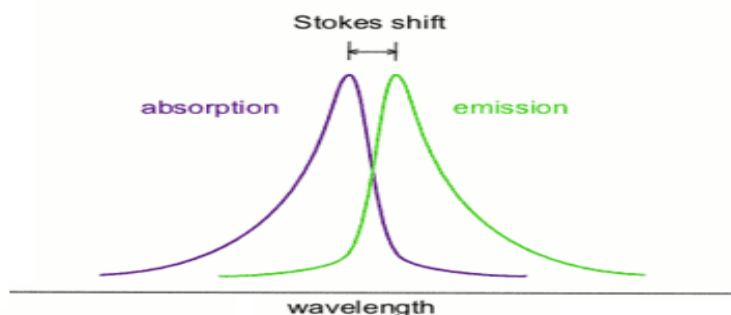


Figure 4. Stokes' shift

Another important characteristic of a fluorophore is its quantum yield. It can be defined as the ratio of number of emitted photons to the number of absorbed photons. To express quantum yield in a formula (Eq. (2)), the processes in Jablonski diagram can be collected in two groups as emissive rate of the fluorophore (Γ) and nonradiative decay rate to S_0 (k_{nr}).

$$Q = \frac{\Gamma}{\Gamma + k_{nr}} \quad (2)$$

Due to Stokes' losses quantum yield is always less than unity. When the rate of nonradiative decay is much smaller than rate of radiative decay, the quantum yield approaches to unity. Substances with larger quantum yields display brighter emission. In order to make quantum yield measurements, a standard sample is chosen with known quantum yield. Rhodamine 6G,²⁷ rhodamine 101,²⁸ cresyl violet,²⁹ fluorescein,³⁰ and zinc phthalocyanine³¹ are some examples for most widely used standard samples. The criterion for standard selection is that it should absorb at the excitation wavelength of choice for test sample. Additionally, if possible, it should emit in a similar region to test sample. Quantum yield is determined by using Eq. (3).

$$Q_{sample} = Q_{ref} \times \frac{I_{sample}}{I_{ref}} \times \frac{n_{sample}^2}{n_{ref}^2} \times \frac{1 - 10^{-A_{ref}}}{1 - 10^{-A_{sample}}} \quad (3)$$

I represents the integrated area of fluorescence spectrum. A is the absorbance value at the excitation wavelength of choice. n is refractive index value of the solvent used for measurements.

1.3 BODIPY[®] Dyes

The design and synthesis of new fluorescent probes for imaging techniques is a growing field today. Those probes are attached to biological molecules, such as DNA, proteins, and they allow us to follow the events in living cells by fluorescence.^{32,33} However this is limited to the probes available. There are few

probes that emit at or above 800 nm, the wavelength at which tissues are most transparent to light. Among the large variety of fluorescent dyes, the boradiazaindacene family has gained recognition as being one of the most versatile fluorophores. BODIPY dyes were first discovered by Treibs and Kreuzer in 1968.³⁴ Since then many applications of BODIPY were reported in a wide range of fields like biomolecular labeling, ion sensing, drug delivery reagents, molecular logic, light harvesting systems, sensitizers for solar cells.

BODIPY has a high molar extinction coefficient and high fluorescence quantum yield. Its lower sensitivity to solvent polarity and pH make it a stable compound to physical conditions. Good solubility, intense absorption profile and negligible triplet state formation are additional advantages of BODIPY dyes. The excitation and emission wavelengths of BODIPY can be changed with structural modifications. Especially, modifications on positions 1-3 and 5-7 (Figure 5) extend the conjugation and make it possible to tune visible spectrum. Functional units can also be added with modifications on positions 4 and 8. There are many research groups working on derivatization and functionalization of BODIPY dyes. These groups are those of Akkaya, Burgess, Boens, Nagano, Rurack, Ziessel et al.

1.3.1 Applications of BODIPY Dyes

Due to the chemical and photochemical properties of BODIPY dyes mentioned above, these dyes have been used in many different applications. First applications of BODIPY were shown in protein labeling.³⁵⁻³⁷

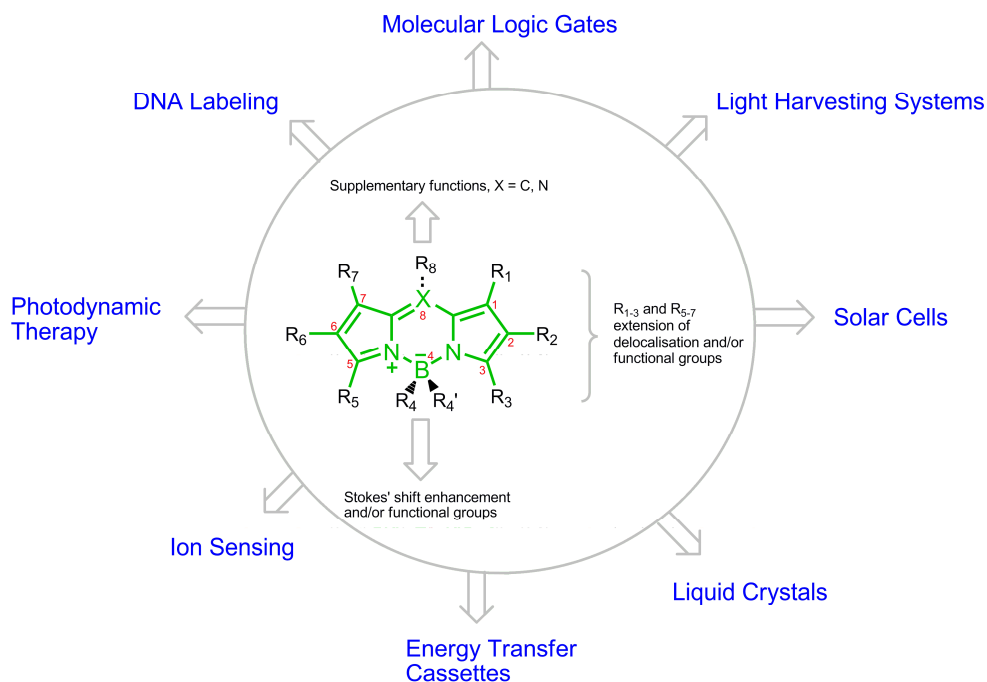


Figure 5. Applications and chemistry of BODIPY

Fluorescent chemosensor design for both cations and anions is a challenging field in supramolecular chemistry. In biological and environmental aspect, chemosensors for heavy and transition metal cations are very important. Selectivity and sensitivity are key parameters in signaling of desired molecular or ionic species. Additionally fluorophores emitting beyond 650 nm are great candidates for sensing in biological media. That is due to the reduced scattering of light at longer wavelengths. The absorption properties of BODIPY can be tuned in the visible spectrum with proper modifications. Red-emitting BODIPY fluorophores and chemosensors have been developed by Akkaya et al (Compounds **1**, **2**, **3**).³⁸⁻⁴⁰ Some other chemosensor examples, **4**⁴¹ and **5**⁴², are shown in Figure 6.

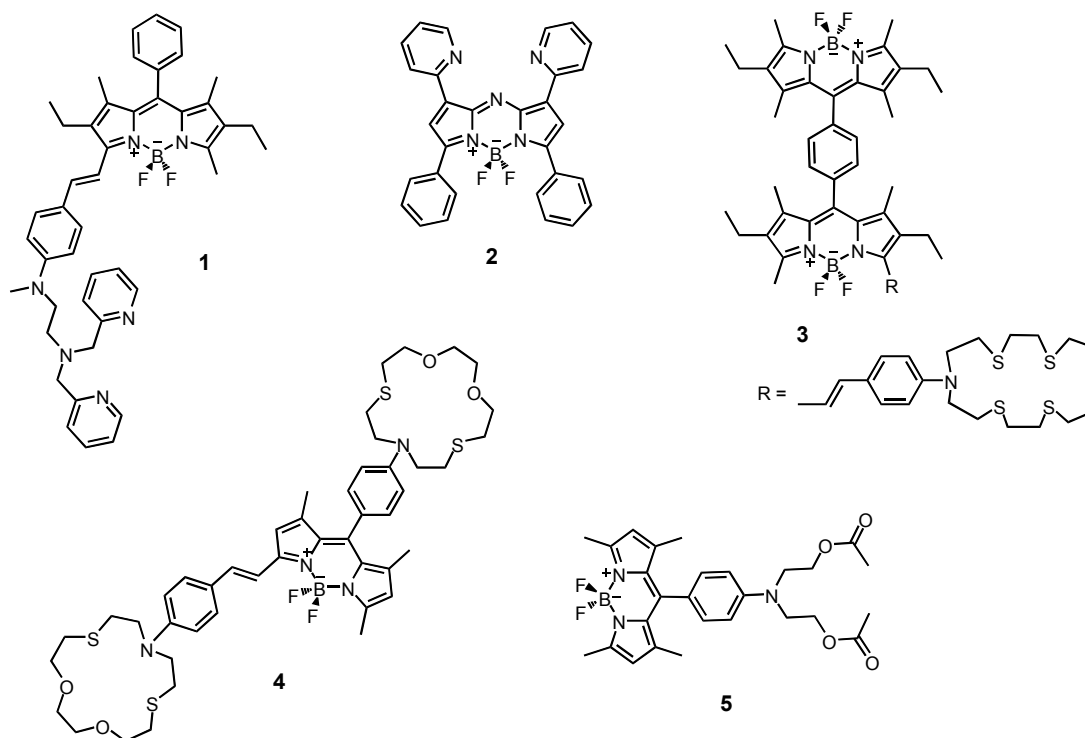


Figure 6. Selective BODIPY-based chemosensors

Photodynamic therapy for treatment of cancer is another application of BODIPY dyes. BODIPY has high absorption coefficient and high efficiency of reactive oxygen species generation which are good properties for being a photosensitizer. In both examples in Figure 7, heavy atoms attached to 2 and 6 positions of BODIPY favor the intersystem crossing, thus increase the triplet yield of dyes. It was observed that in compound **6** the quantum efficiency of fluorescence dropped from 0.70 to 0.02 and high efficiency of singlet oxygen generation was reported.⁴³ Akkaya et al. synthesized compound **7**, in which extension of conjugation by condensation reaction from 3 and 5 positions provided longer wavelength absorption (650-680 nm).⁴⁴ Water solubility was achieved via attaching oligoethyleneglycol groups. Efficient singlet oxygen generation was obtained as well.

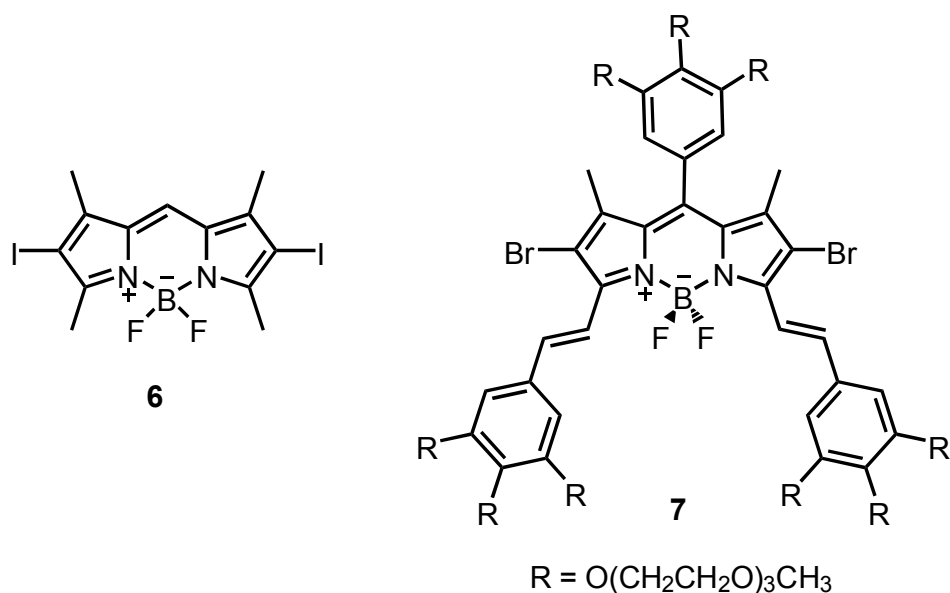


Figure 7. Photosensitizers for photodynamic therapy

A weakness of BODIPY dyes, actually for most of the organic dyes, is small Stokes' shift. This limits the sensitivity of detection in chemical sensing and fluorescence labeling (imaging). For that purpose dual-chromophore dyes have been developed in which "virtual" Stokes' shift is observed. Ziessel et al. reported examples of BODIPY based dual-chromophore dyes by substitution with fluorine atoms at boron center as shown in Figure 8.⁴⁵ Photons are absorbed by the secondary chromophore (pyrene, anthracene) and final emission is observed at BODIPY core as a result of intramolecular energy transfer. In this way, the energy gap between excitation and emission wavelengths was increased by 10-fold.

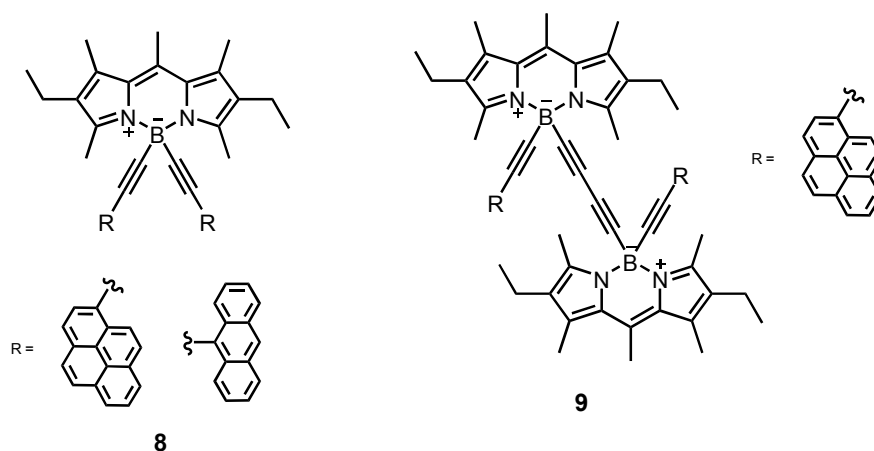


Figure 8. BODIPY dyes with ancillary light absorbers

A BODIPY-based molecular logic, which can function as a unimolecular half-subtractor (compound **10**), was synthesized by Akkaya et al.⁴⁶ Using acid and/or base as inputs, the photochemical response of compound **10** was observed and explained. The core of BODIPY dyes is hydrophobic and it has no functionality to attach to biological units. Water-solubility is important in order to study in living cells. There are few examples of water-soluble BODIPY dyes in literature. Compounds **11** and **12** are examples of water-soluble BODIPYs.^{47,48} The use of luminescent molecules incorporated into soft materials, such as gels and liquid crystalline materials, is challenging in colorimetric sensing, electrooptical devices, photovoltaic devices and as templates to prepare nanoporous materials. BODIPY dyes can be used instead of metallic luminophores so that fluorescent mesomorphic dyes are obtained. Compound **13** is an example luminescent gel that exhibits outstanding features.⁴⁹

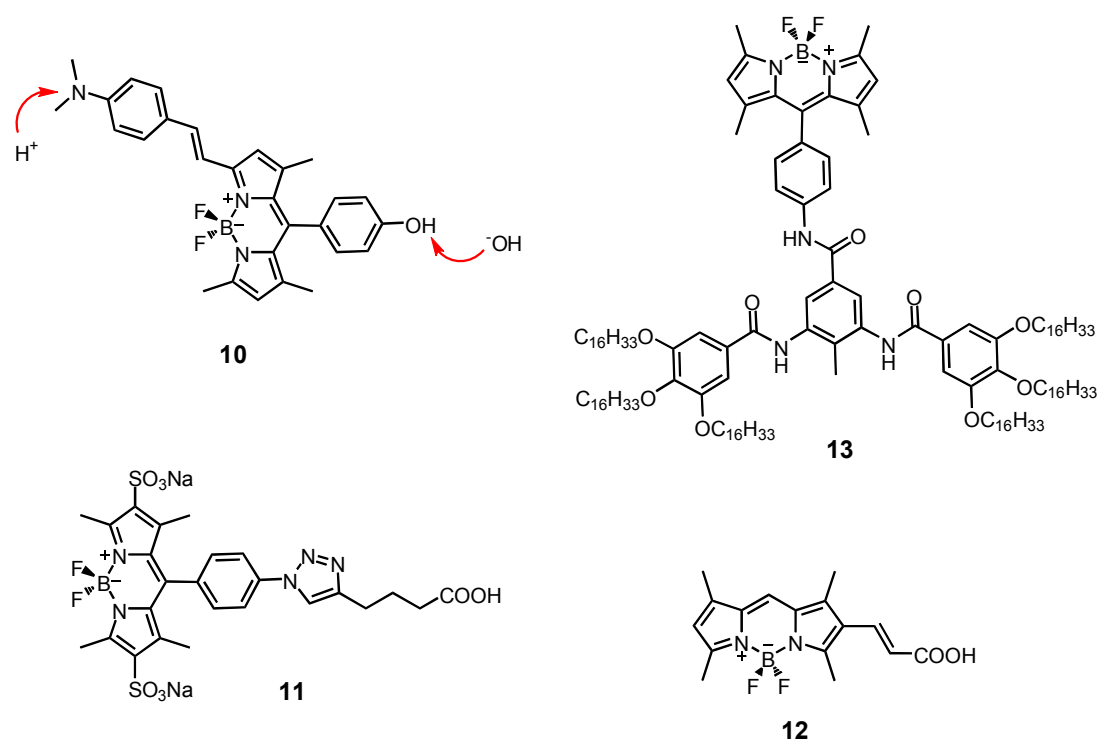


Figure 9. BODIPY as logic gate operator and liquid crystal, and water-soluble derivatives

These examples show that BODIPY chemistry has high versatility. Applications in light harvesting systems and dye-sensitized solar cells will be discussed in following parts.

1.4 Light Harvesting and Energy Transfer

Photosynthesis is a natural process in which the sunlight is collected effectively by a vast array of light-harvesting chromophores and absorbed energy is channeled into a single reaction center. Nature uses antennae systems to overcome the problem of light-harvesting efficiency (Figure 10). Collecting light by means of antenna system provides tuning the sunlight over a wide range and also provides much more concentrated energy in the core. The term “antenna effect” was first used in the luminescence of lanthanide ion which was sensitized by surrounding strongly absorbing ligands.⁵⁰

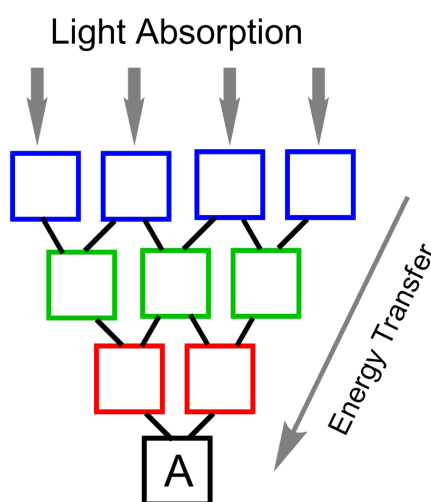


Figure 10. Schematic representation of a light-harvesting antenna system

The most widely studied natural antennae are the light-harvesting complexes of photosynthetic purple bacteria.⁵¹ Figure 11 is the schematic representation of overall process in purple bacteria. The crystal structure of light-harvesting antennae complex LH2 was determined by high resolution X-ray.⁵² It is composed of chlorophyll molecules and carotenoids. Chlorophyll molecules function as light-harvesting antennae. The energy collected by LH2 is transferred to LH1 antennae complex, which surrounds the reaction center. The reaction center is the final destination of collected energy. The structure of LH1 complex is similar to that of LH2, but it is not known as well as LH2 antennae complex.

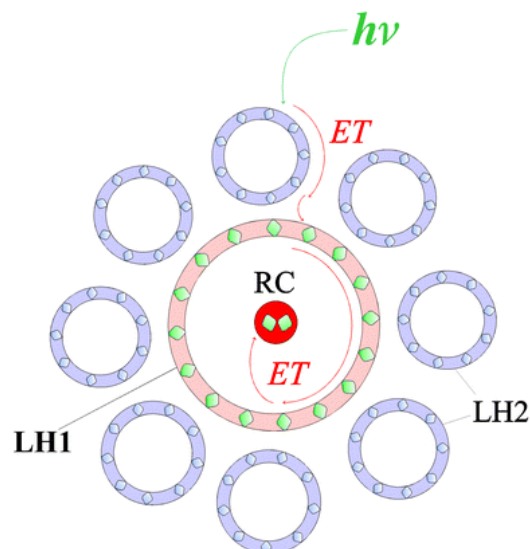


Figure 11. Schematic representation of the overall light-harvesting process by LH2 and LH1

With the assistance of supramolecular chemistry, artificial light-harvesting antenna systems can be obtained, especially dendritic macromolecules. These artificial models are used in signal amplifiers,⁵³ dye-sensitized solar cells,⁵⁴ light emitting diodes,⁵⁵ and exciton sources⁵⁶ in near field and scanning exciton microscopy. In order to observe antennae effect in supramolecular models, the organization in dimensions of time, energy and space is required.⁵⁷ Transfer of energy to next component must occur before undergoing radiative or nonradiative deactivation of donor component (time dimension). In energy dimension the components should be organized such that the energy of the acceptor excited state is lower or, at most, equal to the energy of donor excited state. Finally, overall energy transfer process must lead the excitation energy towards a selected component of array (space dimension).

1.4.1 Energy Transfer Mechanisms

A simple bichromophoric system contains an energy donor chromophore (D) and an energy acceptor chromophore (A). When the donor chromophore is excited, energy transfer occurs so that the donor returns to its ground state and the acceptor goes to excited state. This transfer occurs by either through-bond⁵⁸ (Dexter-type or exchange) mechanism or through-space^{59,60} (Förster-type or coulombic) mechanism.

1.4.1.1 Dexter-type Energy Transfer

A simultaneous electron exchange occurs in this mechanism (Figure 12).⁵⁷ It is a double electron-transfer process, one moving from the LUMO of the donor to the LUMO of the acceptor and the other moving from acceptor HOMO to the donor HOMO.

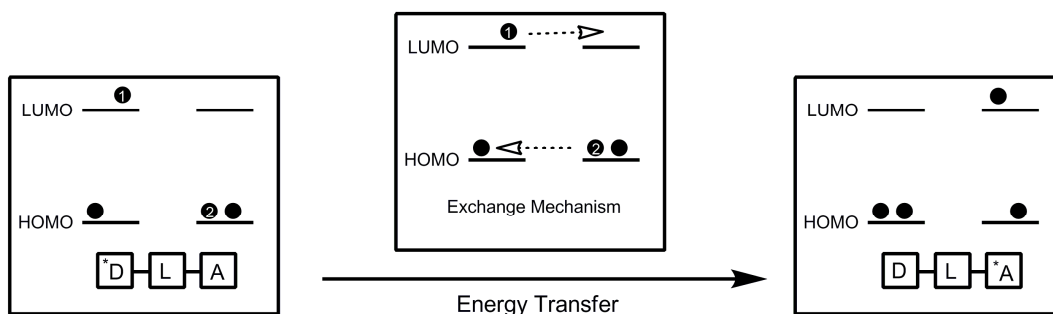


Figure 12. Pictorial representation of exchange energy transfer mechanism

The Dexter-type mechanism requires D-A orbital overlap which can be provided either directly or by the bridge. Therefore it is a short-range ($<10 \text{ \AA}$) interaction and it diminishes exponentially with distance.⁶¹ The literature on molecules that exhibit through-bond energy transfer may be divided into that which deals with oligomeric conjugated materials, and other contributions featuring models for biological systems (e.g. porphyrin-containing systems). Overlap between the emission spectrum of the donor and the lowest energy excited states of the acceptor is not required in through-bond energy transfer. For conjugated cassettes (Figure 13), it may not be possible to determine how much energy transfer proceeds via through-bond mechanisms relative to the through-space mechanisms. Yet the overall rates of energy transfer can be measured. The structure of the donor, acceptor, and linker fragments and the orientation of those fragments influence the rates of energy transfer.

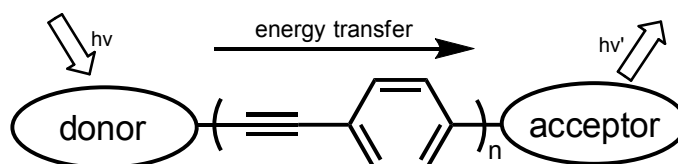


Figure 13. Through-bond energy transfer

Compounds **14** and **15**, in Figure 14, were synthesized in order to observe rates of energy transfer in donor-acceptor cassettes when the orientation of donor and acceptor moieties is changed.⁶²

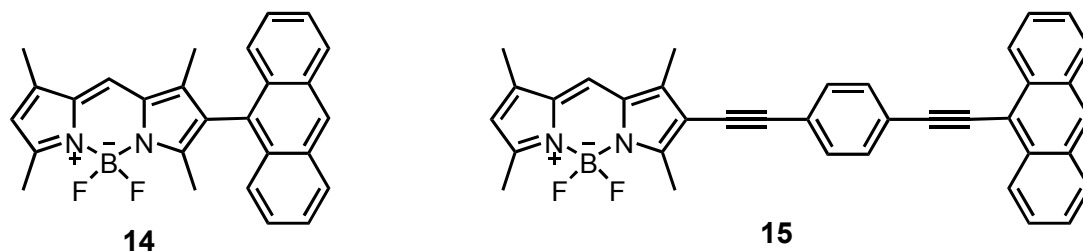


Figure 14. Through-bond energy transfer cassettes

In compound **14**, anthracene donor and BODIPY acceptor are directly attached to each other and the methyl groups on BODIPY twist the anthracene, so that the structure is not planar. If there is full conjugation in the cassette, as in compound **15**, it is not a true cassette. Conjugation in **15** is proved by the red-shift in absorption spectrum. Both of the compounds exhibit energy transfer when they are excited at the λ_{max} of anthracene donor.

Porphyrins are the main chromophores of natural photosynthesis. Synthetic porphyrin-based light-harvesting arrays are essential for investigating the effects of molecular organization on energy transfer. In compound **16**, a porphyrin array synthesized by Lindsey et al., efficient energy transfer has been reported from the Zn-containing porphyrin units to the free-base porphyrin (Figure 15).⁶³ Free-base porphyrin absorbs and emits at longer wavelengths than zinc porphyrins. Then the fluorescence spectrum of **16** is identical to that of free-base porphyrin (core). The mechanism of energy transfer is predominantly over through-bond via the ethyne linker.

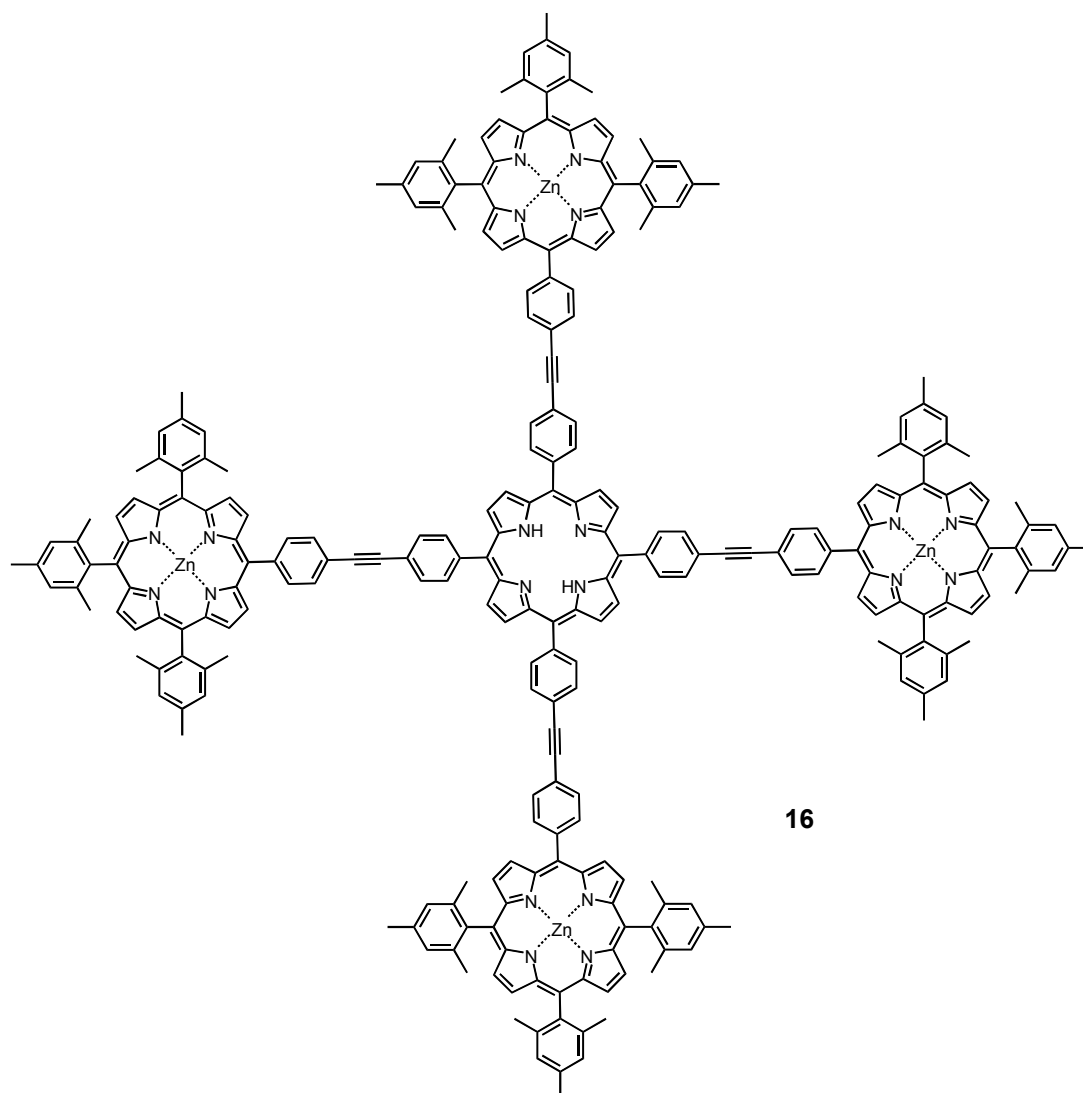


Figure 15. Porphyrin containing Dexter-type cassettes

1.4.1.2 Förster-type Energy Transfer

Fluorescence resonance energy transfer (FRET) is a nonradiative process whereby an excited state donor (D) transfers energy to a ground state acceptor (A) through long-range dipole-dipole interactions.⁶⁴ In contrast to Dexter mechanism, a physical contact between donor and acceptor is not required. D-A orbital overlap is not necessary which allows the chromophores to be separated by a relatively large distance (10-100 Å). In this mechanism, an electron in HOMO of the acceptor molecule is excited with energy released during the relaxation of electron in donor LUMO to its ground state (Figure 16).

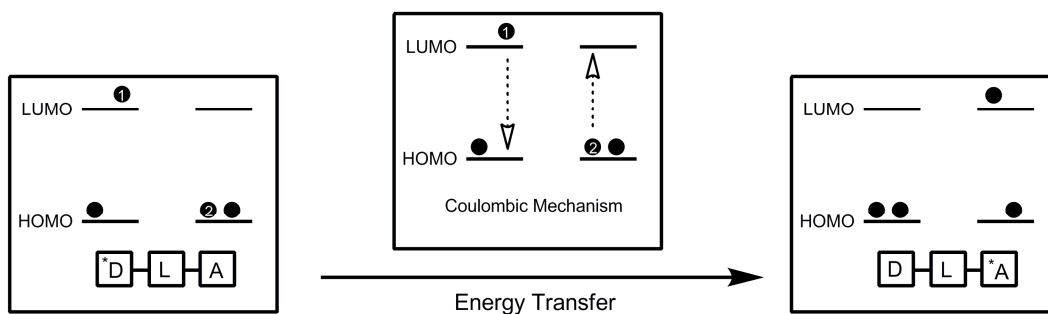


Figure 16. Pictorial representation of coulombic energy transfer mechanism

The acceptor must absorb energy at the emission wavelength of the donor (spectral overlap). The rate of energy transfer is dependent on many factors, such as the extent of spectral overlap, the relative orientation of the transition dipoles, and the distance between donor and acceptor molecules.⁶⁵ The following equations should be considered for a single donor-acceptor pair separated by a fixed distance r . So the energy transfer rate, $k_T(r)$, can be expressed in terms of the Förster distance R_0 . R_0 is the distance between D and A at which 50% of the excited D molecules decay by energy transfer, while the other half decay through other radiative or nonradiative ways. R_0 can be determined from the spectral properties of donor and acceptor molecules.

$$R_0 = 9.78 \times 10^3 [\kappa^2 n^{-4} Q_D J(\lambda)]^{1/6} \text{ (in } \text{Å}^\circ) \quad (4)$$

The term κ is an orientation factor which is related to the dipole-dipole interaction of donor and acceptor. Q and τ are the quantum yield and lifetime of the donor molecule, respectively. n is the refractive index of the solvent. Finally, $J(\lambda)$ refers to the Förster overlap integral between the luminescence spectrum of the donor, $F(\nu)$, and the absorption spectrum of the acceptor, $\varepsilon(\nu)$. That is further expressed by Eq. (5).

$$J = \frac{\int F(\nu)\varepsilon(\nu)/\nu^4 d\nu}{\int F(\nu)d\nu} \quad (5)$$

J parameter plays a crucial role in Förster energy transfer. The values for J and R_0 increase with higher acceptor extinction coefficients and greater overlap

between the donor emission spectrum and the acceptor absorption spectrum. The distance (r), that FRET will be effective, is estimated as $R_0 \pm 50\% R_0$. The efficiency of the energy transfer is determined from Eq. (6) where F is the relative donor fluorescence intensity in the absence (F_D) and presence (F_{DA}) of the acceptor.

$$E = 1 - \frac{F_{DA}}{F_D} \quad (6)$$

The use of Förster energy transfer has been in practice for more than 50 years. Biological purposes, light frequency conversion, cascade systems, artificial photosynthetic antenna, singlet oxygen generation and switching element in molecular machines are major application areas of FRET. Some selected examples of Förster energy transfer are summarized below.

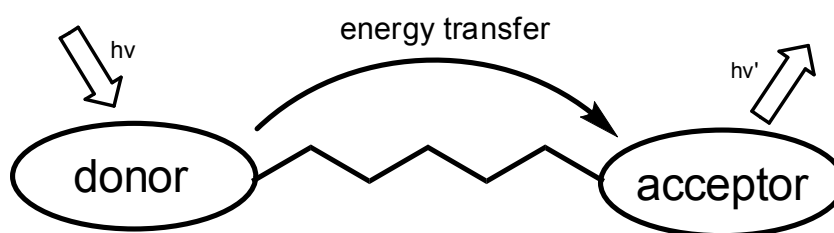


Figure 17. Through-space energy transfer

1.4.2 Light Frequency Conversion

Light frequency conversion is the basic property of most light-harvesting molecules actually. However, in some cases, it becomes most interesting function of the system. This happens when there is a strong frequency difference between absorbed and emitted light (large Stokes' shift).

Compound **17** is a dendritic material that transforms ultraviolet (UV) directly into near-infrared (NIR) radiation.⁶⁶ The donor, coumarin 2, has an absorption band at 345 nm and an emission band at 445 nm. The acceptor core, perylene, shows absorption at 435 and 685 nm and emission band at 770 nm. The emission of coumarin 2 at 445 nm overlaps with the absorption of perylene which leads to a 99%

FRET. Perylene core absorbs strongly in most regions of visible spectrum. So the energy of any photon absorbed either by donor or acceptor of **17** is converted to single NIR emission of perylene core. Evidence of FRET is the quenching of donor emission and amplification of core emission due to the antennae effect (Figure 18).

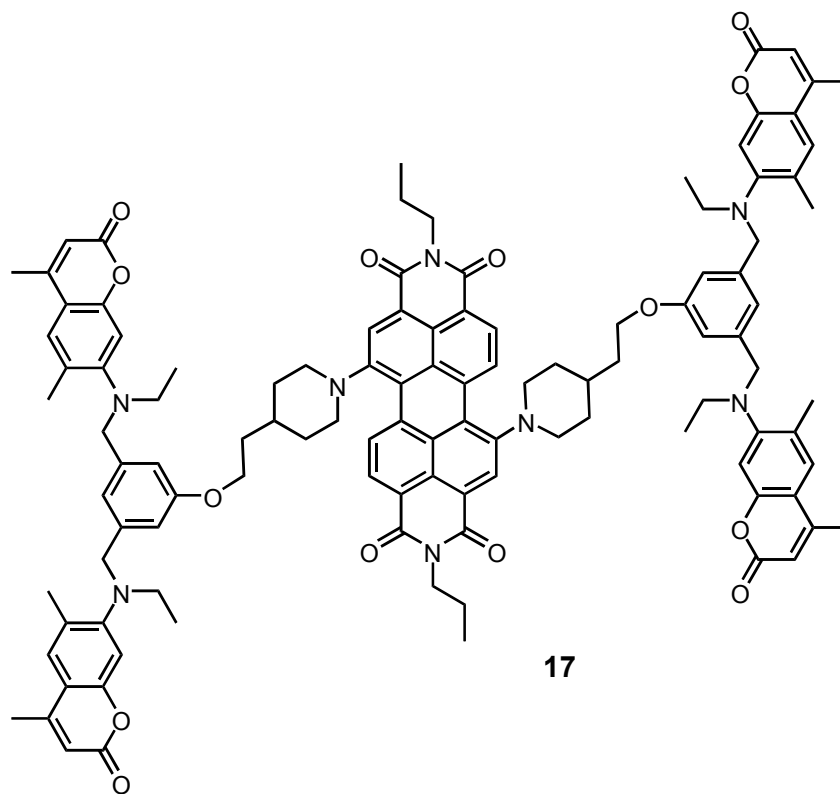


Figure 18. Chemical structure of compound **17**

Another interesting example of light frequency conversion is two-photon absorbing system developed by Frechet et al.⁶⁷ These kinds of materials are promising materials for biomedical imaging. The core of compound **18**, a Nile red derivative, absorbs at 530 nm and shows a broad emission at 595 nm. The donor chromophore exhibits absorptions at 320 and 410 nm and emits at 500 nm. Like in the example above, the excitation of donor chromophore followed by FRET results in the emission of core at 595 nm. What makes compound **18** interesting is not only the single photon absorption but also its two-photon absorption properties. The donor chromophore has large two-photon absorbing cross section. Therefore excitation of donor part with high intensity IR light (815 nm) results in amplified emission of Nile red chromophore at 595 nm due to FRET.

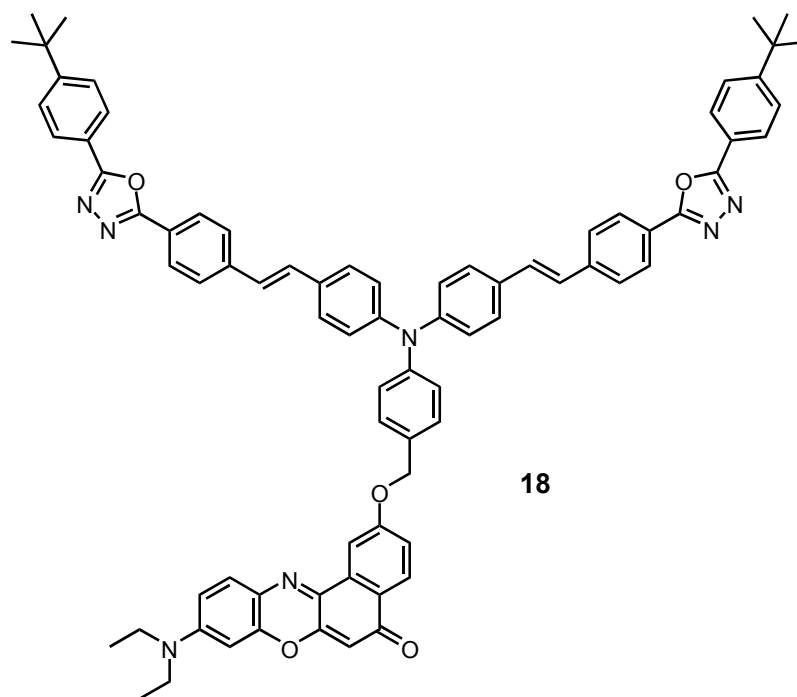


Figure 19. Chemical structure of compound **18**

1.4.3 Cascade Systems

Systems capable of directional FRET between several chromophores have attracted much attention since in natural photosynthetic systems energy is transferred through many chromophores. Compound **19** has been designed to investigate cascade energy transfer without self-quenching (Figure 20).⁶⁸ The system contains three chromophores; coumarin 2 (blue), fluorol 7GA (green), and perylene core (red) which show absorptions at 350 nm, 415 nm, and 555 nm respectively. There are two possible pathways for FRET in this structure. One is from coumarin 2 part to the perylene core and other is from coumarin 2 groups to fluorol 7GA units to perylene core. Former is not favored compared to latter because of the poor overlap between emission spectrum of coumarin 2 and absorption spectrum of perylene. In second pathway, the efficiency of first FRET is 98% and that of second FRET is 97%, which results in overall 95% FRET efficiency in compound **19**. Furthermore the upper limit of transfer efficiency is 79% if the transfer is directly from coumarin 2 to perylene.

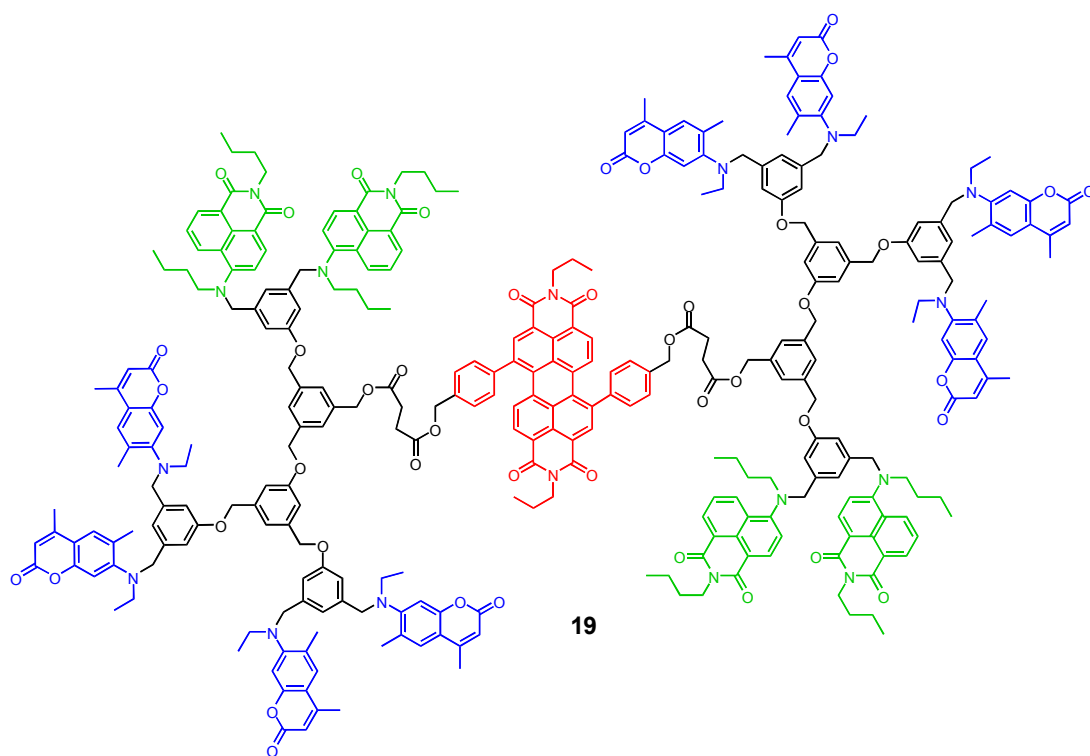


Figure 20. The structure of cascade system 19

1.4.4 Artificial Photosynthetic Antenna

Photosynthesis is one of the most important natural processes. It is the main source of energy for living organisms. The importance of photosynthesis has driven many scientists to look for ways of achieving it in simplified systems. The investigation of light-harvesting antenna complex LH2 of purple bacterium has led to the design and synthesis of cyclic porphyrin arrays. These are constructed either by means of covalent bonds, noncovalent bonds, or metal coordination bonds.⁶⁹⁻⁷¹ Energy transfer in cyclic porphyrin arrays has been observed successfully and even ultrafast energy transfer rates that rival in the natural LH2 have been identified.⁷²⁻⁷⁴

Compounds **20** and **21** are the examples for covalently linked porphyrin arrays (Figure 21). In compound **20**, Förster energy transfer is observed from a zinc porphyrin to a free base porphyrin.⁷⁵ This is a type of linear *meso-meso* linked porphyrin array. However efficient energy transfer has also been reported in compound **21** where all the porphyrin units are coordinated to a zinc ion.⁷⁶

Compound **21** is a directly *meso-meso* linked porphyrin array and orientation of transition dipole moments provides energy transfer to occur with quite efficient rates.

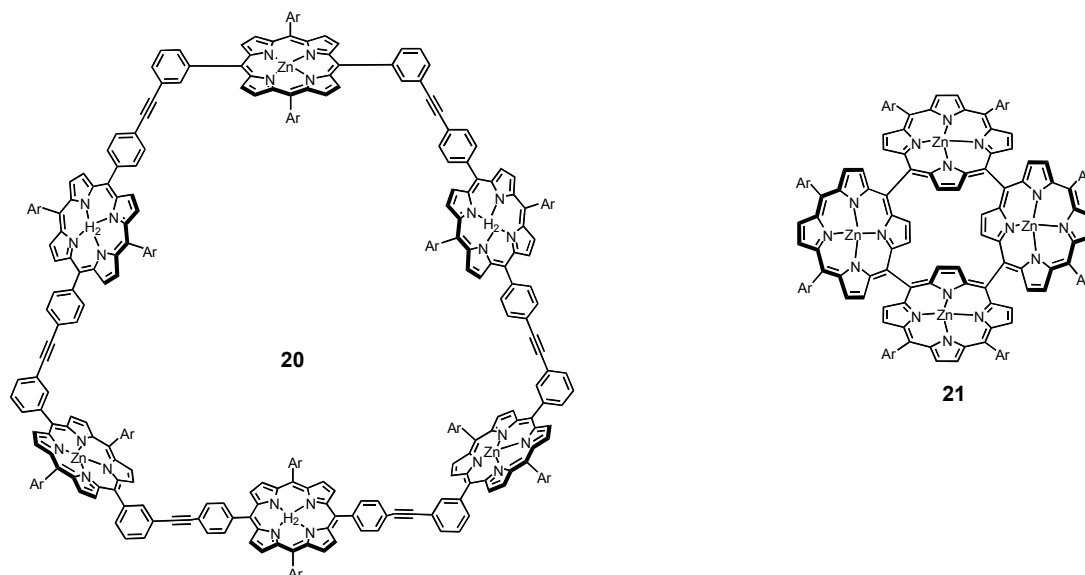
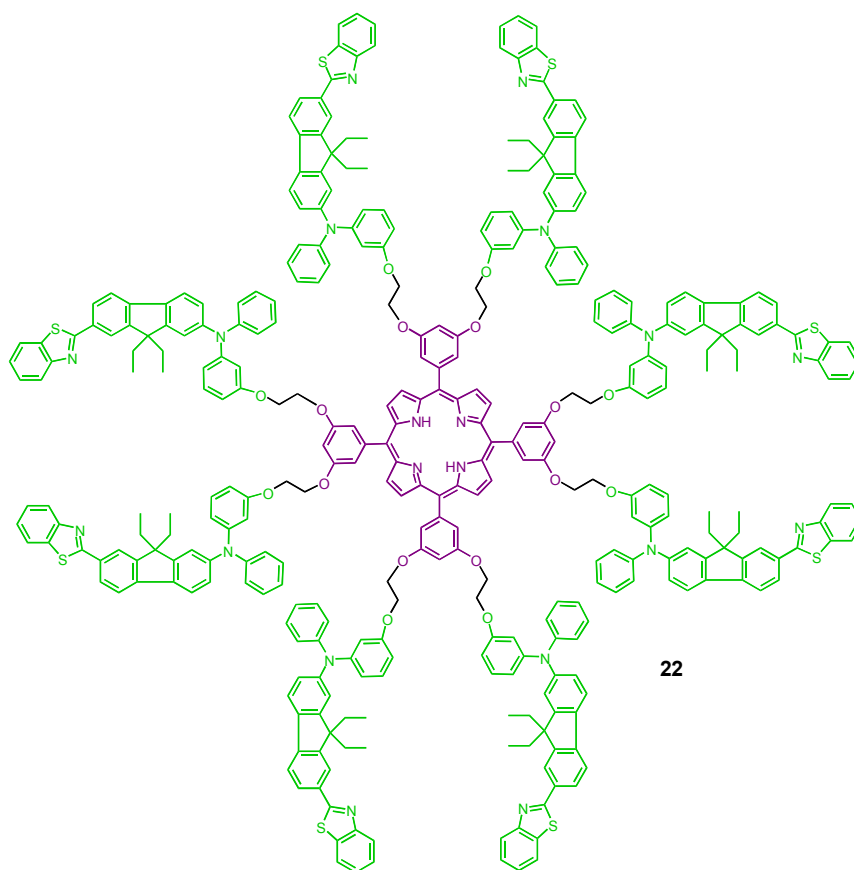


Figure 21. Artificial photosynthetic antenna systems

1.4.5 FRET for Biological Purposes and Fluorescent Signaling Systems

Singlet oxygen generation is an important process for photodynamic therapy to tumors below the skin surface. Compound **22** is capable of generating singlet oxygen efficiently via FRET (Figure 22).⁷⁷ The donor chromophores, surrounding the core, have high two-photon absorption cross section. After absorption of photons by donor parts at 780 nm, excited state energy is transferred to porphyrin core via FRET, and there occurs intersystem crossing and consequently, singlet oxygen generation. Porphyrin core itself is not capable of two-photon absorption efficiently but with simple modification of porphyrin, incorporating donor fragments, it becomes so. Working with near-infrared light is an essential for photodynamic therapy, which makes the idea and design of compound **22** promising.



22

Figure 22. Singlet oxygen generation via FRET

The design of fluorescent chemosensor has received much attention because of its applications in biology, medicine, environment, etc. Compound **23** is a kind of proton sensing agent acting via electron and energy transfer (Figure 23).⁷⁸ Anthracene and chalcone moieties are linked by piperazine in this compound. When anthracene is excited with near-ultraviolet light, energy transfer does not occur to the chalcone moiety. That's because fast electron transfer occurs from piperazine to anthracene. However, when piperazine is protonated, electron transfer is blocked and energy transfer takes place to chalcone moiety which is followed by emission at 510 nm.

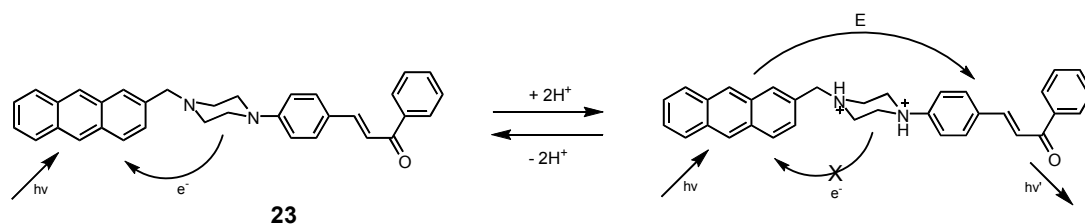


Figure 23. Electron and energy transfers in compound **23**

1.4.6 BODIPY dyes as Light Harvesters

BODIPY is a versatile compound that can be modified from its different positions leading to changes in photophysical properties. Thus it is a promising compound in design of light-harvesting systems. By changing its absorption and emission properties, BODIPY can act as either donor or acceptor in a light-harvesting array. Compound **24** is synthesized by Akkaya et al (Figure 24).⁷⁹ It is composed of four BODIPY donors and a perylene-3,4,9,10-tetracarboxylic diimide (PDI) acceptor. Absorption properties of both fragments exist in the spectrum. Upon excitation of BODIPY donors at 526 nm, no green fluorescence emission was observed indicating efficient energy transfer (99%). Additionally 3.5-fold enhancement in core emission was obtained by antenna effect relative to direct excitation of core at 588 nm.

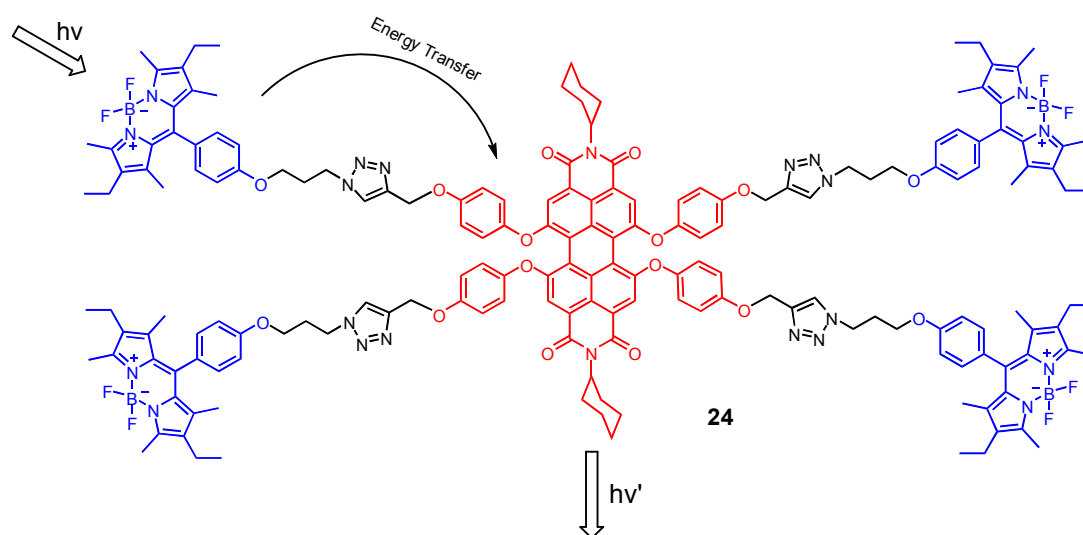


Figure 24. Light-harvesting dendrimer **24**

The following compound **25** is a supramolecular triad.⁸⁰ Here the idea is that the energy transfer occurs from BODIPY donor to zinc porphyrin (ZnP) and then electron transfer takes place to the fullerene (C₆₀-Im) unit. ZnP connects to fullerene via metal-ligand coordination. Both energy and electron transfer steps were efficient in the study. The whole system was designed to mimic “combined antenna-reaction center” events in natural photosynthesis (Figure 25).

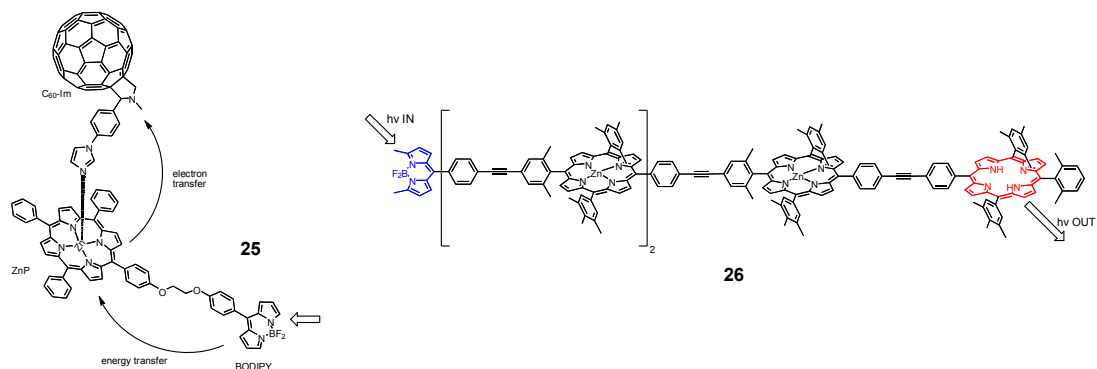


Figure 25. Light-harvesting arrays with BODIPY energy donors

Compound **26** is a design of light-harvesting system that can function as a “molecular photonic wire”.⁸¹ When BODIPY, at one end of the molecule, is excited at 485 nm, it results in an emission from free base porphyrin. The percentage of emission from free base porphyrin is 92%. Zinc-porphyrins act as efficient signal transmission element (Figure 25).

A novel BODIPY based light-harvesting system was reported by Xiao et al. recently (Figure 26).⁸² The compound contains three types of BODIPY derivatives, each absorbing at different wavelengths. The acceptor part is a long wavelength BODIPY. Upon the excitation of **27** either at 490 nm (from green fragment) or at 560 nm (from pink fragment), the emission of central BODIPY dye (purple part) was observed. The energy transfer efficiency is over 99%.

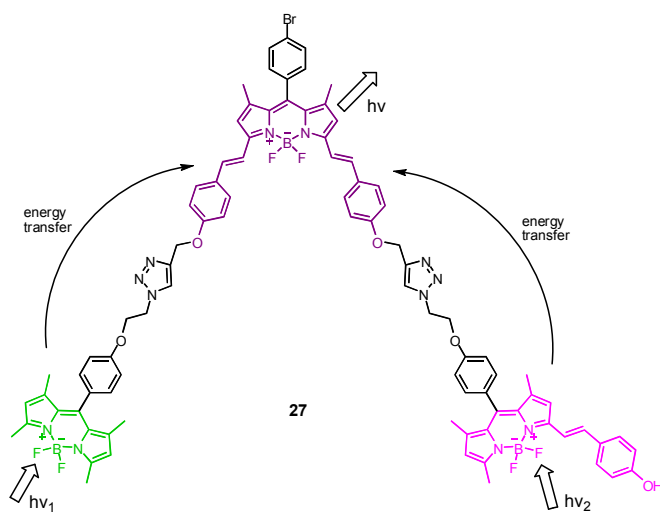


Figure 26. Light-harvesting cassette with BODIPY donors and acceptor

1.5 Dye-sensitized Solar Cells

The quality of human life depends almost on the availability of energy. It is threatened if new energy resources cannot be developed in the near future. The earth's oil reserves will run out during this century. Additionally, environmental pollution arising from oil spills and out comings of greenhouse effect as a result of combustion of fossil fuels make people concerned about the problem. The energy supply from the sun is gigantic, 3×10^{24} J year⁻¹ or, in other words, it is about 10^4 times more than current consumption. Thus the effective conversion of solar energy seems challenging. Covering 0.1% of the earth's surface with solar cells with an efficiency of 10% would satisfy our current needs.

Until now, the research on solar cells has been focused on inorganic solid state materials, usually doped forms of crystalline or amorphous silicon. Silicon has been studied widely and its availability has led to study it on solar cells. However, there is still great research on these materials in order to lower production costs and to increase production yields and stability. It is now possible to depart from classical solid state cells. The dye-sensitized solar cells (DSSC) were invented by Gratzel in 1991.⁸³ This novel type of solar cell offers very low cost fabrication, compatibility with flexible substrates, and a variety of appearances to facilitate market entry. Dye-sensitized solar cells have shown conversion efficiencies which compete with those of inorganic solar cells.⁸⁴⁻⁸⁶ Efficiency of cell is defined as conversion efficiency from solar to electrical power.

1.5.1 Working Principle of DSSCs

The cell design contains three primary parts. In the middle of the system there is a mesoscopic semiconductor oxide film. This material is usually chosen as TiO₂, whereas other wide-band-gap oxides (ZnO, Nb₂O₅) have also been studied. These oxides are deposited in nanoparticle form onto a glass covered with a transparent conducting layer of fluorine-doped tin oxide (FTO) or tin-doped indium oxide (ITO). The average size of TiO₂ nanoparticles are 20 nm. In order to ensure

that particles are interconnected electronically and to improve the light-harvesting efficiency of the film in red or near-infrared region, larger size of TiO₂ nanoparticles (200-400 nm) are also added.

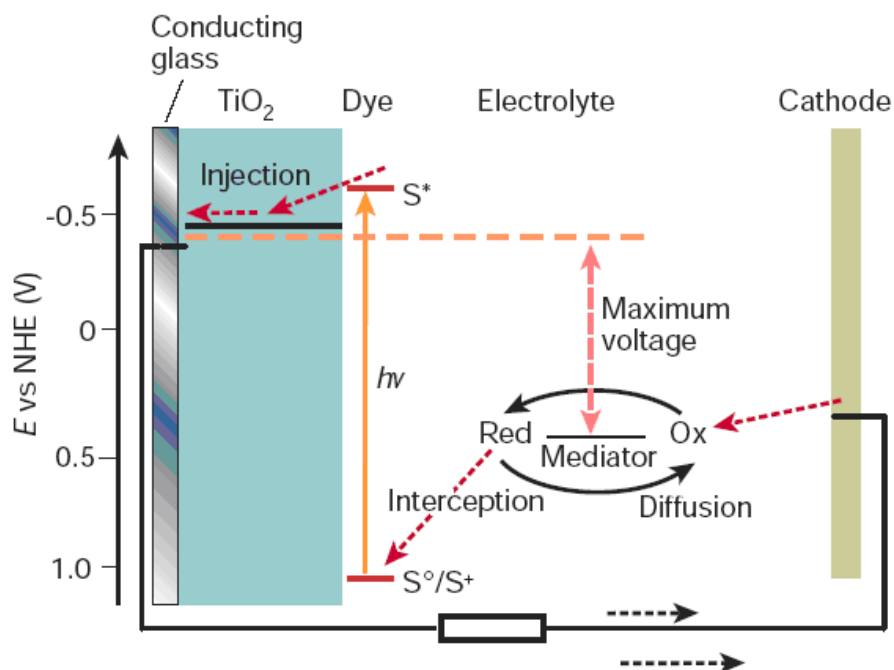


Figure 27. Principle of operation of DSSC

The dye sensitizer is attached as a layer to the surface of TiO₂ film. The sensitizer molecules usually contain functional groups such as carboxylate, hydroxamate, and phosphonate for successful attachment onto the TiO₂ nanoparticles. S^o, S^{*} and S⁺ represents the ground, excited, and oxidized states of the sensitizer respectively in Figure 27. The sensitizer is excited with light at certain wavelength and the electron in excited state is transferred to the conduction band of semiconductor TiO₂ film. Thus electron flow is started in the external circuit. The dye in ground state is regenerated by redox system. The redox system is composed of iodide/triiodide couple. The electrons, passed through the load, at the counter electrode are captured by triiodide and formation of iodide results in the reduction of oxidized dye molecule.



The light-harvesting efficiency for photons of wavelength λ is expressed as in Eq. (9) where α is the reciprocal absorption length and d is the thickness of the nanocrystalline film.⁸⁷

$$LHE(\lambda) = 1 - 10^{-\alpha d} \quad (9)$$

The incident photon to current conversion efficiency (IPCE) is the number of electrons measured as photocurrent in the external circuit divided by the monochromatic photon flux that strikes the cell.⁸⁷

$$IPCE(\lambda) = LHE(\lambda) \cdot \varphi_{inj} \cdot \eta_{coll} \quad (10)$$

φ_{inj} is the quantum yield for electron injection from the excited sensitizer in the conduction band of the semiconductor oxide, and η_{coll} is the electron collection efficiency. The parameter φ_{inj} is the ratio of injection rate to the sum of injection and deactivation rates. Deactivation comes from radiative or radiationless ways. In other words, achievement of charge separation is an important step in cell efficiency. IPCE values exceed 80% in the wavelength range near the absorption maximum of the sensitizer. The overall conversion efficiency of the dye-sensitized cell is determined by the photocurrent density measured at short circuit (I_{sc}), the open-circuit voltage (V_{oc}), the fill factor of the cell (ff), and the intensity of the incident light (I_s).⁸⁷

$$\eta(\%) = \frac{I_{sc} \cdot V_{oc} \cdot (ff)}{I_s} \times 100 \quad (11)$$

Taking these facts into account, a good sensitizer should have a high molar extinction coefficient and absorb over a wide range in visible spectrum. The dye molecule must be attached to the surface of semiconductor metal oxide well so that electrons are injected into the conduction band with high quantum yield. The HOMO and LUMO levels of the sensitizer should be adjusted to maintain the electron injection and to be reduced to ground state by electrolyte. A photovoltaic device must remain serviceable for 20 years without significant loss performance, which corresponds to 10^8 turnovers for the dye. To enhance the conversion

efficiency, the aggregation of dye molecules due to π - π interactions should be prevented, which is overcome by using bulky groups in dye molecules. Aggregation results in self-quenching of sensitizer and inhibition of electron transfer to the conduction band of semiconductor.

1.5.2 Photosensitizers for DSSCs

Ruthenium-based sensitizers, developed by Gratzel et al., have been investigated intensively and solar-energy-to-electricity conversion efficiencies up to 11% (under AM 1.5 sunlight irradiation) have been reported for ruthenium-based dye-sensitized solar cells.⁸⁷⁻⁸⁹ The structures of N3 (**28**), N719 (**29**), and black dye (**30**) are shown in Figure 28. The compounds are made of bipyridyl complexes of ruthenium. Carboxylate groups enable the interaction of sensitizer with TiO₂ surface. Those ruthenium complexes absorb over a wide range spectrum including visible and near-infrared region.

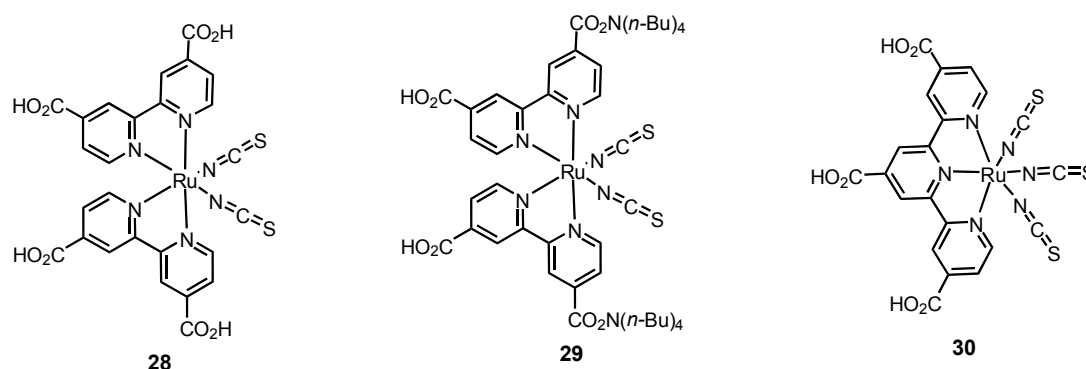


Figure 28. The structures of N3, N719, and black dye

Incorporation of triphenyl amine groups as electron donors to the structures enhances the charge separation and as a consequence, it increases cell efficiency. In compound **31**, a polymer chain of triphenyl amine groups have been attached to the ruthenium complex (Figure 29).⁹⁰ After the excitation of sensitizer, electrons are injected to TiO₂ semiconductor. The back electron transfer from TiO₂ to sensitizer is avoided through the fast reduction ruthenium by triphenyl amine groups. Therefore overall process results in a very long-lived charge separated state. Compound **32** has

extended π electron delocalization, so that it has high molar extinction coefficient.⁹¹ The HOMO of **32** is spread over the triphenyl amine moieties. The increased separation of the HOMO from TiO₂ surface results in an efficient charge separation. The overall conversion efficiency was found out as 6.1%.

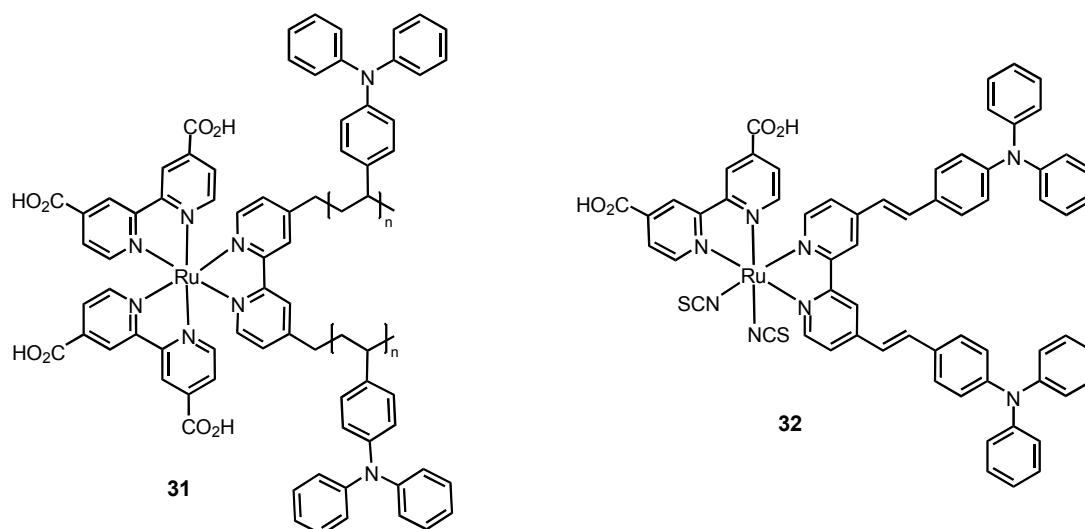


Figure 29. Ruthenium complexes with electron donor groups

In recent years, it is of great interest to design organic dye sensitizers, which are not based on ruthenium complexes. Organic dyes have many advantages such as large molar extinction coefficient, control of absorption wavelength, facile design and synthesis, and lower cost than ruthenium complexes. Derivatives of coumarine, indoline, phthalocyanine and conjugated oligo-ene dyes have reported as photosensitizers.⁹²⁻⁹⁴ Until now, none of them has shown an overall efficiency that ruthenium complexes exhibited.

Figure 30 shows some examples of organic dyes as photosensitizers. The efficiency of compound **33** was reported as 7.4%.⁹⁵ It was found out that electron injection from dye into the conduction band of TiO₂ occurs within <100 fs, which is much faster than the emission lifetime of the dye (1.0 ns). Thus it results in almost unity quantum yield of electron injection. The dye molecule has also high thermal stability. Compound **34** is an indoline-based organic dye with a conversion efficiency of 8.00%.⁹⁶ That higher efficiency was achieved by optimizing with a cholic acid derivative. Cholic acid derivatives prevent aggregation of dyes on TiO₂

surface. Finally, compound **35** is a simple π -conjugated oligo-phenylenevinylene unit containing an electron donor-acceptor moiety.⁹⁷ Although it does not have absorption beyond 500 nm, the overall solar-to-energy conversion efficiency was 9.1% which is the highest value for ruthenium free solar cells.

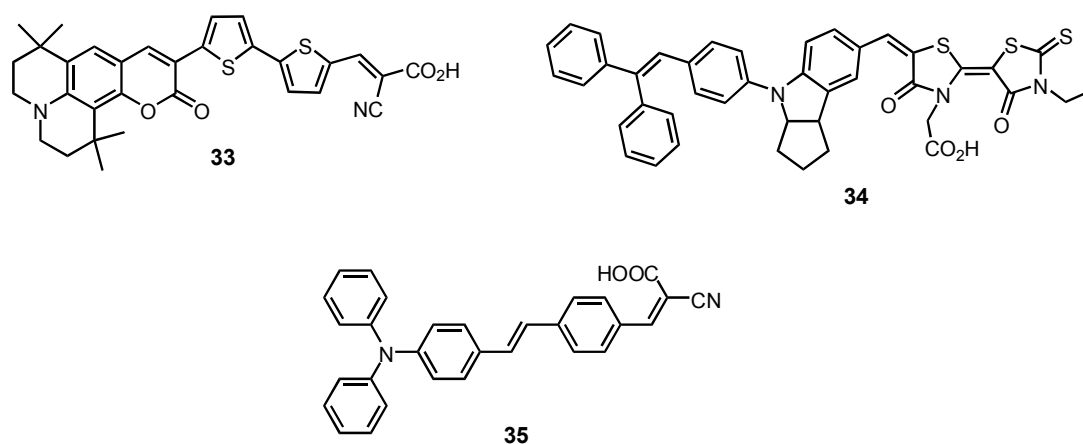


Figure 30. Organic dyes as DSSC

Following compounds (Figure 31) was designed and synthesized in order to investigate the position effect of carboxylic group.⁹⁸ The position of carboxyl group has negligible influence of photophysical and electrochemical properties. However, in dye-sensitized solar cells, they exhibit different efficiencies. The carboxylic group in compound **36** acts as electron acceptor, it interacts well with TiO_2 surface and as a consequence electrons are injected effectively to TiO_2 semiconductor. For **37**, carboxylic group is still anchoring group for attachment to TiO_2 surface, but it is no longer an electron acceptor moiety. Cyanide group acts as acceptor rather. Free rotation of butyl group prevents the injection of electrons to TiO_2 surface even through cyanide unit. The cell efficiency of **36** is 1.00% and that of **37** is 0.34%.

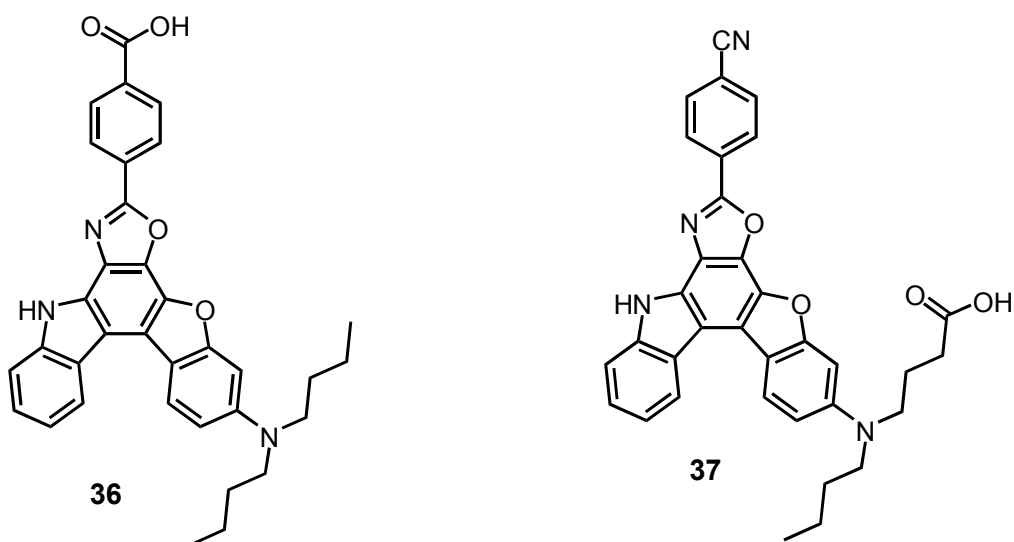


Figure 31. Effect of COOH position on cell efficiency

BODIPY was used as a photosensitizer firstly by Nagano et al.⁹⁹ Compounds **38** and **39** was designed and synthesized as shown in Figure 32. Both of them attach to the TiO₂ surface. Compound **38** contains electron donor methoxyl groups, whereas compound **39** does not. Charged separated state for compound **38** was observed and it has the ability to inject electron to the conduction band of TiO₂. For **39**, the photoexcitation of the dye results in direct electron injection from the singlet excited state of the dye. Both compounds lead to the photocurrent generation. The conversion efficiencies are 0.13% and 0.16% for **38** and **39** respectively. The reason for lower values of cell efficiency was presumed to be due to the aggregation of dyes on TiO₂ surface.

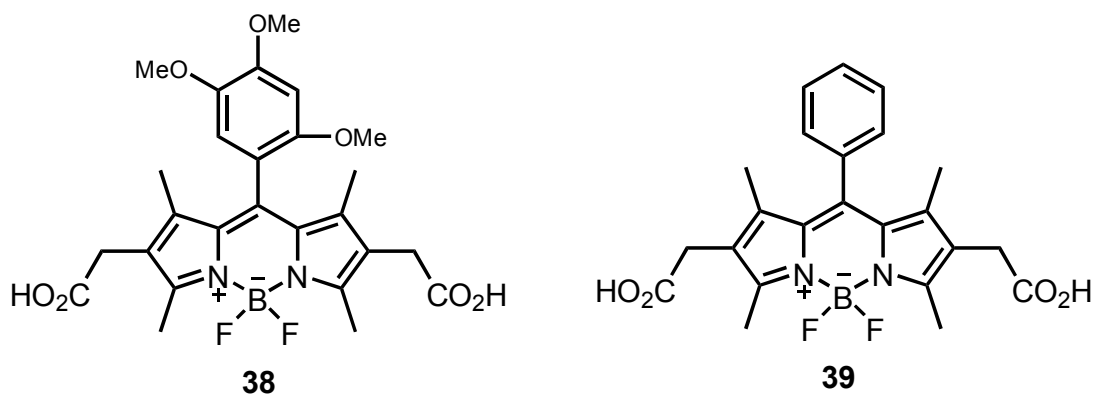


Figure 32. BODIPY photosensitizers

CHAPTER 2

EXPERIMENTAL

2.1 Instrumentation

All chemicals and solvents purchased from Aldrich were used without further purification. Compounds **40**, **51**, and **53** were prepared following the procedures as described in the literature. Column chromatography of all products was performed using Merck Silica Gel 60 (particle size: 0.040-0.063 mm, 230-400 mesh ASTM). Reactions were monitored by thin layer chromatography using fluorescent coated aluminum sheets.

¹H NMR and ¹³C NMR spectra were recorded using a Bruker DPX-400 in CDCl₃ with TMS as internal reference. Splitting patterns are designated as s (singlet), d (doublet), t (triplet), q (quartet), m (multiplet), p (pentet), dt (doublet of triplet), and br (broad).

Absorption spectrometry was performed using a Varian spectrophotometer. Fluorescence spectra were determined on a Varian Eclipse spectrofluorometer. Excitation slit was set at 2.5 nm and emission slit was set at 5 nm. Fluorescence quantum yields were measured in CHCl₃ vs. Rhodamine 6G ($\Phi=0.95$ in ethanol). Solvents used for spectroscopy experiments were spectrophotometric grade. Mass spectrometry measurements were done at the Ohio State University Mass Spectrometry and Proteomics Facility, Ohio, USA.

PART I

2.2.1 Synthesis of 4,4-difluoro-8-{4-(1,3-dioxolan-2-yl)}phenyl- 1,3,5,7-tetramethyl-2,6-diethyl-4-bora-3a,4a-diaza-s-indacene (41)

3-ethyl-2,4-dimethyl pyrrole (13.89 mmol, 1.71 g) and compound **40** (6.73 mmol, 1.2 g) were dissolved in 300 mL absolute CH₂Cl₂ (argon gas was bubbled through CH₂Cl₂ for 25 min) under argon atmosphere. One drop of TFA was added and the solution was stirred at room temperature overnight. Then a solution of DDQ (6.94 mmol, 1.71 g) in 50 mL of absolute CH₂Cl₂ was added. Stirring was continued for 45 min followed by the addition of 5 mL of TEA and 5 mL of BF₃.OEt₂. The reaction was monitored by TLC (eluent CHCl₃). After stirring 2 h, the reaction mixture was washed three times with water and dried over Na₂SO₄. The solvent was evaporated and the residue was purified by silica gel column chromatography (CHCl₃). Orange solid (875 mg, 30%).

¹H NMR (400 MHz, CDCl₃) δ 7.52 (d, *J*=7.9 Hz, 2H), 7.23 (d, *J*=7.9 Hz, 2H), 5.8 (s, 1H), 4.1 (t, *J*=5.3 Hz, 2H), 3.99 (t, *J*=5.3 Hz, 2H), 2.45 (s, 6H), 2.21 (q, *J*=7.5 Hz, 4H), 1.19 (s, 6H), 0.9 (t, *J*=7.5 Hz, 6H).

¹³C NMR (100 MHz, CDCl₃) δ 153.8, 139.7, 138.7, 138.4, 136.8, 132.8, 130.7, 128.4, 127.3, 103.4, 65.4, 17.1, 14.6, 12.5, 11.8.

HRMS (ESI) calcd for C₂₃H₂₇BF₂N₂Na (M+Na) 474.2381, found 474.2355. Δ=5.5 ppm.

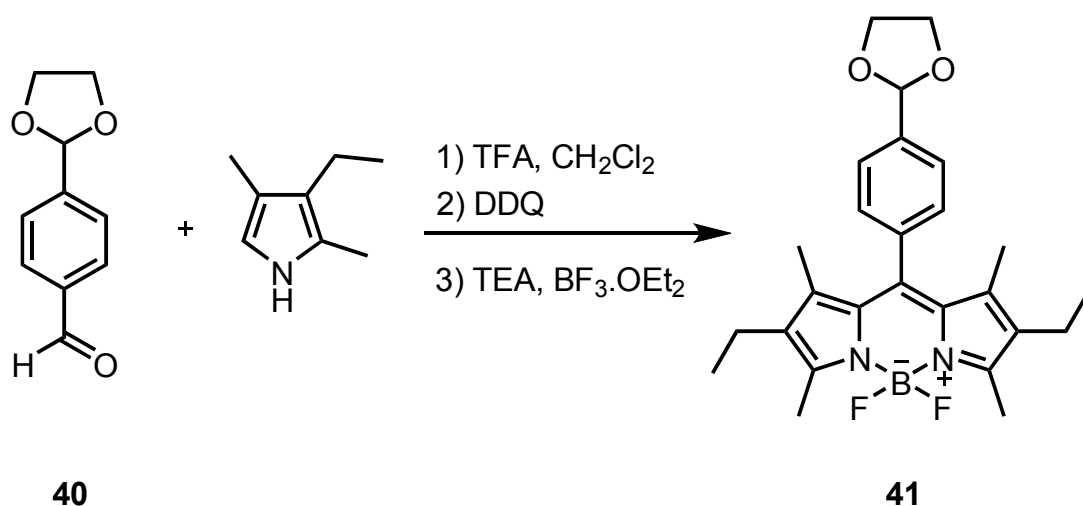


Figure 33. Synthesis of compound **41**

2.2.2 Synthesis of 4-[3,5-di{2-(4-methylphenyl)ethenyl}-4,4-difluoro-1,3,5,7-tetramethyl-2,6-diethyl-4-bora-3a,4a-diaza-s-indacen-8-yl]-benzaldehyde (**42**)

Compound **41** (0.66 mmol, 300 mg) and p-tolualdehyde (3.39 mmol, 410 mg) were refluxed in a mixture of benzene (50 mL), glacial acetic acid (0.5 mL), and piperidine (0.6 mL). Any water formed during the reaction was removed azeotropically by heating overnight in a Dean-Stark apparatus. Crude product was concentrated under vacuum. Without further purification, deprotection of acetal group was followed. The crude product was stirred in a mixture of THF (20 mL) and HCl (5%, 10 mL) at room temperature overnight. The reaction was monitored by TLC. THF was evaporated and remaining solution was extracted with CHCl₃. After the separation of organic phase and evaporation of CHCl₃, the crude product was purified by silica gel column chromatography (CHCl₃/Hexane (2:1)). Brown solid (247 mg, 61%).

¹H NMR (400 MHz, CDCl₃) δ 10.1 (s, 1H), 7.97 (d, *J*=7.9 Hz, 2H), 7.68 (d, *J*=16.7 Hz, 2H), 7.53-7.42 (m, 6H), 7.22-7.11 (m, 6H), 2.54 (q, *J*=7.4 Hz, 4H), 2.32 (s, 6H), 1.23 (s, 6H), 1.09 (t, *J*=7.4 Hz, 6H).

^{13}C NMR (100 MHz, CDCl_3) δ 191.5, 161.0, 136.6, 134.2, 132.4, 130.3, 129.9, 129.5, 127.4, 119.1, 114.8, 26.4, 21.4, 18.4, 14.0, 11.7.

HRMS (ESI) calcd for $\text{C}_{40}\text{H}_{39}\text{BF}_2\text{N}_2\text{ONa}$ ($\text{M}+\text{Na}$) 634.3057, found 634.3008. $\Delta=7.7$ ppm.

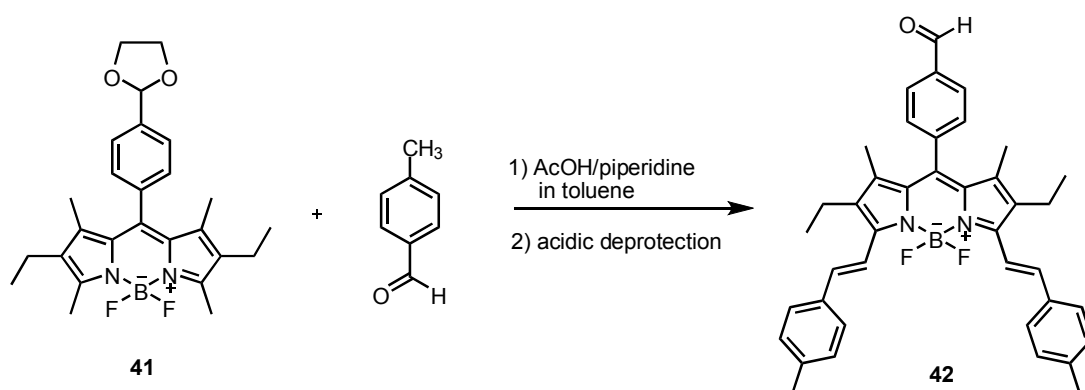


Figure 34. Synthesis of compound **42**

2.2.3 Synthesis of 1-{4,4-difluoro-1,3,5,7-tetramethyl-2,6-diethyl-4-bora-3a,4a-diaza-s-indacen-8-yl}-4-[3,5-di{2-(4-methylphenyl)ethenyl}-4,4-difluoro-1,3,5,7-tetramethyl-2,6-diethyl-4-bora-3a,4a-diaza-s-indacen-8-yl]-benzene (**43**)

A similar procedure, which was applied in the synthesis of compound **41**, was followed here. Compound **42** (0.28 mmol, 171 mg), 3-ethyl-2,4-dimethyl pyrrole (0.56 mmol, 68.7 mg), DDQ (0.28 mmol, 68.6 mg), TEA (3 mL), and $\text{BF}_3\cdot\text{OEt}_2$ (3 mL) were used in this reaction. The residue was purified by silica gel column chromatography (first CHCl_3 /Hexane (2:1), then CHCl_3 /Hexane (1:1)). The green fraction which has red fluorescence was collected. Green solid (84 mg, 34%).

^1H NMR (400 MHz, CDCl_3) δ 7.7 (d, $J=16.7$ Hz, 2H), 7.49-7.44 (m, 8H), 7.21-7.12 (m, 6H), 2.56 (q, $J=7.3$ Hz, 4H), 2.49 (s, 6H), 2.32 (s, 6H), 2.26 (q, $J=7.4$ Hz, 4H), 1.45 (s, 6H), 1.43 (s, 6H), 1.11 (t, $J=7.3$ Hz, 6H), 0.94 (t, $J=7.4$ Hz, 6H).

^{13}C NMR (100 MHz, CDCl_3) δ 153.3, 152.5, 149.8, 137.9, 137.4, 136.9, 135.3, 133.6, 132.9, 132.0, 129.1, 128.8, 128.7, 128.5, 127.1, 126.4, 28.7, 20.4, 17.4, 16.1, 13.6, 13.5, 13.1, 12.3, 12.1, 11.6, 11.5, 10.7.

HRMS (ESI) calcd for $\text{C}_{56}\text{H}_{60}\text{B}_2\text{F}_4\text{N}_4\text{Na}$ ($\text{M}+\text{Na}$) 907.4910, found 907.4002. $\Delta=0.9$ ppm.

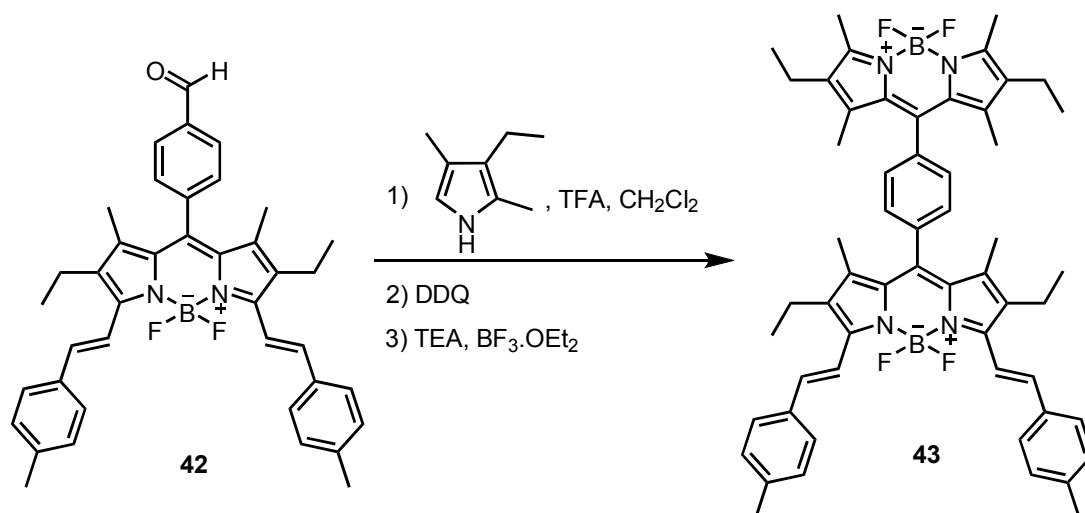


Figure 35. Synthesis of energy transfer cassette 43

2.2.4 Synthesis of 4,4-difluoro-8-phenyl-1,3,5,7-tetramethyl-2,6-diethyl-4-bora-3a,4a-diaza-s-indacene (44)

Benzoyl chloride (3.95 mmol, 556 mg) and 3-ethyl-2,4-dimethyl pyrrole (8.12 mmol, 1.0 g) were refluxed for 3 h in CH_2Cl_2 . The reaction was monitored by TLC (eluent CH_2Cl_2), after 3h, TEA (3 ml) and $\text{BF}_3\cdot\text{OEt}_2$ (3 ml) were added. Immediately after the addition of $\text{BF}_3\cdot\text{OEt}_2$ bright yellowish fluorescence was observed. Crude product washed three times with water, dried over Na_2SO_4 and concentrated in vacuo. Then crude product purified by silica gel column chromatography (eluent $\text{CH}_2\text{Cl}_2/\text{Hexane}(2:1)$). The orange fraction which has bright yellow fluorescence was collected. Orange solid (810 mg, 54 %).

^1H NMR (400 MHz, CDCl_3) δ 7.40-7.37 (m, 3H), 7.21-7.17 (m, 2H), 2.45 (s, 6H), 2.22 (q, $J=7.5$ Hz, 4H), 1.20 (s, 6H), 0.90 (t, $J=7.5$ Hz, 6H).

^{13}C NMR (100 MHz, CDCl_3) δ 153.7, 140.2, 138.4, 135.8, 132.7, 130.8, 128.9, 128.7, 128.3, 17.1, 14.5, 14.1, 12.5, 11.6.

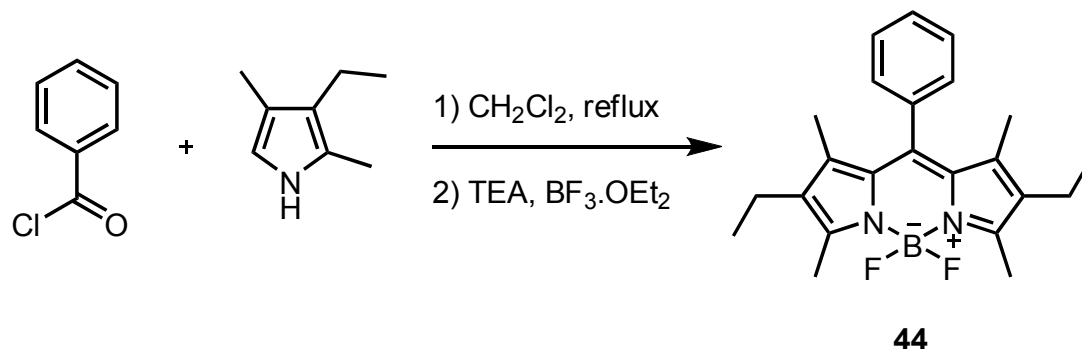


Figure 36. Synthesis of compound 44

2.2.5 Synthesis of 3,5-di{2-(4-methanoylphenyl)ethenyl}-4,4-difluoro-8-phenyl-1,3,5,7-tetramethyl-2,6-diethyl-4-bora-3a,4a-diaza-s-indacene (45)

Compound **44** (1.08 mmol, 410 mg) and Compound **40** (2.69 mmol, 479 mg) were refluxed in a mixture of benzene (50 mL), glacial acetic acid (0.5 mL), and piperidine (0.6 mL). Any water formed during the reaction was removed azeotropically by heating overnight in a Dean-Stark apparatus. Crude product was concentrated under vacuum. The crude product was purified by silica gel column chromatography (CHCl_3). The green fraction was collected and concentrated under vacuum. The collected fraction was stirred in a mixture of glacial acetic acid (20 mL) and water (2.5 mL) at 50°C overnight. The reaction was monitored by TLC. Additional amount of water (100 mL) was added and precipitation of product was observed. The mixture was filtered by suction and washed with water several times. The brown solid was dried. (550 mg, 90%).

^1H NMR (400 MHz, CDCl_3) δ 9.95 (s, 2H), 7.89-7.78 (m, 6H), 7.68 (d, $J=7.9$ Hz, 4H), 7.5-7.42 (m, 3H), 7.3-7.15 (m, 4H), 2.56 (q, $J=7.4$ Hz, 4H), 1.28 (s, 6H), 1.11 (t, $J=7.4$ Hz, 6H).

^{13}C NMR (100 MHz, CDCl_3) δ 191.5, 149.9, 143.2, 139.9, 136.0, 135.6, 134.6, 134.3, 133.8, 130.2, 129.3, 129.2, 128.4, 127.7, 123.1, 18.3, 14.0, 11.5.

HRMS (ESI) calcd for $\text{C}_{39}\text{H}_{35}\text{BF}_2\text{N}_2\text{O}_2\text{Na}$ ($\text{M}+\text{Na}$) 634.2693, found 634.2644. $\Delta=7.7$ ppm.

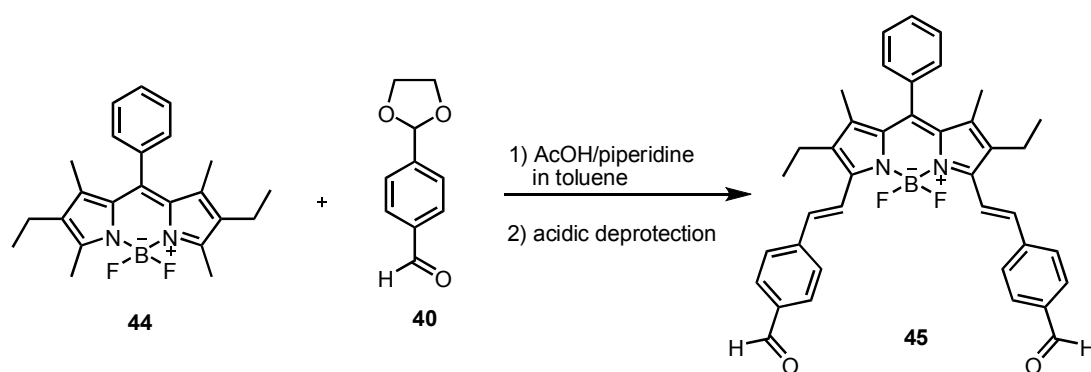


Figure 37. Synthesis of compound 45

2.2.6 Synthesis of 3,5-di[2-{4-(4,4-difluoro-1,3,5,7-tetramethyl-2,6-diethyl-4-bora-3a,4a-diaza-s-indacen-8-yl)phenyl}ethenyl]-4,4-difluoro-8-phenyl-1,3,5,7-tetramethyl-2,6-diethyl-4-bora-3a,4a-diaza-s-indacene (46)

A similar procedure, as in the synthesis of compound 41, was carried out. Compound 45 (0.18 mmol, 100 mg), 3-ethyl-2,4-dimethyl pyrrole (0.36 mmol, 44.3 mg), DDQ (0.36 mmol, 90 mg), TEA (3 mL), and $\text{BF}_3\cdot\text{OEt}_2$ (3 mL) were used in this reaction. Before the addition of DDQ, the mixture was stirred for two days rather than overnight stirring. The residue was purified by silica gel column chromatography (first CHCl_3 , then $\text{CHCl}_3/\text{Hexane}$ (2:1)). The purple fraction which has red fluorescence was collected. Purple solid (40 mg, 20%).

^1H NMR (400 MHz, CDCl_3) δ 7.84 (d, $J=16.7$ Hz, 2H), 7.68 (d, $J=7.9$ Hz, 4H), 7.49-7.42 (m, 4H), 7.32-7.22 (m, 7H), 2.6 (q, $J=7.4$ Hz, 4H), 2.46 (s, 12H), 2.23 (q, $J=7.5$ Hz, 8H), 1.29 (s, 18H), 1.15 (t, $J=7.4$ Hz, 6H), 0.91 (t, $J=7.5$ Hz, 12H).

^{13}C NMR (100 MHz, CDCl_3) δ 153.8, 150.2, 139.7, 138.4, 137.7, 136.1, 135.0, 134.3, 133.4, 132.8, 130.7, 129.2, 128.5, 127.8, 120.6, 118.9, 46.4, 29.7, 18.4, 17.7, 17.2, 15.4, 14.6, 14.1, 12.5, 11.5, 11.3.

MS (MALDI) calcd for $\text{C}_{71}\text{H}_{77}\text{B}_3\text{F}_6\text{N}_6$ 1160.639, found 1160.639.

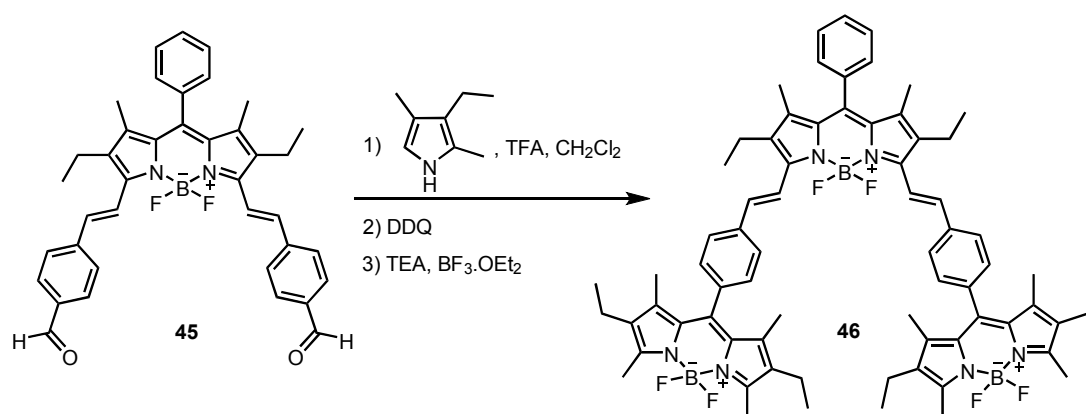


Figure 38. Synthesis of energy transfer cassette **46**

2.2.7 Synthesis of 4-[3,5-di{2-(4-methanoylphenyl)ethenyl}-4,4-difluoro-1,3,5,7-tetramethyl-2,6-diethyl-4-bora-3a,4a-diaza-s-indacen-8-yl]-benzaldehyde (**47**)

Compound **40** (2.43 mmol, 433 mg) and compound **41** (0.81 mmol, 366 mg) were refluxed in a mixture of benzene (50 mL), glacial acetic acid (0.5 mL), and piperidine (0.6 mL). Any water formed during the reaction was removed azeotropically by heating overnight in a Dean-Stark apparatus. Crude product was concentrated under vacuum. Without further purification, deprotection of acetal groups was carried. The crude product was stirred in a mixture of glacial acetic acid (20 mL) and water (2.5 mL) at 50°C for two days. The reaction was monitored by TLC. Additional amount of water (100 mL) was added and no precipitation was observed. Then the solution was neutralized with NaOH (5M) and precipitation of brown solid was observed. The mixture was filtered by suction and washed with water several times. The crude product was purified by silica gel column chromatography (CHCl_3). (275 mg, 53%).

^1H NMR (400 MHz, CDCl_3) δ 10.1 (s, 1H), 9.98 (s, 2H), 8.02 (d, $J=7.7$ Hz, 2H), 7.8-7.78 (m, 6H), 7.7 (d, $J=7.9$ Hz, 4H), 7.5 (d, $J=7.7$ Hz, 2H), 7.25 (d, $J=16.7$ Hz, 2H), 2.57 (q, $J=7.4$ Hz, 4H), 1.27 (s, 6H), 1.11 (t, $J=7.4$ Hz, 6H).

^{13}C NMR (100 MHz, CDCl_3) δ 190.5, 190.4, 149.5, 142.0, 140.9, 135.8, 135.1, 134.0, 133.9, 129.4, 129.2, 128.6, 126.8, 126.3, 121.8, 28.7, 17.3, 13.1, 12.9, 10.8.

HRMS (ESI) calcd for $\text{C}_{40}\text{H}_{35}\text{BF}_2\text{N}_2\text{O}_3\text{Na}$ ($\text{M}+\text{Na}$) 662.2643, found 662.2581. $\Delta=9.4$ ppm.

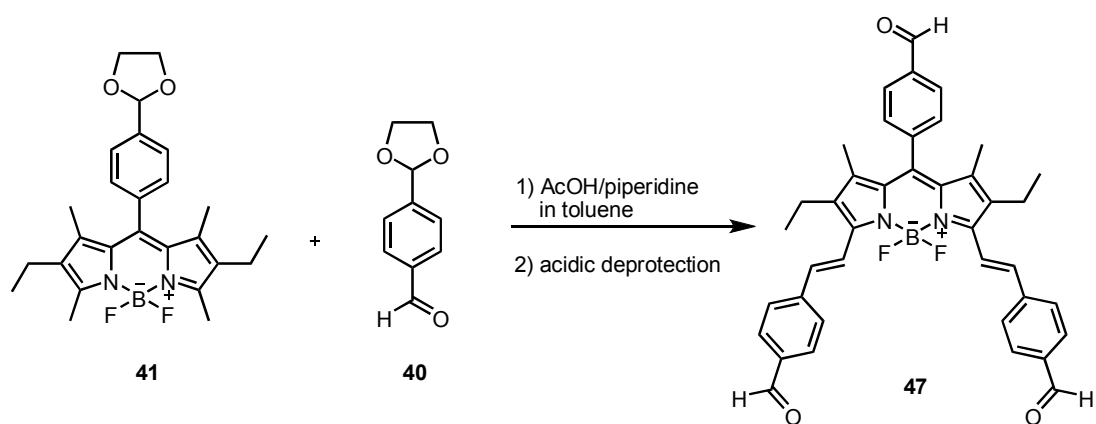


Figure 39. Synthesis of compound 47

2.2.8 Synthesis of 1-[3,5-di{2-(4-(4,4-difluoro-1,3,5,7-tetramethyl-2,6-diethyl-4-bora-3a,4a-diaza-s-indacen-8-yl)phenyl)ethenyl}-4,4-difluoro-1,3,5,7-tetramethyl-2,6-diethyl-4-bora-3a,4a-diaza-s-indacen-8-yl]-4-(4,4-difluoro-1,3,5,7-tetramethyl-2,6-diethyl-4-bora-3a,4a-diaza-s-indacen-8-yl)-benzene (48)

A similar procedure, which was applied in the synthesis of compound 41, was followed. Compound 47 (0.43 mmol, 275 mg), 3-ethyl-2,4-dimethyl pyrrole (2.66 mmol, 327 mg), DDQ (1.29 mmol, 317 mg), TEA (5 mL), and $\text{BF}_3\cdot\text{OEt}_2$ (5 mL) were used in this reaction. Before the addition of DDQ, the mixture was stirred for two days. The residue was purified by silica gel column chromatography (CHCl_3). Green solid (76 mg, 12%).

^1H NMR (400 MHz, CDCl_3) δ 7.86 (d, $J=16.7$ Hz, 2H), 7.69 (d, $J=7.9$ Hz, 4H), 7.55-7.49 (m, 4H), 7.32-7.25 (m, 6H), 2.63 (q, $J=7.4$ Hz, 4H), 2.51 (s, 6H), 2.46 (s, 12H), 2.32-2.19 (m, 12H), 1.51 (s, 6H), 1.45 (s, 6H), 1.31 (s, 12H), 1.17 (t, $J=7.4$ Hz, 6H), 0.99-0.88 (m, 18H).

^{13}C NMR (100 MHz, CDCl_3) δ 153.4, 152.9, 149.5, 138.7, 137.9, 137.3, 137.1, 136.8, 136.6, 135.8, 135.3, 134.5, 133.4, 132.4, 132.0, 131.8, 129.8, 129.7, 129.0, 128.0, 126.9, 119.5, 115.2, 112.6, 109.2, 101.4, 17.5, 16.1, 13.6, 13.1, 12.3, 12.2, 11.6, 11.5, 11.0.

HRMS (ESI) calcd for $\text{C}_{88}\text{H}_{98}\text{B}_4\text{F}_8\text{N}_8\text{Na}$ ($\text{M}+\text{Na}$) 1483.8140, found 1483.8055. $\Delta=5.7$ ppm.

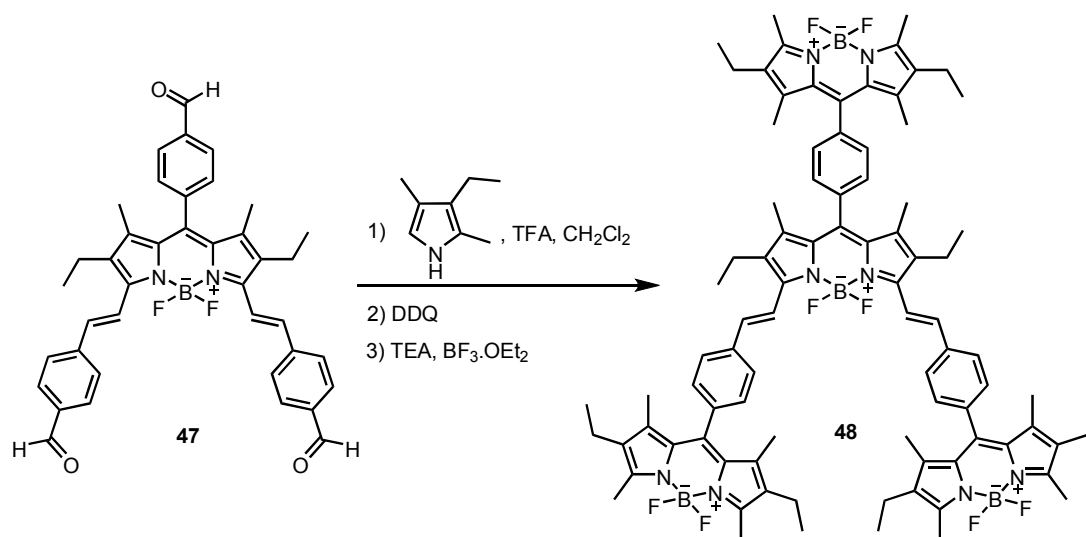


Figure 40. Synthesis of energy transfer cassette **48**

PART II

2.3.1 Synthesis of 4,4-difluoro-8-(4-carboxy)phenyl-1,3,5,7-tetramethyl-4-bora-3a,4a-diaza-*s*-indacene (49)

2,4-dimethyl pyrrole (21.98 mmol, 2.1 g) and 4-formylbenzoic acid (9.99 mmol, 1.5 g) were dissolved in 500 mL absolute CH₂Cl₂ (argon gas was bubbled through CH₂Cl₂ for 30 min) under argon atmosphere.. One drop of TFA was added and the solution was stirred at room temperature overnight. Then a solution of DDQ (9.99 mmol, 2.46 g) in 50 mL of absolute CH₂Cl₂ was added. Stirring was continued for 45 min followed by the addition of 5 mL of TEA and 5 mL of BF₃.OEt₂. The reaction was monitored by TLC (eluent CHCl₃/MeOH (97:3)). After stirring 2 h, the reaction mixture was washed three times with water and dried over Na₂SO₄. The solvent was evaporated and the residue was purified by silica gel column chromatography (CHCl₃/MeOH (97:3)). Red solid (1.0 g, 27%).

¹H NMR (400 MHz, DMSO-*d*₆ + CDCl₃) δ 8.07 (d, *J*=8.2 Hz, 2H), 7.45 (d, *J*=8.2 Hz, 2H), 6.1 (s, 2H), 2.4 (s, 6H), 1.3 (s, 6H).

¹³C NMR (100 MHz, CDCl₃) δ 167.2, 155.6, 143.0, 141.2, 138.9, 132.0, 130.8, 130.6, 128.6, 121.8, 14.7, 14.5.

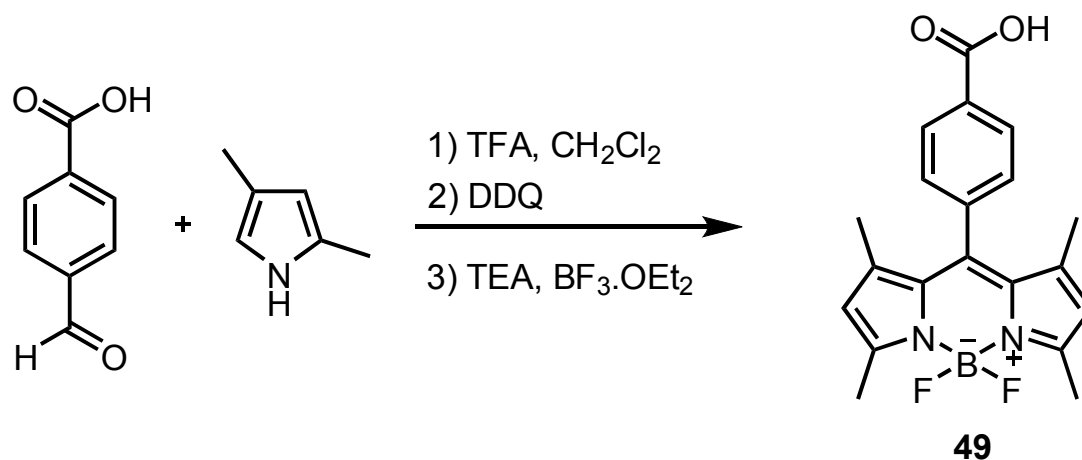


Figure 41. Synthesis of compound 49

2.3.2 Synthesis of 4,4-difluoro-8-(4-carboxy)phenyl -2,6-diiodo-1,3,5,7-tetramethyl-4-bora-3a,4a-diaza-s-indacene (50)

Compound **49** (1.41 mmol, 0.52 g) and iodine (3.53 mmol, 0.897 g) were added to a 500 mL round-bottomed flask and to this solution was added iodic acid (2.82 mmol, 0.497 g) dissolved in 2 mL of water. The reaction mixture was stirred at 60°C and was monitored by TLC using CHCl₃/MeOH (97:3). When TLC indicated that all the starting material had been consumed, saturated Na₂S₂O₃ solution in water was added and the product was extracted into CHCl₃. The solvent was evaporated under vacuo. Red solid (0.875 g, 100%).

¹H NMR (400 MHz, CDCl₃) δ 8.2 (d, *J*=8.0 Hz, 2H), 7.35 (d, *J*=8.2 Hz, 2H), 2.55 (s, 6H), 1.3 (s, 6H).

HRMS (ESI) calcd for C₂₀H₁₇BF₂I₂N₂O₂Na (M+Na) 641.9375, found 641.9351. Δ=3.7 ppm.

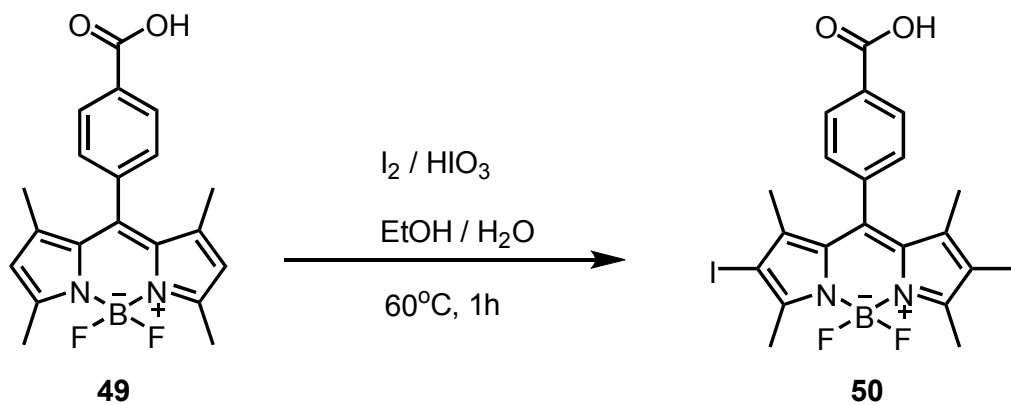


Figure 42. Synthesis of compound **50**

2.3.3 Synthesis of 4-[3,5-bis{4-(diphenylamino)styryl}-4,4-difluoro-1,3,5,7-tetramethyl-2,6-diiodo-4-bora-3a,4a-diaza-s-indacen-8-yl]-benzoic acid (52)

Compound **50** (0.645 mmol, 400 mg) and Compound **51** (2.58 mmol, 705 mg) were refluxed in a mixture of toluene (50 mL), glacial acetic acid (0.5 mL), and

piperidine (0.6 mL). Any water formed during the reaction was removed azeotropically by heating for 4 hours in a Dean-Stark apparatus. The reaction was monitored by TLC (eluent CHCl₃/MeOH (93:7)). Crude product was concentrated with the evaporation of reaction solvent. The crude product was purified by silica gel column chromatography (CHCl₃/MeOH (93:7)). Purple-black solid (620 mg, 85%).

¹H NMR (400 MHz, CDCl₃) δ 8.19 (d, *J*=8 Hz, 2H), 8.07 (d, *J*=16.5 Hz, 2H), 7.51 (d, *J*=16.5 Hz, 2H), 7.44 (d, *J*=8.5 Hz, 4H), 7.38 (d, *J*=8 Hz, 2H), 7.25-7.2 (m, 8H), 7.06 (d, *J*=7.5 Hz, 8H), 7.04-6.95 (m, 8H), 1.2 (s, 6H).

¹³C NMR (100 MHz, CDCl₃) δ 165.7, 149.1, 147.1, 145.1, 139.4, 138.6, 136.0, 132.4, 131.1, 130.3, 129.4, 128.9, 125.1, 123.7, 122.5, 116.7, 14.4.

HRMS (ESI) calcd for C₅₈H₄₃BF₂I₂N₄O₂Na (M+Na) 1152.1471, found 1152.1416. Δ=4.8 ppm.

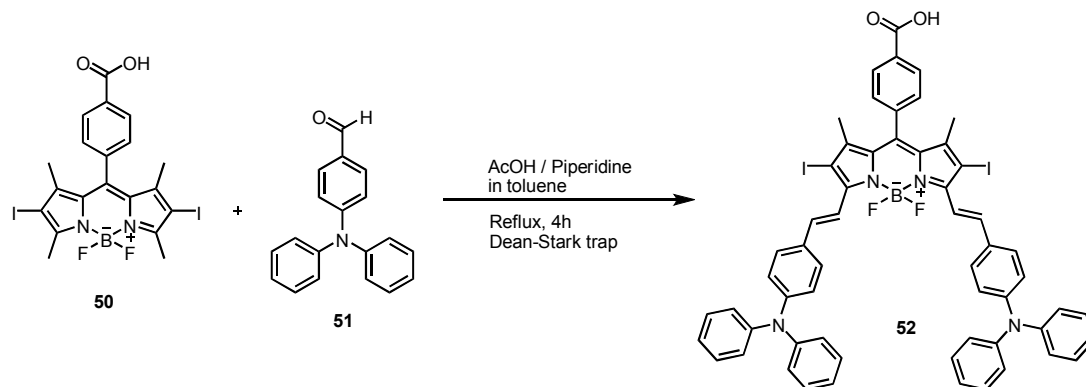


Figure 43. Synthesis of compound 52

2.3.4 Synthesis of 4,4-difluoro-8-{4-(prop-2-ynyloxy)phenyl}-2,6-diethyl-1,3,5,7-tetramethyl-4-bora-3a,4a-diaza-s-indacene (54)

3-ethyl-2,4-dimethyl pyrrole (9.63 mmol, 1.19 g) and compound 53 (4.37 mmol, 0.7 g) were dissolved in 500 mL absolute CH₂Cl₂ (argon gas was bubbled through CH₂Cl₂ for 30 min) under argon atmosphere.. One drop of TFA was added

and the solution was stirred at room temperature overnight. Then a solution of DDQ (4.37 mmol, 1.08 g) in 50 mL of absolute CH_2Cl_2 was added. Stirring was continued for 45 min followed by the addition of 6 mL of TEA and 6 mL of $\text{BF}_3 \cdot \text{OEt}_2$. The reaction was monitored by TLC (eluent CHCl_3). After stirring 3 h, the reaction mixture was washed three times with water and dried over Na_2SO_4 . The solvent was evaporated and the residue was purified by silica gel column chromatography (first CHCl_3 , then $\text{CHCl}_3/\text{Hexane}$ (2:1)). Red-orange solid (0.57 g, 30%).

^1H NMR (400 MHz, CDCl_3) δ 7.21 (d, $J=8.8$ Hz, 2H), 7.10 (d, $J=8.8$ Hz, 2H), 4.78 (s, 2H), 2.55 (s, 6H), 2.32 (q, $J=7.5$ Hz, 4H), 1.57 (s, 1H), 1.33 (s, 6H), 1.0 (d, $J=7.5$ Hz, 6H).

^{13}C NMR (100 MHz, CDCl_3) δ 157.9, 153.6, 139.9, 138.4, 132.7, 131.1, 129.5, 128.9, 115.5, 78.1, 75.8, 56.0, 17.1, 14.6, 12.5, 11.8.

HRMS (ESI) calcd for $\text{C}_{26}\text{H}_{29}\text{BF}_2\text{N}_2\text{ONa}$ ($\text{M}+\text{Na}$) 456.2275, found 456.2246. $\Delta=6.4$ ppm.

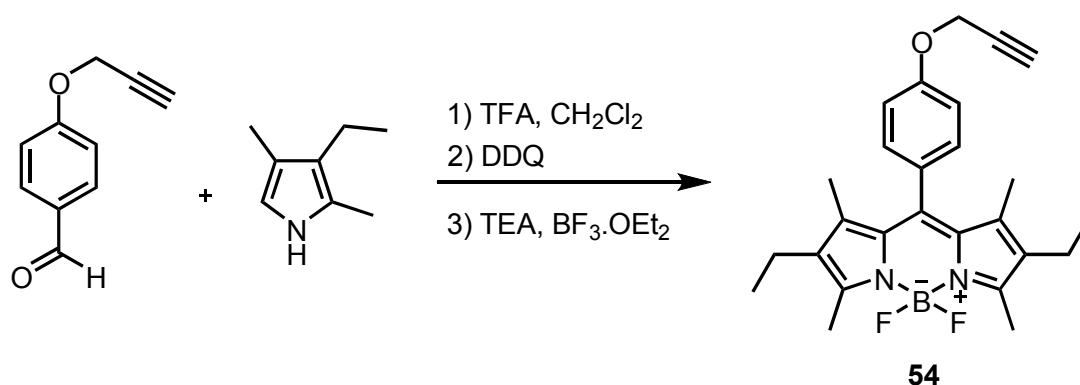


Figure 44. Synthesis of compound 54

2.3.5 Synthesis of compound 55

Compound 52 (0.194 mmol, 219 mg), $\text{Pd}(\text{PhCN})_2\text{Cl}_2$ (0.0194 mmol, 7.4 mg), and CuI (0.0155 mmol, 3 mg) were dissolved in 5 mL of distilled THF. Then argon gas was bubbled through the mixture for 10 min which was followed by

addition of $\text{P}(\text{t-Bu})_3$ (0.0387 mmol, 40 μL of a 1.0 M solution in toluene), and $\text{H}_2\text{N}(\text{i-Pr})_2$ (0.484 mol, 70 μL) via syringe. Finally compound 54 (0.484 mmol, 210 mg) was added, reaction flask was filled with argon gas and the mixture was stirred at 30°C for two days. The reaction was monitored by TLC (eluent $\text{CHCl}_3/\text{MeOH}$ (97:3)). Upon the completion of reaction, THF was evaporated and crude product was purified by silica gel column chromatography ($\text{CHCl}_3/\text{MeOH}$ (97:3)). Several preparative TLC purifications were applied. Red solid (30 mg, 9%).

^1H NMR (400 MHz, CDCl_3) δ 8.17 (d, $J=8.0$ Hz, 2H), 8.16 (d, $J=16.2$ Hz, 2H), 7.53 (d, $J=16.2$ Hz, 2H), 7.40 (d, $J=8.6$ Hz, 4H), 7.34 (d, $J=8.0$ Hz, 2H), 7.22-7.15 (m, 8H), 7.07-6.96 (m, 20H), 6.93 (d, $J=8.6$ Hz, 4H), 4.98 (s, 4H), 2.44 (s, 12H), 2.19 (q, $J=7.5$ Hz, 8H), 1.18 (s, 6H), 1.13 (s, 12H), 0.98 (t, $J=7.5$ Hz, 12H).

^{13}C NMR (100 MHz, CDCl_3) δ 158.0, 153.6, 152.9, 149.3, 147.0, 144.9, 139.9, 139.1, 138.4, 132.7, 131.1, 130.1, 129.5, 129.0, 128.7, 125.2, 123.8, 122.1, 115.5, 92.5, 82.1, 56.9, 17.1, 14.6, 13.3, 12.5, 11.8.

MS (MALDI) calcd for $\text{C}_{110}\text{H}_{98}\text{B}_3\text{F}_6\text{N}_8\text{O}_4$ (M-H) 1741.796, found 1741.178.

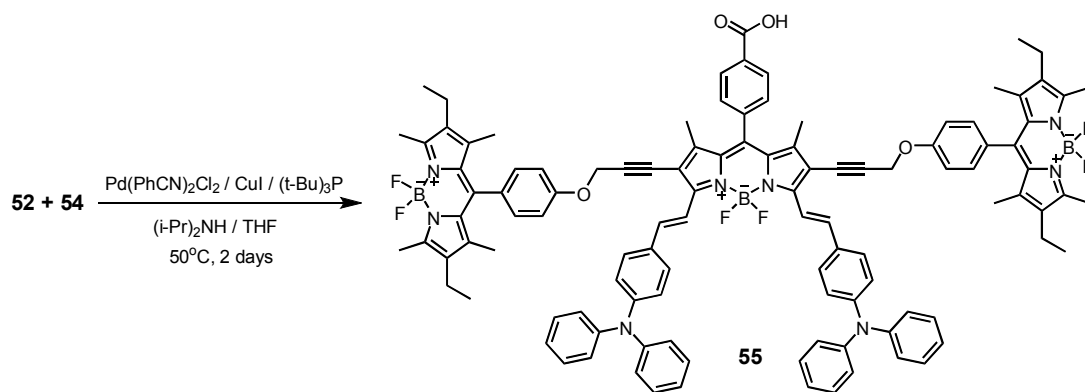


Figure 45. Synthesis of compound 55

CHAPTER 3

RESULTS AND DISCUSSIONS

3.1 Synthesis and Spectroscopic Properties of Light-Harvesting Cassettes 43, 46, and 48

Design and synthesis of supramolecular systems which can function as light-harvesting system have attracted much attention due to its importance especially in photochemical conversion of solar energy. Light-harvesting arrays collect the light at different wavelengths by antenna (donor molecules) and emit at one wavelength. In other words these systems concentrate the energy in one molecular unit which is referred as acceptor or core. As mentioned, energy transfer can take place through either Dexter mechanism (through-bond) or Förster mechanism (through-space). For efficient energy transfer in through-space mechanism, it is essential to choose proper chromophores, which have spectral overlap between donor and acceptor parts and are close enough in terms of distance for energy transfer. BODIPYs are bright chromophores with high quantum yields and large extinction coefficients. Structural modifications of BODIPYs allow us to generate dyes absorbing in visible region from green to red. There are many examples of energy transfer cassettes in which BODIPY is used as an energy donor component. However, there are few of them as an acceptor component. In this work, we designed and synthesized energy transfer cassettes with an increasing number of energy donor component (Figure 46). These cassettes are entirely composed of BODIPY derivatives.

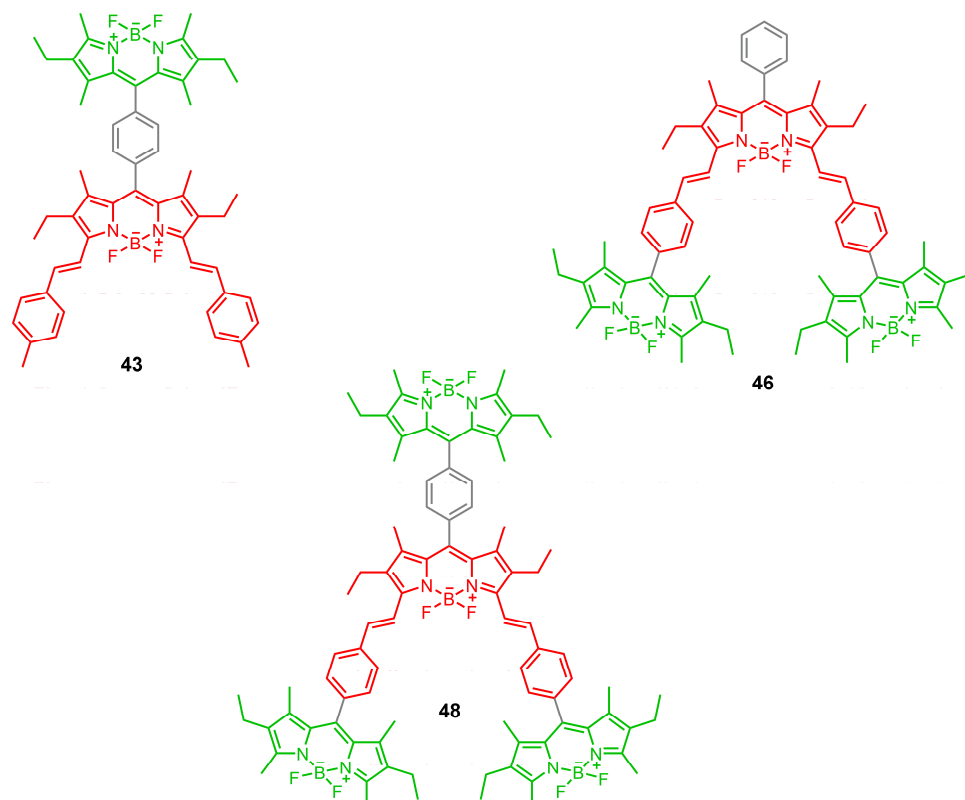


Figure 46. The structures of cassettes **43**, **46**, and **48**

First, we synthesized the compound **40** by protecting one of the carbonyl groups of terephthalaldehyde with ethylene glycol. So we ensure that only one aldehyde group yields BODIPY. Compound **40** was then used to obtain **41** in the usual manner in the synthesis of a BODIPY dye, reacting with 3-ethyl-2,4-dimethylpyrrole in the presence of TFA and DDQ at room temperature, followed by the addition of $\text{BF}_3 \cdot \text{Et}_2\text{O}$ and Et_3N . Methyl groups neighboring the BF_2 bridges are slightly acidic and the condensation of these groups with aldehyde results in distyryl BODIPY derivative which has longer wavelength absorption due to the extension of conjugation.¹⁰⁰ Thus we targeted to use it as energy acceptor component. Condensation of **41** with p-tolualdehyde and then acidic deprotection of acetal group in crude product gave distyryl BODIPY derivative **42**. Finally, the aldehyde group formed after acidic deprotection was reacted with 3-ethyl-2,4-dimethylpyrrole to obtain cassette **43** which is composed of one energy donor BODIPY dye (green part) and one energy acceptor distyryl BODIPY derivative (red part). Cassettes **46** and **48** were synthesized by using same synthetic strategy. Compound **40** was used for condensation reactions so that aldehyde groups could be placed in desired positions

before final steps giving **46** and **48**. Cassette **46** has two energy donor BODIPY dyes at the bottom positions and cassette **48** has three of them. The structures of cassettes were confirmed by ^1H NMR, ^{13}C NMR and mass spectroscopy (Appendix A and B).

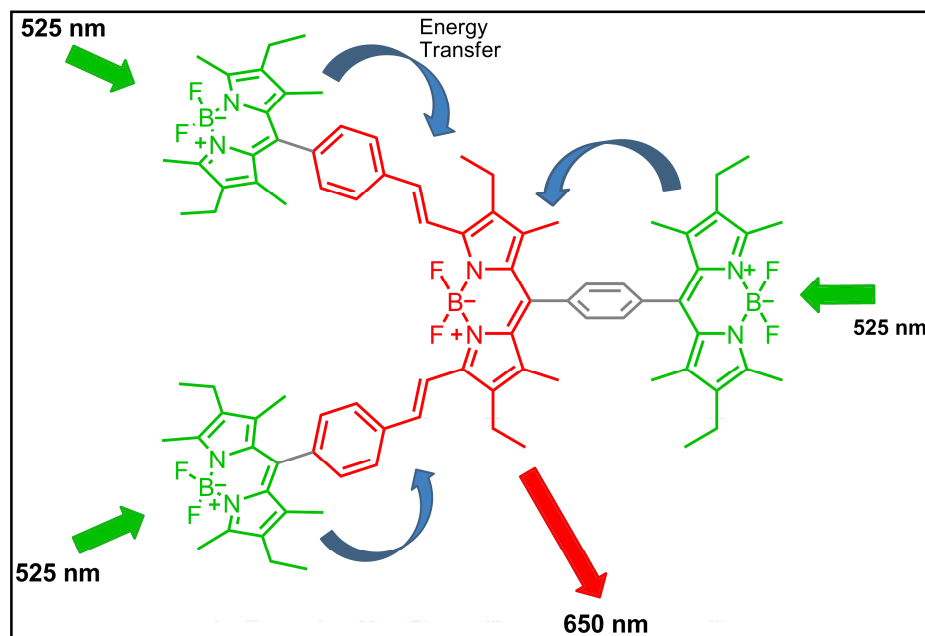


Figure 47. Schematic representation of energy transfer in cassette **48**

A schematic representation of whole energy transfer process achieved in this work is shown above in Figure 47. The absorption spectra of all three cassettes prove the presence of two noninteracting chromophores in each cassette with no-ground state interactions (Figure 48). Methyl groups on 1 and 7 positions of BODIPY makes the phenyl ring perpendicular to BODIPY plane (the gray fragments in Figure 46). Therefore conjugation is cut beyond these points. The absorption band around 525 nm belongs to BODIPY fragments (green, donor chromophore) and the band around 650 nm arises from distyryl BODIPY fragment (red, acceptor chromophore). The absorbance of compounds **43**, **46**, and **48** was normalized to 0.1 at 650 nm, the λ_{max} of distyryl BODIPY core, so that we would be able to observe the change in emission spectrum of acceptor chromophore due to energy transfer. The absorbance around 525 nm increases with increasing number of donor chromophores, which correlates well with the structures of cassettes as designed. The fact is further justified with the extinction coefficient values at λ_{max} of

donor chromophore which was found out to be $72073 \text{ M}^{-1}\text{cm}^{-1}$ (527 nm), $114880 \text{ M}^{-1}\text{cm}^{-1}$ (528 nm), $191746 \text{ M}^{-1}\text{cm}^{-1}$ (529 nm) for **43**, **46**, and **48** respectively (Table 1).

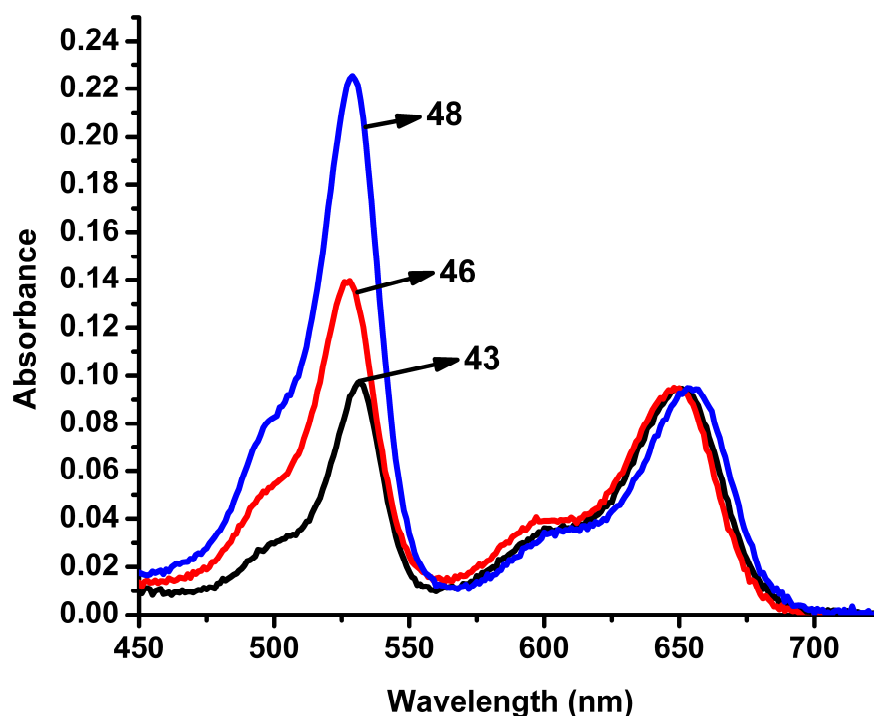


Figure 48. Absorbance spectra of compounds **43**, **46**, and **48** at equal absorbances at 650 nm in CHCl_3

The emission spectra of compounds **43**, **46**, and **48** are shown in Figure 49. Blue colored line is emission spectrum of a single donor chromophore which is not incorporated to the cassette. It shows an intense emission peak at 540 nm. However, it is not observed in cassettes **43**, **46** and **48**. There is very little residual emission corresponding to donor BODIPY chromophores. Therefore we estimate the efficiency of energy transfer as 99%. The spectral overlap between the donor emission peak and the absorption peak of the distyryl BODIPY chromophore is apparent when Figures 48 and 49 are inspected carefully. When compounds **42**, **45** and **47** (the distyryl compounds before the incorporation donor components) are excited at 525 nm, they obviously emit poorly because of small extinction coefficients at this wavelength. Photoexcitation of cassettes **43**, **46** and **48** at 525 nm, from donor chromophores, results in the strong emission from acceptor at around

665 nm. The intensity of emission peaks increases with the number of donor chromophores. To assess the magnitude of antenna effect in these cassettes, we compared the emission intensities of acceptor chromophore with and without donor chromophores at 665 nm upon excitation at 525 nm. The increase in cassette **43**, with one donor chromophore, is 30-fold. Another evidence for energy transfer is the quantum yield values of chromophores. The quantum yield of BODIPY dye alone is 0.61. In cassettes **43**, **46** and **48**, quantum yields were found 0.24, 0.24, and 0.22 ($\lambda_{\text{ex}}=525$ nm) which are very close to those of acceptor chromophore without donor fragments (Table 1). This is the verification of quenching of emission of donor BODIPY chromophores. Furthermore quantum yields did not vary significantly whether the cassettes were excited at the donor's ($\lambda_{\text{ex}}=525$ nm) or acceptor's absorbance ($\lambda_{\text{ex}}=645$ nm). The absence of quantum yield dependence indicates almost complete energy transfer from the donor to the acceptor.

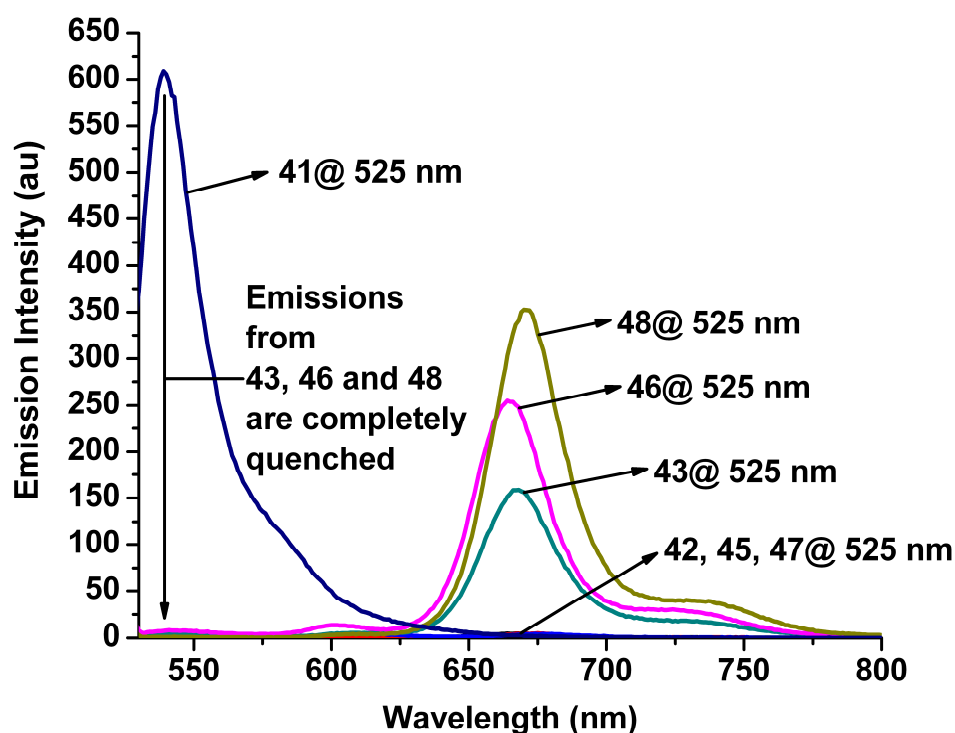


Figure 49. The emission spectra of compounds in CHCl_3 ($\lambda_{\text{exc}} = 525$ nm)

In the fluorescence excitation spectra of all cassettes, all absorption bands of donor and acceptor chromophores were observed (Figure 50). The absorption spectra and excitation spectra matched well. This indicated high yield of singlet-state energy transfer in cassettes.

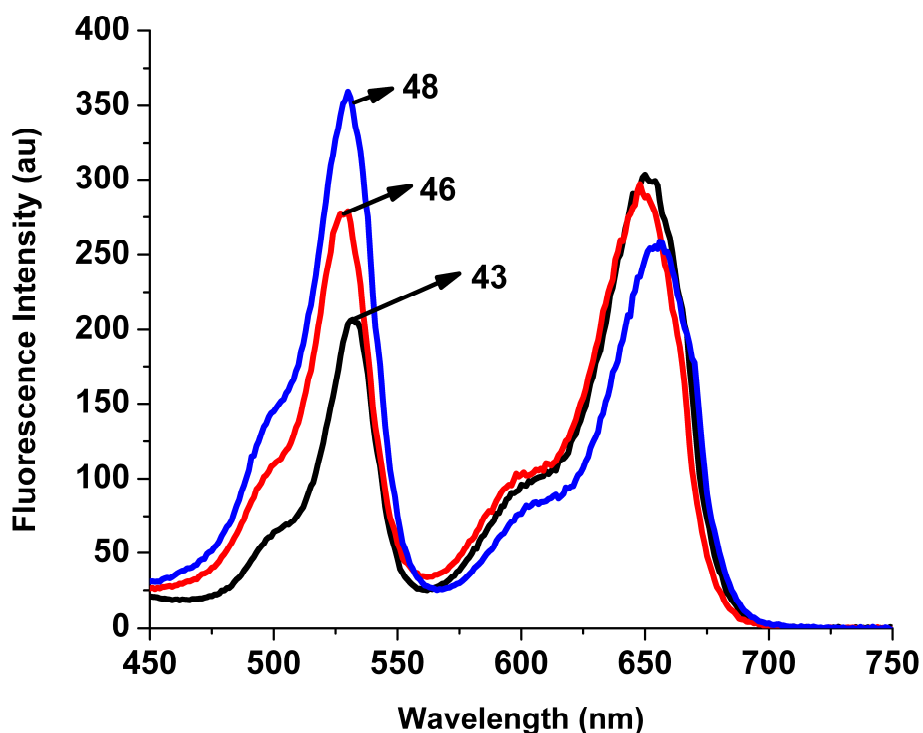


Figure 50. Excitation spectra of compounds 43, 46, and 48 in CHCl_3

Table 1. Photophysical Properties of Compounds in CHCl_3

Compound	$\epsilon (\lambda_{\text{max}})/(\text{M}^{-1}\text{cm}^{-1})$ (nm)	$\lambda_{\text{em}}/\text{nm}$	Φ_{F}	
			$\lambda_{\text{ex}}=525$ nm	$\lambda_{\text{ex}}=645$ nm
41	79922 (528)	539	0.61	-
42	81374 (649)	667	0.18	-
45	61830 (656)	675	0.18	-
47	62237 (660)	676	0.21	-
43	72073 (527), 71128 (651)	668	0.24	0.33
46	114880 (528), 77478 (649)	664	0.24	0.33
48	191746 (529), 80497 (654)	670	0.22	0.31

3.2 Novel Light-Harvesting Photosensitizer

It has always been a hot topic to convert solar energy into the form we can use. Design and synthesis of DSSCs are great of interest since their invention in 1991 by Gratzel. Low cost production and being less harmful to environment differ DSSCs from other types of solar cells. Up to now, lots of organic dyes, free of ruthenium metal, have been synthesized as photosensitizers and some high conversion efficiency requirements are defined. First of all, the dye compound must interact well with TiO₂ surface via proper functional groups. Presence of electron donor groups increases conversion efficiency. Absorption properties of dye molecule are important that it should harvest the sunlight as much as it can. Finally, aggregation of dye molecules due to π - π interactions, which significantly effects conversion efficiency, should be prevented.

BODIPY dyes have remarkable properties such as high molar extinction coefficient, stability, and good solubility. These properties make BODIPY dyes promising material in dye-sensitized solar cells. However, there are few examples of them in the literature. Taking these facts into account, we targeted bichromophoric light-harvesting dendritic molecule, **55**, as photosensitizer (Figure 51). We preferred to use carboxyl group to attach the molecule to TiO₂ surface. Based on theoretical calculations, the meso position of BODIPY, where carboxyl group is placed, has high electron density in LUMO level. So the electron flow within the molecule should occur towards this point. As electron donor groups, triphenyl amine moieties were used which are fairly electron rich compounds. The more electron is injected into TiO₂ surface, the more electric current is formed in external circuit. Therefore it results in a higher conversion efficiency. It should be noted that after the incorporation of triphenyl amine groups we obtain a distyryl BODIPY derivative (red). The absorption band of molecule is expected to shift into near-IR region due to extension of conjugation. To harvest the sunlight over a wide range, we attached another BODIPY chromophore (blue) on 2 and 6 positions as energy donor fragments. We intended to obtain energy transfer from side BODIPY chromophores to the distyryl BODIPY core. Therefore photosensitization would be facilitated not only at the absorption wavelength of core but also that of donor chromophore via

energy transfer. Triphenyl amine groups are capable of preventing the aggregation of dye molecules. Additionally donor BODIPY fragments (blue) were presumed to prevent aggregation because they are not on the same plane with core. We synthesized compound **55** and studied the energy transfer in this work.

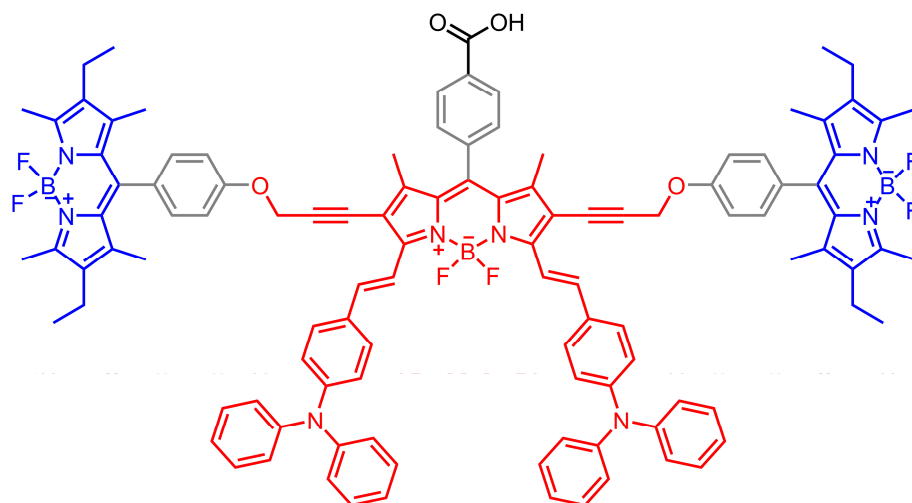


Figure 51. The structure of light-harvesting photosensitizer **55**

We synthesized the compound **49** from 4-formylbenzoic acid in the usual manner of BODIPY synthesis. Iodination of **49** in the presence of excess iodine resulted in formation of di-iodo BODIPY derivative **50** with excellent yield. The formylation of triphenyl amine was achieved by Viels-Meier reaction yielding compound **51**. The condensation of compound **51** with di-iodo BODIPY derivative **50** was carried out which yielded the core component of final product. Finally the distyryl core component with two iodine atoms was reacted with compound **54** containing a terminal alkyne in the presence of palladium catalyst via Sonogashira coupling reaction. The structures of compounds were confirmed by ^1H NMR, ^{13}C NMR and mass spectroscopy (Appendix A and B).

The absorption spectra of compounds **52**, **54**, and **55** at equal absorbance values at 527 nm (for **54** and **55**) and at 725 nm (**52** and **55**) are shown in Figure 52. The spectrum of **55** is equal to the sum of two spectra as expected. The extinction coefficient of **55** is $57668\text{ M}^{-1}\text{cm}^{-1}$ at 735 nm and $107884\text{ M}^{-1}\text{cm}^{-1}$ at 527 nm. The

latter value indicates presence of two donor BODIPY chromophores (blue fragments in Figure 51).

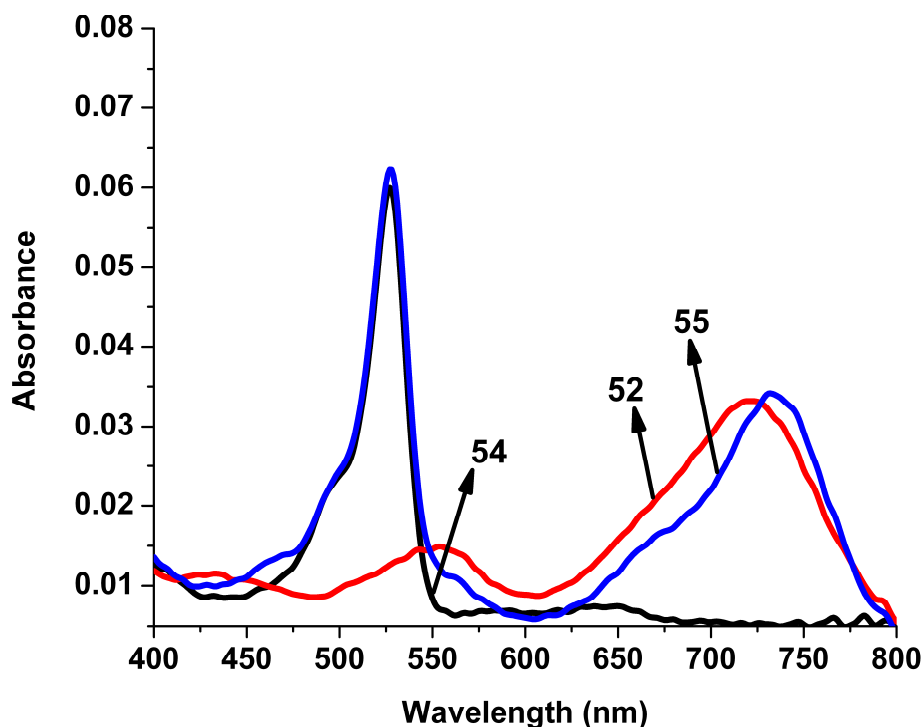


Figure 52. Absorption spectra of compounds **52**, **54**, and **55** in CHCl_3

The emission spectra of **52**, **54**, and **55** are shown in Figure 53. The emission of antenna BODIPY donors at 540 nm is not observed in spectrum of **55**. Since we normalized the absorbance values of **54** and **55**, the great difference in emission at 540 nm is the indication of efficient energy transfer from BODIPY donors (blue fragments) to the core (red fragment). The quantum yield of emission for compound **54** was determined 0.75, whereas that of BODIPY donor units in compound **55** was 0.05 due to the antenna effect. The efficiency of energy transfer is 96%. As a consequence, the effect of energy transfer was observed as enhancement of core emission (inset spectrum in Figure 53). Core fragment itself, compound **52**, emits poorly when excited at 520 nm. However, upon the excitation of light-harvesting molecule **55** at 520 nm resulted in enhanced emission peak centered at 785 nm. The increase in emission intensity at 785 nm is calculated as 13-fold. If we consider the

emission intensity upon direct excitation of core at 730 nm, the emission intensity of core fragment at 785 nm increases significantly due to the energy transfer (inset spectrum in Figure 53).

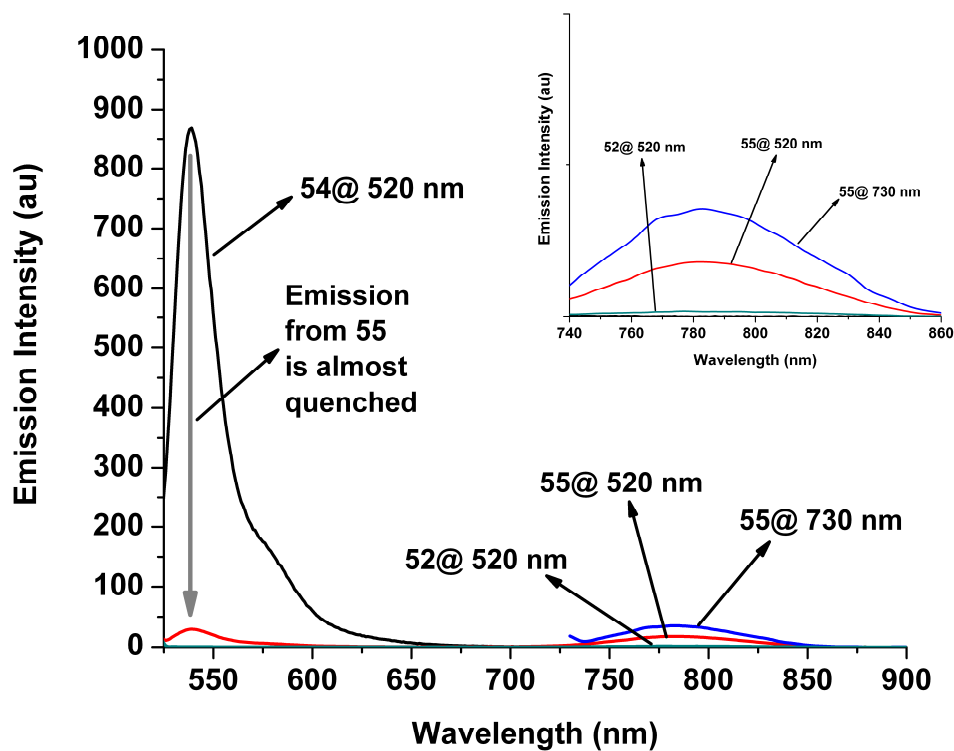


Figure 53. The emission spectra of compounds **52**, **54**, and **55** in CHCl_3 . Inset: expanded spectrum in the region of core emission

Table 2. Photophysical Properties of Compounds **52**, **54**, and **55** in CHCl_3

Compound	$\epsilon (\lambda_{\text{max}})/(\text{M}^{-1}\text{cm}^{-1})$ (nm)	$\lambda_{\text{em}}/\text{nm}$	$\Phi_{\text{bodipy}} (\lambda_{\text{ex}} = 520 \text{ nm})$
52	68885 (726)	785	-
54	81193 (527)	540	0.75
55	57668 (735), 107884 (527)	785	0.05

CHAPTER 4

CONCLUSION

Novel BODIPY-based bichromophoric light-harvesting systems have successfully been designed and synthesized. Efficient fluorescence resonance energy transfer (FRET) has been demonstrated between BODIPY donor chromophore and acceptor distyryl BODIPY derivatives.

In the first part of the thesis, a series of energy transfer cassettes were synthesized. The effect of donor chromophore number was investigated. Location of spectral and spatial concentration of UV-Vis radiation at the core of cassettes was achieved. The compounds also exhibited large pseudo-Stokes' shift. The efficiency of energy transfer was 99%.

In the second part of the thesis, due to the results obtained in first part, we introduced a light-harvesting photosensitizer **55**. Efficient energy transfer (96%) was demonstrated. We presume that light-harvesting BODIPY dye **55** is a promising photosensitizer for dye-sensitized solar cells. Bichromophoric design of the molecule provides absorption of light from 400 nm to 800 nm which spans visible spectrum and near-IR region due to the extension of conjugation. Sunlight would be harvested efficiently and photosensitizer **55** is expected to show high solar energy to electrical power conversion efficiency. With remarkable photophysical properties, BODIPY dyes are currently being investigated extensively for DSSC purposes.

REFERENCES

1. Lehn, J.M. *Supramolecular Chemistry: Concepts and Perspectives*, VCH, Weinheim, **1995**.
2. Balzani, V.; Scandola, F. *Supramolecular Photochemistry*, Horwood, Chichester, **1991**.
3. Lindsey, J.S. *New J. Chem.*, **1991**, *15*, 153.
4. Whitesides, G.M.; Mathias, J.P.; Seto, C.T. *Science.*, **1991**, *254*, 1312.
5. Lehn, J.M. in *Perspectives in Coordination Chemistry*, VCH, Basel, **1992**, p. 447.
6. Lehn, J.M. *Angew. Chem. Int. Ed. Engl.*, **1988**, *27*, 89.
7. Philip, D.; Stoddart, J.F. *Angew. Chem. Int. Ed.*, **1996**, *35*, 1155.
8. Lehn, J.M.; Ball, P. in *The New Chemistry*, ed. Hall, N. (Cambridge Univ. Press, Cambridge, U.K.), **1995**, pp. 300-351.
9. Ziener, U.; Lehn, J.M.; Mourran, A.; Möller, M. *Chem. Eur. J.*, **2002**, *8*, 951.
10. Rebek, J. *Chem. Commun.*, **2000**, 637.
11. Leung, K.C.-F.; Nguyen, T.D.; Stoddart, J.F.; Zink, J.I. *Chem. Matter.*, **2006**, *18*, 5919.
12. Feringa, B.L. *J. Org. Chem.*, **2007**, *72*, 6635.
13. Nijhuis, C. A.; Huskens, J.; Reinhoudt, D. N. *J. Am. Chem. Soc.*, **2004**, *126*, 12266.
14. Credo, G. M.; Boal, A. K.; Das, K.; Galow, T. H.; Rotello, V. M.; Feldheim, D. L.; Gorman, C. B. *J. Am. Chem. Soc.*, **2002**, *124*, 9036.
15. Sugou, K.; Sasaki, K.; Kitajima, K.; Iwaki, T.; Kuroda, Y. *J. Am. Chem. Soc.*, **2002**, *124*, 1182.
16. McQuade, D. T.; Hegedus, A. H.; Swager, T. M. *J. Am. Chem. Soc.*, **2000**, *122*, 12389.
17. Kim, S.; Choi, H.; Kim, D.; Song, K.; Kang, S.O.; Ko, J. *Tetrahedron*, **2007**, *63*, 9206.
18. Lo, S.-C.; Burn, P. L. *Chem. Rev.*, **2007**, *107*, 1097.
19. Pischel, U. *Angew. Chem. Int. Ed.*, **2007**, *46*, 4026.

20. Credi, A. *Angew. Chem. Int. Ed.*, **2007**, *46*, 5472.
21. Paul, D.; Suzumura, A.; Sugimoto, H.; Teraoka, J.; Shinoda, S.; Tsukube, H. *J. Am. Chem. Soc.*, **2003**, *125*, 11478.
22. Pauvert, M.; Laine, P.; Jonas, M.; Wiest, O. *J. Org. Chem.*, **2004**, *69*, 543.
23. Yukruk, F.; Dogan, A. L.; Canpinar, H.; Guc, D.; Akkaya, E. U. *Org. Lett.*, **2005**, *7*, 2885.
24. Regehly, M.; Greish, K.; Rancan, F.; Maeda, H.; Bohm, F.; Roder, B. *Bioconjugate Chem.*, **2007**, *18*, 494.
25. Stokes, G.G. *Phil. Trans. R. Soc. London*, **1852**, *142*, 463.
26. Kasha, M. *Disc. Faraday Soc.*, **1950**, *9*, 14.
27. Olmsted, J. *J. Phys. Chem.*, **1979**, *83*, 2581.
28. Karstens, T.; Kobs, K. *J. Phys. Chem.*, **1980**, *84*, 1871.
29. Magde, D.; Brannon, J.H.; Cremers, T.L.; Olmsted, J. *J. Phys. Chem.*, **1979**, *83*, 696.
30. Umberger, J.Q.; Lamer, V.K. *J. Am. Chem. Soc.*, **1945**, *67*, 1099.
31. Melhuish, W.H. *J. Phys. Chem.*, **1961**, *65*, 229.
32. Ross, A.H.; Daou, M.-C.; McKinnon, C.A.; Condon, P.J.; Lachyankar, M.B.; Stephens, R.M.; Kaplan, D.R.; Wolf, D.E. *J. Cell Biol.*, **1996**, *132*, 945.
33. Metzker, M.L. WO Patent WO/2003/066812, **2003**.
34. Treibs, A.; Kreuzer, F.-H. *Justus Liebigs Ann. Chem.*, **1968**, *718*, 208.
35. Karolin, J.; Johansson, L.B.-A.; Strandberg, L.; Ny, T. *J. Am. Chem. Soc.*, **1994**, *116*, 7801.
36. Haugland, R.P. *Handbook of Fluorescent Probes and Research Chemicals*, 6th ed.; Molecular Probes: Eugene, OR, **1996**.
37. Tan, K.; Jaquinod, L.; Paolesse, R.; Nardis, S.; Di Natale, C.; Di Carlo, A.; Prodi, L.; Montalti, M.; Zaccheroni, N.; Smith, K.M. *Tetrahedron*, **2004**, *60*, 1099.
38. Coskun, A.; Yilmaz, M.D.; Akkaya, E. U. *Org. Lett.*, **2007**, *9*, 607.
39. Coskun, A.; Deniz, E.; Akkaya, E. U. *Tetrahedron. Lett.*, **2007**, *48*, 5359.
40. Coskun, A.; Akkaya, E. U. *J. Am. Chem. Soc.*, **2005**, *127*, 10464.
41. Yuan, M.; Li, Y.; Li, J.; Li, C.; Liu, X.; Lv, J.; Xu, J.; Liu, H.; Wang, S.; Zhu, D. *Org. Lett.*, **2007**, *9*, 2313.

42. Qi, X.; Jun, E. J.; Xu, L.; Kim, S.-J.; Joong Hong, J. S.; Yoon, Y. J.; Yoon, J. *J. Org. Chem.*, **2006**, *71*, 2881.
43. Yogo, T.; Urano, Y.; Ishitsuka, Y.; Maniwa, F.; Nagano, T. *J. Am. Chem. Soc.*, **2005**, *127*, 12162.
44. Atilgan, S.; Ekmekci, Z.; Dogan, A.L.; Guc, D.; Akkaya, E.U. *Chem. Commun.*, **2006**, 4398.
45. Goze, C.; Ulrich, G.; Ziesel, R. *Org. Lett.*, **2006**, *8*, 4445.
46. Coskun, A.; Deniz, E.; Akkaya, E. U. *Org. Lett.*, **2005**, *7*, 5187.
47. Li, L.; Han, J.; Nguyen, B.; Burgess, K. *J. Org. Chem.*, **2008**, *73*, 1963.
48. Thivierge, C.; Bandichhor, R.; Burgess, K. *Org. Lett.*, **2007**, *9*, 2135.
49. Camerel, F.; Bonardi, L.; Schmutz, M.; Ziesel, R. *J. Am. Chem. Soc.*, **2006**, *128*, 4548.
50. Alpha, B.; Balzani, V.; Lehn, J.M.; Perathoner, S.; Sabbatini, N. *Angew. Chem. Int. Ed.*, **1987**, *26*, 1266.
51. Hu, X.; Damjanovic, A.; Ritz, T.; Schulten, K. *Proc. Natl. Acad. Sci. USA*, **1998**, *95*, 5935.
52. McDermott, G.; Prince, S.M.; Freer, A.A.; Hawthornthwaitelawless, A.M.; Papiz, M.Z.; Cogdell, R.J.; Isaacs, N.W. *Nature*, **1995**, *374*, 517.
53. Balzani, V.; Ceroni, P.; Gestermann, S.; Kauffmann, C.; Gorke, M.; Vögtle, F. *Chem. Commun.*, **2000**, 853.
54. Bignozzi, C.A.; Argazzi, R.; Kleverlaan, C.J. *Chem. Soc. Rev.*, **2000**, *29*, 87.
55. Montes, V. A.; Perez-Bolivar, C.; Estrada, L. A.; Shinar, J.; Anzenbacher, P., Jr. *J. Am. Chem. Soc.*, **2007**, *129*, 12598.
56. Tan, W.; Kopelman, R., in *Fluorescence Spectroscopy and Microscopy*, Wiley, New York, **1996**.
57. Balzani, V.; Credi, A.; Venturi, M. *Molecular Devices and Machines – A Journey into the Nano World*, Wiley-VCH, **2002**.
58. Dexter, D.L. *J. Chem. Phys.*, **1953**, *21*, 836.
59. Förster, T. *Ann. Phys.*, **1948**, *2*, 55.
60. Förster, T. *Z. Naturforsch.*, **1949**, *4*, 321.
61. Turro, N.J., *Modern Molecular Photochemistry*, University Science Books, Sausalito, **1991**.

62. Wan, C.-W.; Burghart, A.; Chen, J.; Bergström, F.; Johansson, L.B.-A.; Wolford, M.F.; Kim, T.G.; Topp, M.R.; Hochstrasser, R.M.; Burgess, K. *Chem. Eur. J.*, **2003**, *9*, 4430.
63. Prathapan, S.; Johnson, T.E.; Lindsey, J.S. *J. Am. Chem. Soc.*, **1993**, *115*, 7519.
64. Förster, T. *Disc. Faraday Soc.*, **1959**, *27*, 7.
65. Lakowicz, J.R., *Principles of Fluorescence Spectroscopy*, 2nd ed., Kluwer/Plenum, New York, **1999**.
66. Serin, J.M.; Brousmiche, D.W.; Frechet, J.M.J. *J. Am. Chem. Soc.*, **2002**, *124*, 11848.
67. Brousmiche, D.W.; Serin, J.M.; Frechet, J.M.J.; He, G.S.; Lin, T.-C.; Chung, S. J.; Prasad, P.N. *J. Am. Chem. Soc.*, **2003**, *125*, 1448.
68. Serin, J.M.; Brousmiche, D.W.; Frechet, J.M.J. *Chem. Commun.*, **2002**, 2605.
69. Imamura, T.; Fukushima, K. *Coord. Chem. Rev.*, **2000**, *198*, 133.
70. Burrell, A.K.; Officer, D.L.; Pleiger P.G.; Reid, D.C.W. *Chem. Rev.*, **2001**, *101*, 2751.
71. Wurthner, F.; You, C.-C.; Saha-Moller, C.R. *Chem. Soc. Rev.*, 2004, *33*, 133.
72. Trinkunas, G.; Herek, J.L.; Polivka, T.; Sundstrom, V.; Pullerits, T. *Phys. Rev. Lett.*, **2001**, *86*, 4167.
73. Bradforth, S.E.; Jimenez, R.; van Mourik, F.; van Grondelle, R.; Fleming, G.R. *J. Phys. Chem.*, **1995**, *99*, 16179.
74. Bruggemann, B.; Herek, J. L.; Sundstrom, V.; Pullerits, T.; May, V. *J. Phys. Chem. B*, **2001**, *105*, 11391.
75. Li, J.; Ambroise, A.; Yang, S.I.; Diers, J.R.; Seth, J.; Wack, C.R.; Bocian, D.F.; Holten, D.; Lindsey, J.S. *J. Am. Chem. Soc.*, **1999**, *121*, 8927.
76. Nakamura, Y.; Hwang, I.-W.; Aratani, N.; Ahn, T.K.; Ko, D.M.; Takagi, A.; Kawai, T.; Matsumoto, T.; Kim, D.; Osuka, A. *J. Am. Chem. Soc.*, **2005**, *127*, 236.
77. Dichtel, W.R.; Serin, J.M.; Edder, C.; Frechet, J.M.J.; Matuszewski, M.; Tan, L.-S.; Ohulchansky, T.Y.; Prasad, P.N. *J. Am. Chem. Soc.*, **2004**, *126*, 5380.
78. Wang, P.; Wu, S. *J. Photochem. Photobiol. A*, **1998**, *118*, 7.
79. Yilmaz, M.D.; Bozdemir, O.A.; Akkaya, E. U. *Org. Lett.*, **2006**, *8*, 2871.

80. D'Souza, F.; Smith, P.M.; Zandler, M.E.; McCarty, A.L.; Itou, M.; Araki, Y.; Ito, O. *J. Am. Chem. Soc.*, **2004**, *126*, 7898.
81. Wagner, R.W.; Lindsey, J.S. *J. Am. Chem. Soc.*, **1994**, *116*, 9759.
82. Zhang, X.; Xiao, Y.; Qian, X. *Org. Lett.*, **2008**, *10*, 29.
83. O'Regan, B.; Gratzel, M. *Nature*, **1991**, *353*, 737.
84. Gratzel, M. *J. Photochem. Photobiol. A.*, **2004**, *164*, 3.
85. Nazeeruddin, M.K.; Gratzel, M. *Comprehensive Coordination Chemistry II*, Vol. 9 (Eds.: J. A. McCleverty, T. J. Meyer), Elsevier, Dordrecht, **2004**.
86. Gratzel, M. *J. Photochem. Photobiol. C.*, **2003**, *4*, 145.
87. Nazeeruddin, M.K.; Kay, A.; Rodicio, R.; Humphry-Baker, R.; Muller, E.; Liska, P.; Vlachopoulos, N.; Gratzel, M. *J. Am. Chem. Soc.*, **1993**, *115*, 6382.
88. Nazeeruddin, M.K.; Zakeeruddin, S.M.; Humphry-Baker, R.; Jirousek, M.; Liska, P.; Vlachopoulos, N.; Shklover, V.; Fischer, C. H.; Gratzel, M. *Inorg. Chem.*, **1999**, *38*, 6298.
89. Nazeeruddin, M.K.; Pechy, P.; Renouard, T.; Zakeeruddin, S. M.; Humphry-Baker, R.; Comte, P.; Liska, P.; Cevey, L.; Costa, E.; Shklover, V.; Spiccia, L.; Deacon, G. B.; Bignozzi, C. A.; Gratzel, M. *J. Am. Chem. Soc.*, **2001**, *123*, 1613.
90. Moser, J.E. *Nat. Mater.*, **2005**, *4*, 723.
91. Shankar, K.; Bandara, J.; Paulose, M.; Wietasch, H.; Varghese, O.K.; Mor, G. K.; LaTempa, T.J.; Thelakkat, M.; Grimes, C.A. *Nano Lett.*, **2008**, ASAP Article.
92. Sayama, K.; Hara, K.; Tsukagoshi, S.; Abe, Y.; Ohga, Y.; Shinpo, A.; Suga S.; Arakawa, H. *New J. Chem.*, **2001**, *25*, 200.
93. Hagberg, D.P.; Edvinsson, T.; Marinado, T.; Boschloo, G.; Hagfeldt, A.; Sun, L. *Chem. Commun.*, **2006**, 2245.
94. Kitamura, T.; Ikeda, M.; Shigaki, K.; Inoue, T.; Anderson, N.A.; Ai, X.; Lian, T.; Yanagida, S. *Chem. Mater.*, **2004**, *16*, 1806.
95. Hara, K., Wang, Z.S.; Sato, T.; Furube, A.; Katoh, R.; Sugihara, H.; Dan-oh, Y.; Kasada, C.; Shinpo, A.; Suga, S. *J. Phys. Chem. B.*, **2005**, *109*, 15476.
96. Horiuchi, T.; Miura, H.; Sumioka, K.; Uchida, S. *J. Am. Chem. Soc.*, **2004**, *126*, 12218.

97. Hwang, S.; Lee, J.H.; Park, C.; Lee, H.; Kim, C.; Park, C.; Lee, M.-H.; Lee, W.; Park, J.; Kim, K.; Park, N.-G.; Kim, C. *Chem. Commun.*, **2007**, 4887.
98. Ooyama, Y.; Shimada, Y.; Kagawa, Y.; Imae, I.; Harima, Y. *Org. Biomol. Chem.*, **2007**, *5*, 2046.
99. Hattori, S.; Ohkubo, K.; Urano, Y.; Sunahara, H.; Nagano, T.; Wada, Y.; Tkachenko, N.V.; Lemmetyinen, H.; Fukuzumi, S. *J. Phys. Chem. B.*, **2005**, *109*, 15368.
100. Dost, Z.; Atilgan, S.; Akkaya, E.U. *Tetrahedron*, **2006**, *62*, 8484.

APPENDIX A

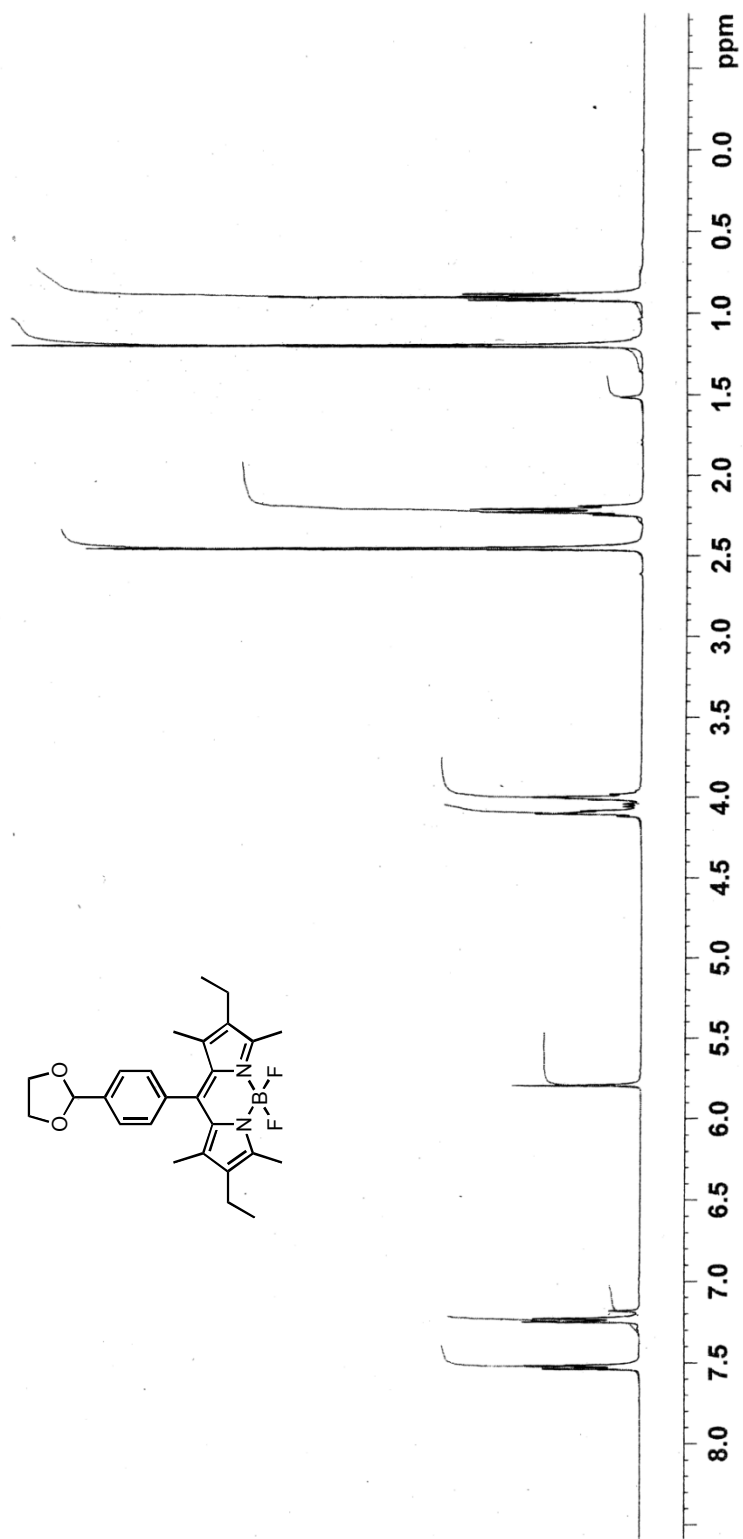


Figure 54. ¹H NMR spectrum of compound 41

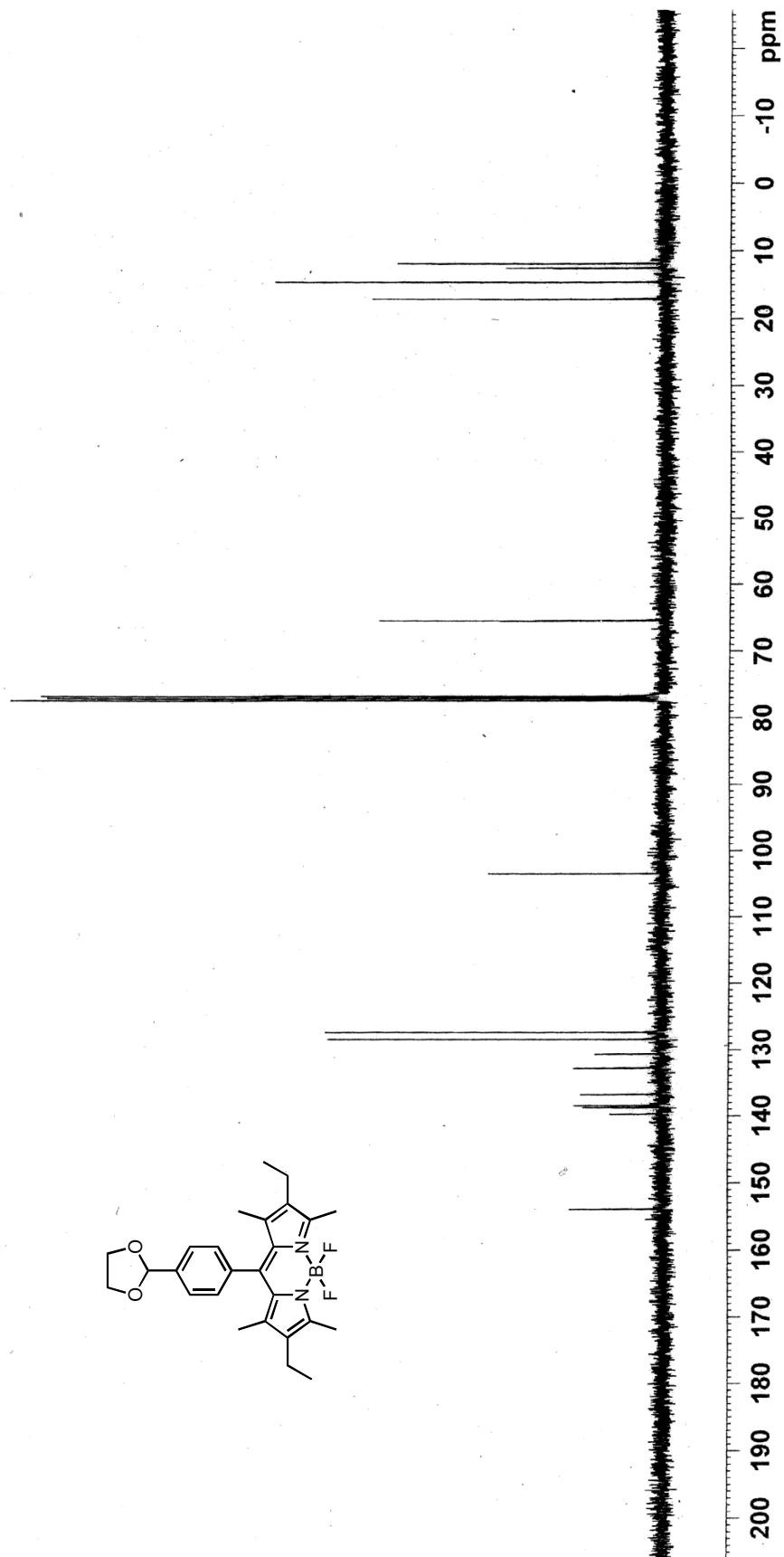


Figure 55. ^{13}C NMR spectrum of compound 41

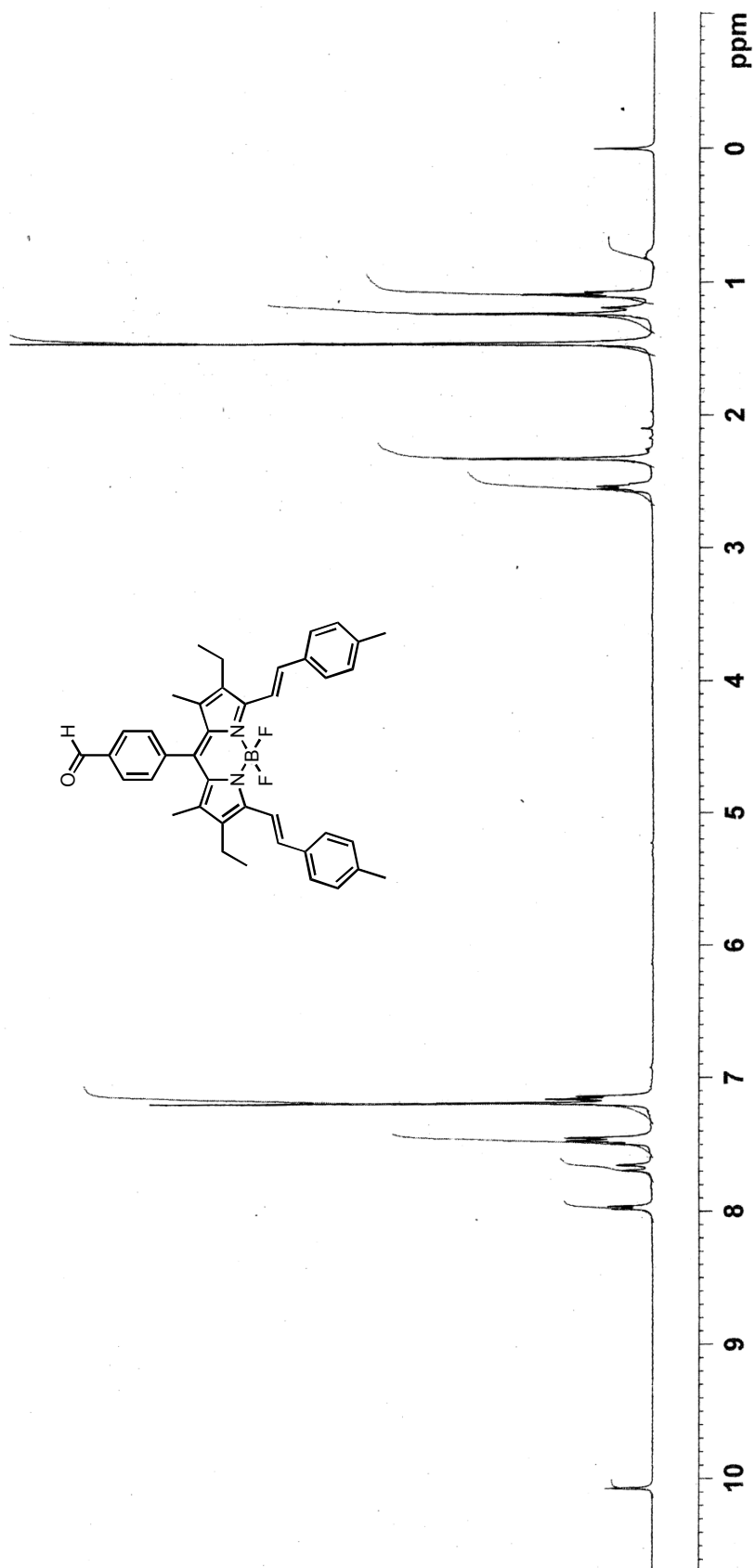


Figure 56. ¹H NMR spectrum of compound 42

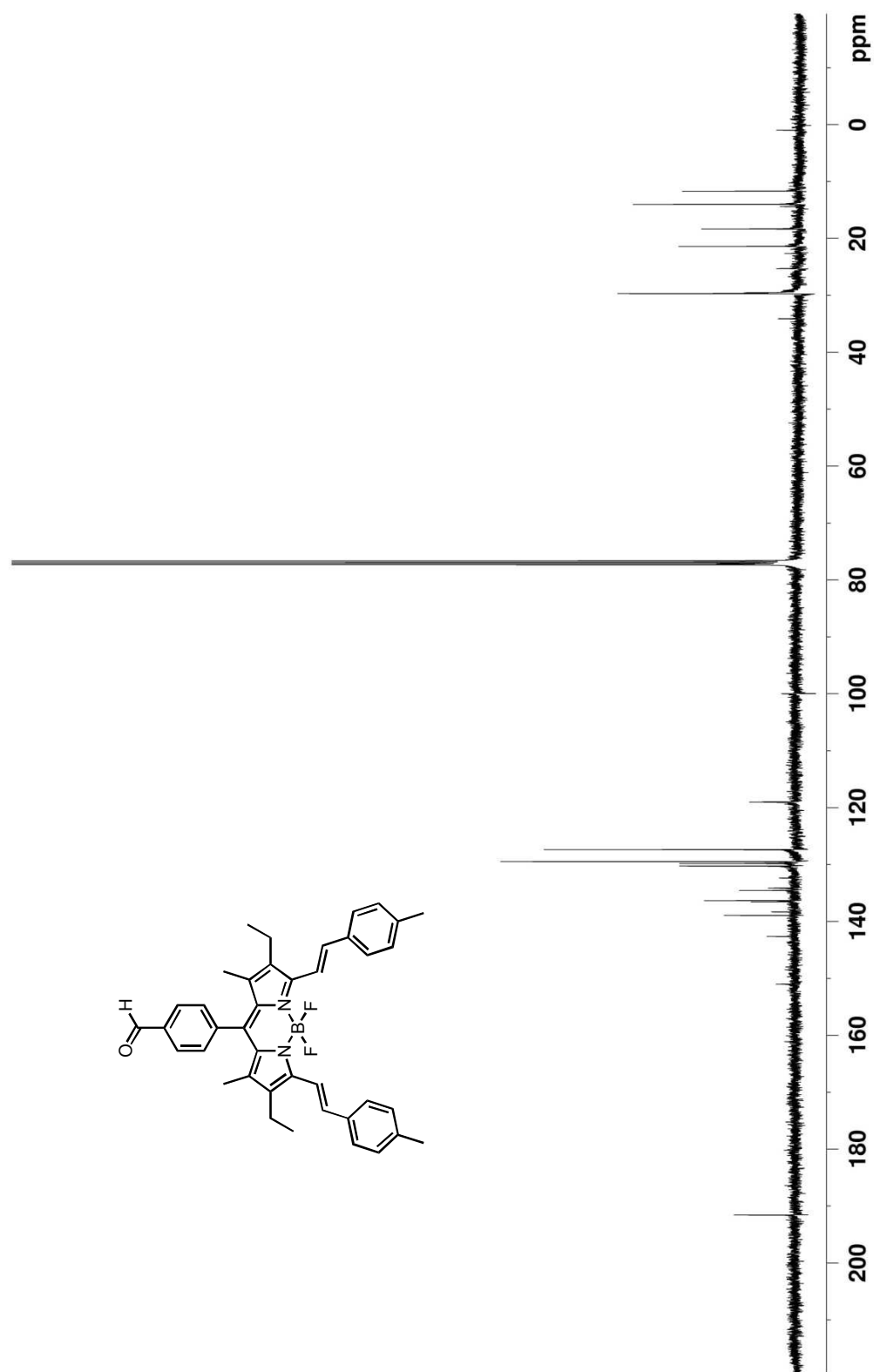


Figure 57. ^{13}C NMR spectrum of compound 42

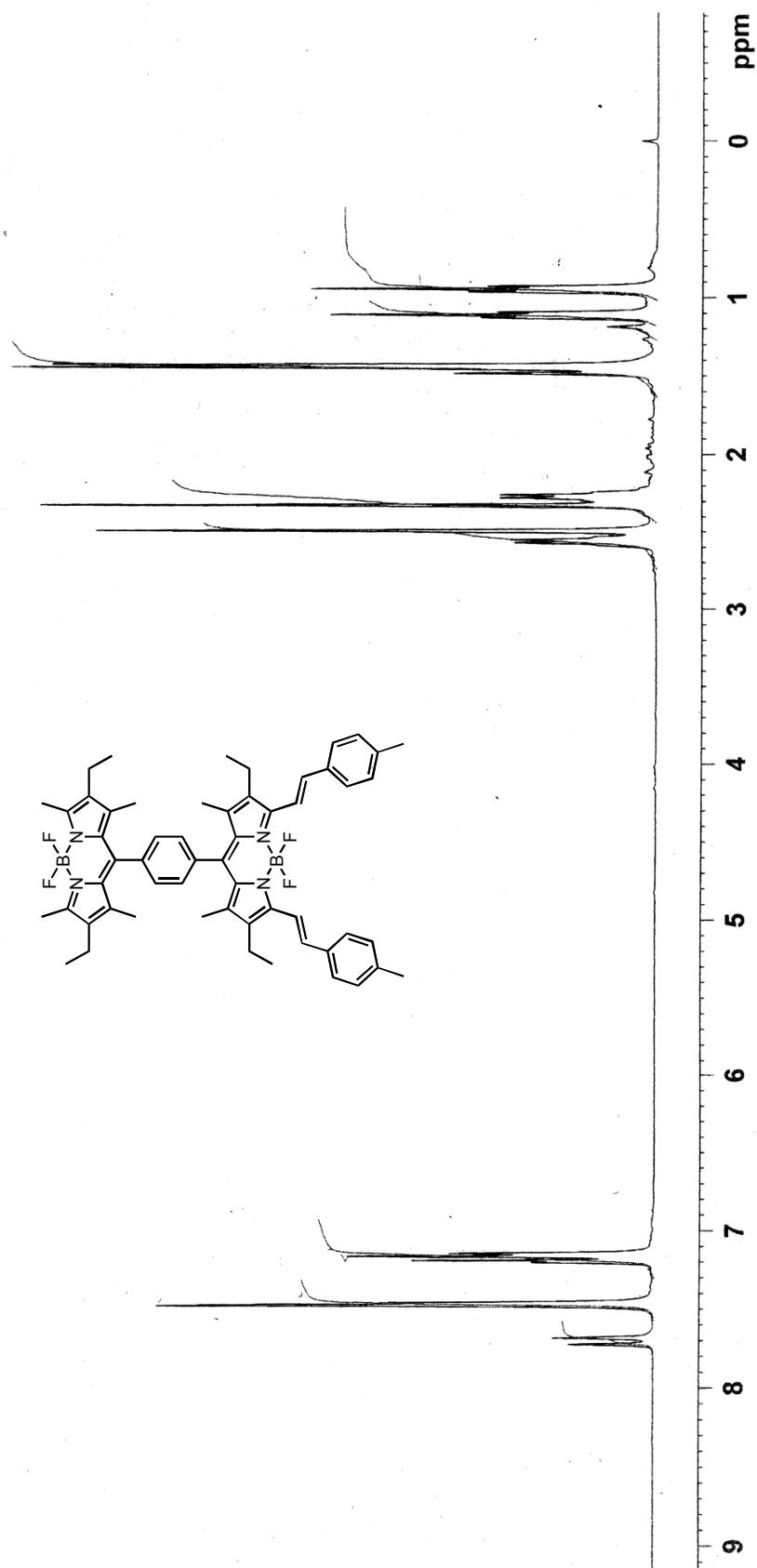


Figure 58. ¹H NMR spectrum of compound 43

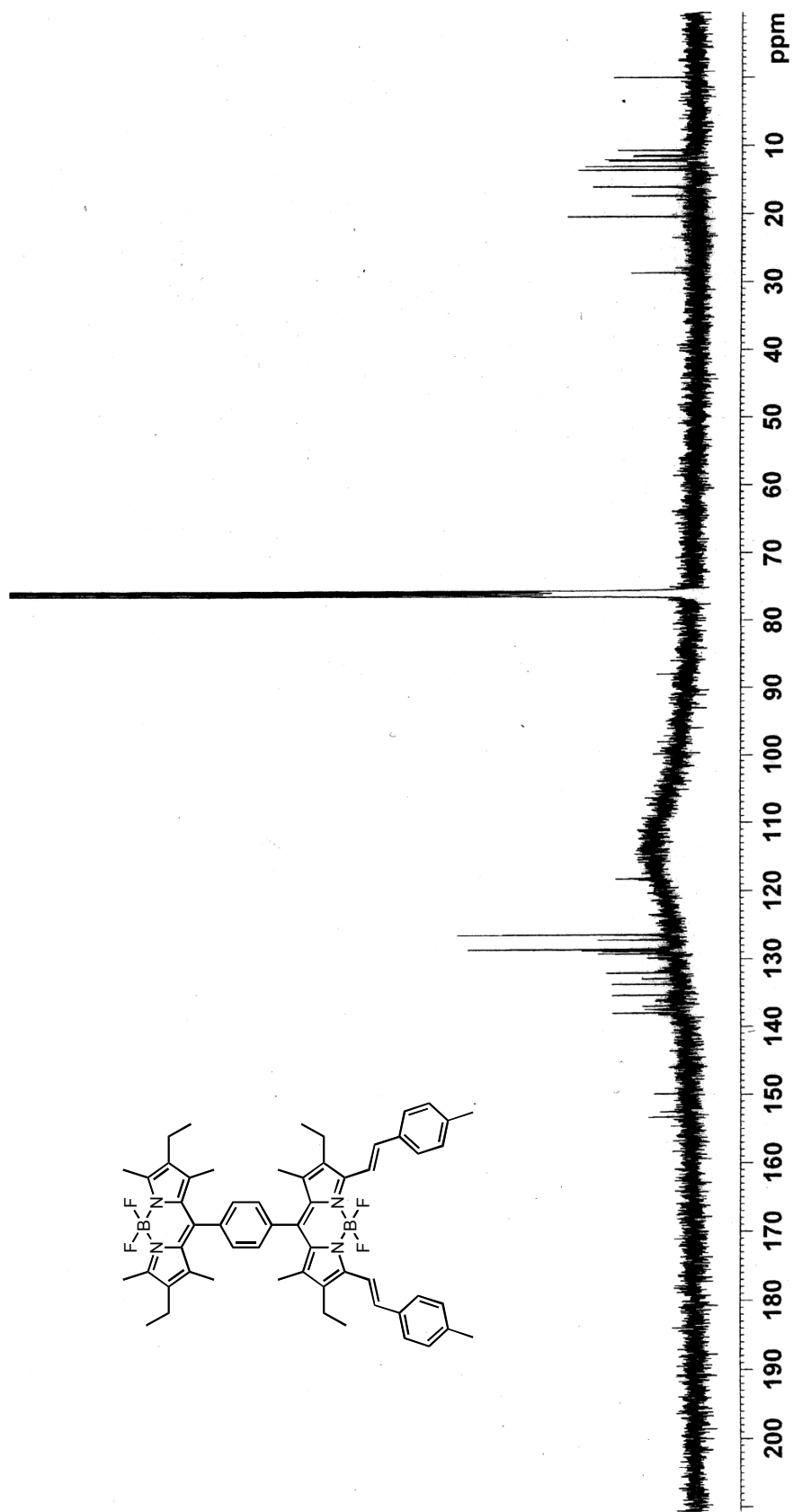


Figure 59. ^{13}C NMR spectrum of compound 43

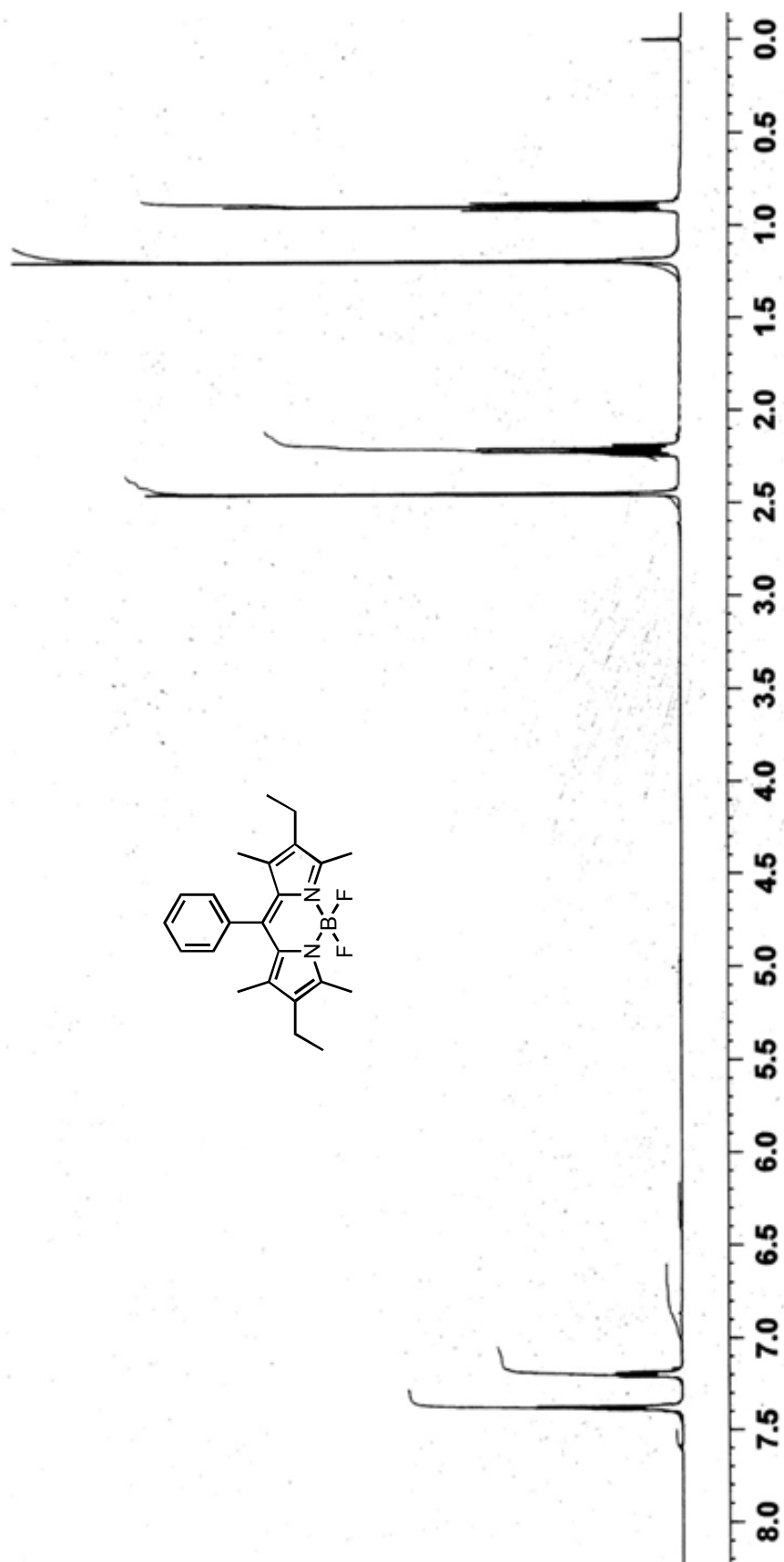


Figure 60. ¹H NMR spectrum of compound 44

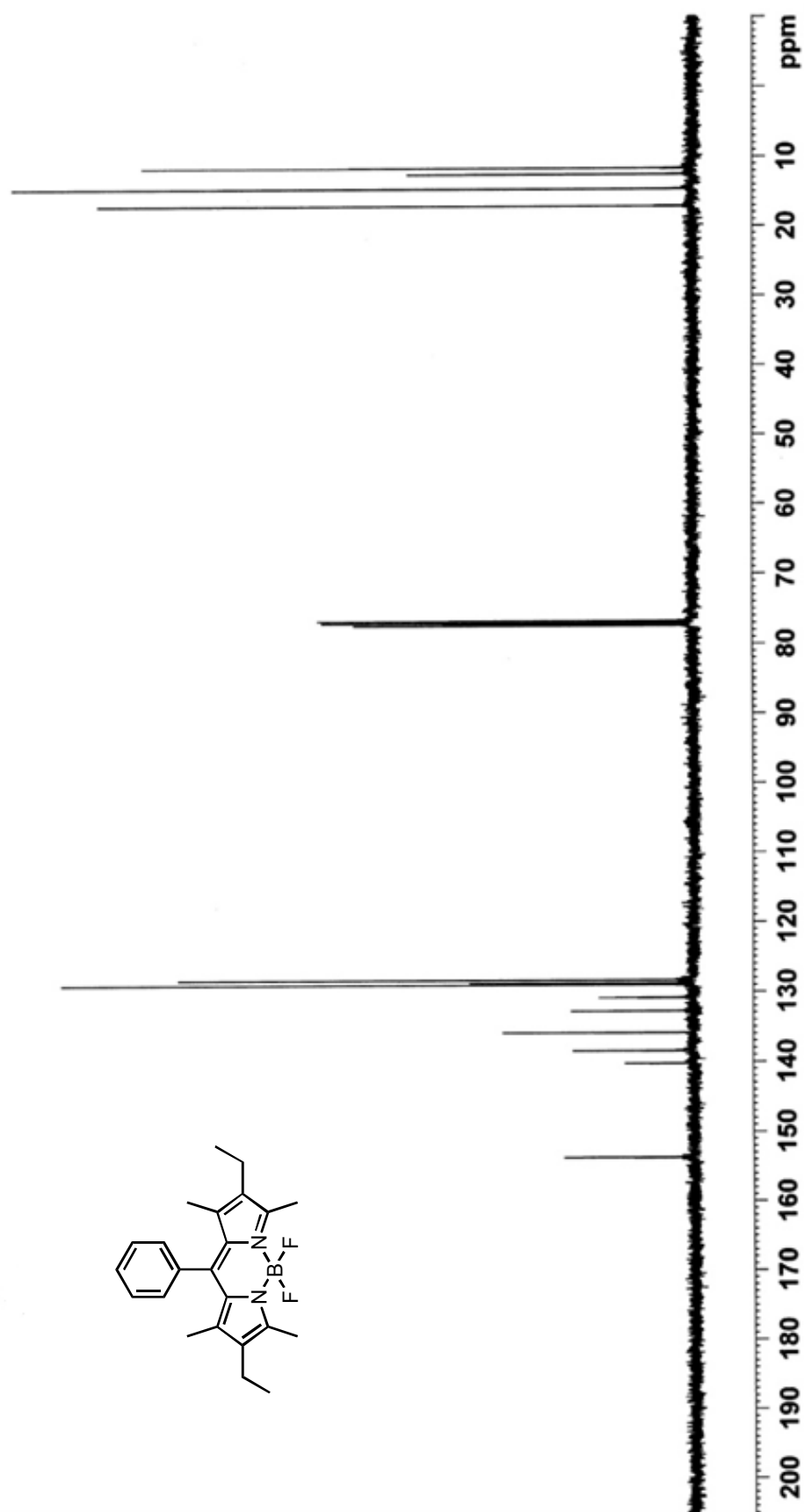


Figure 61. ^{13}C NMR spectrum of compound 44

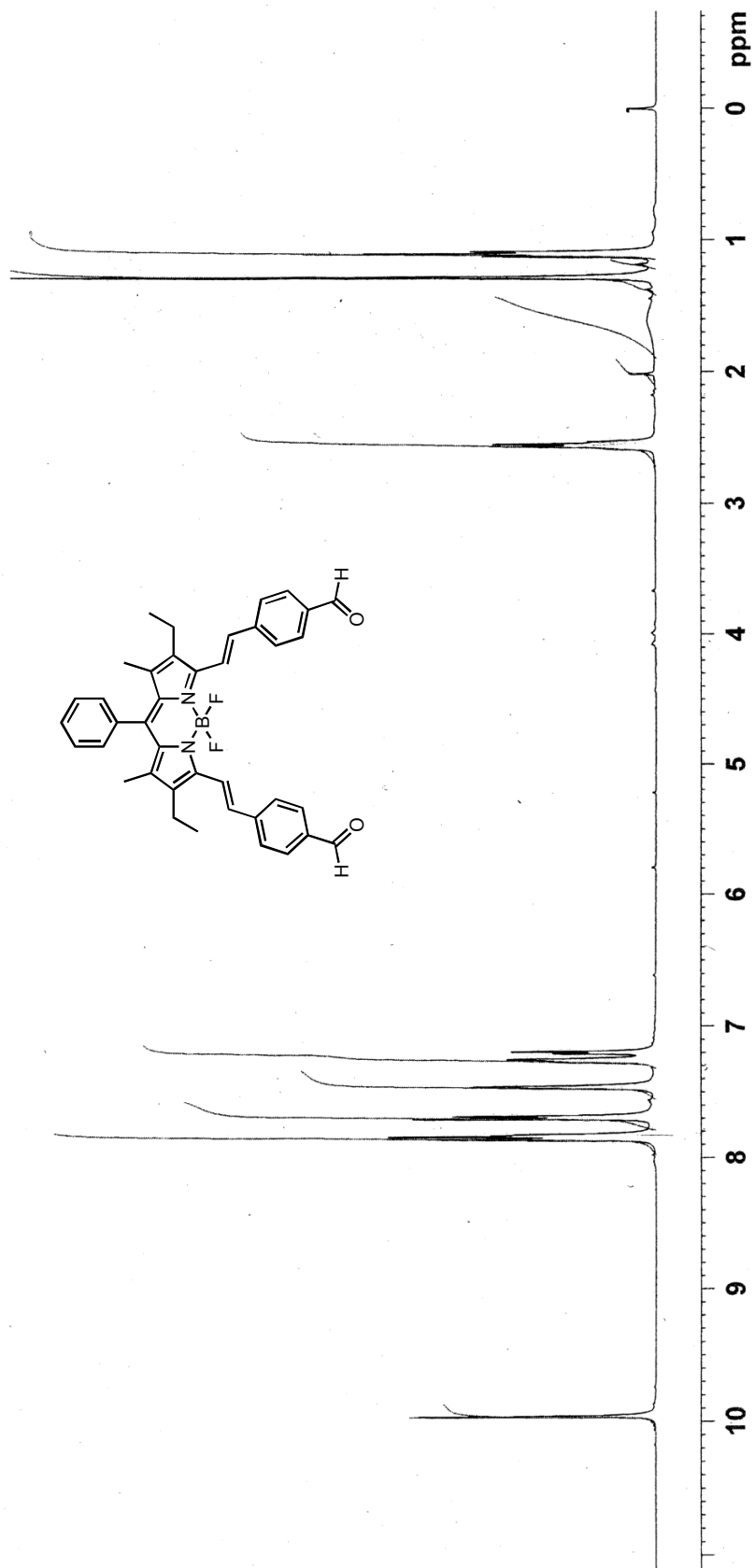


Figure 62. ^1H NMR spectrum of compound 45

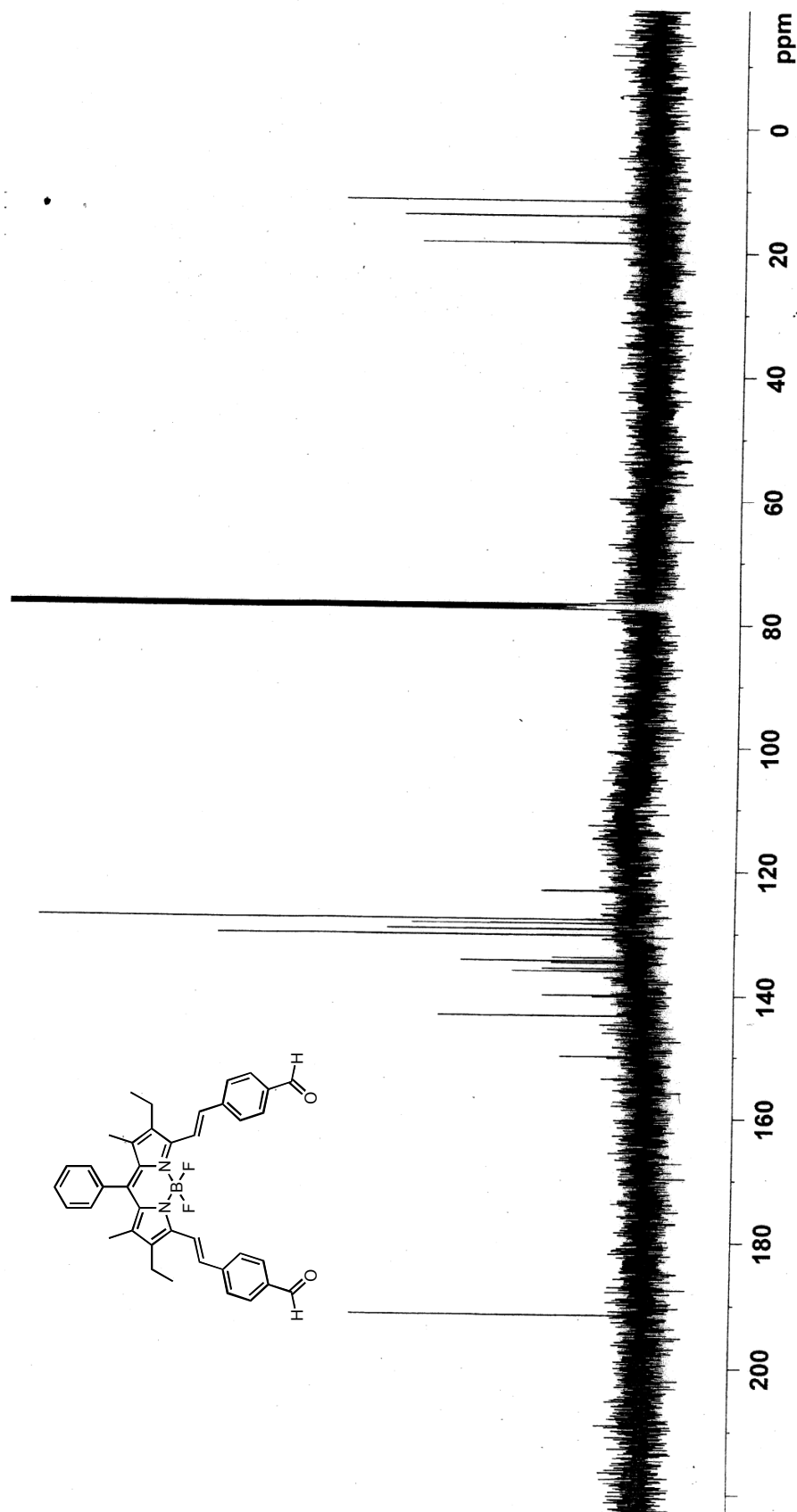


Figure 63. ^{13}C NMR spectrum of compound 45

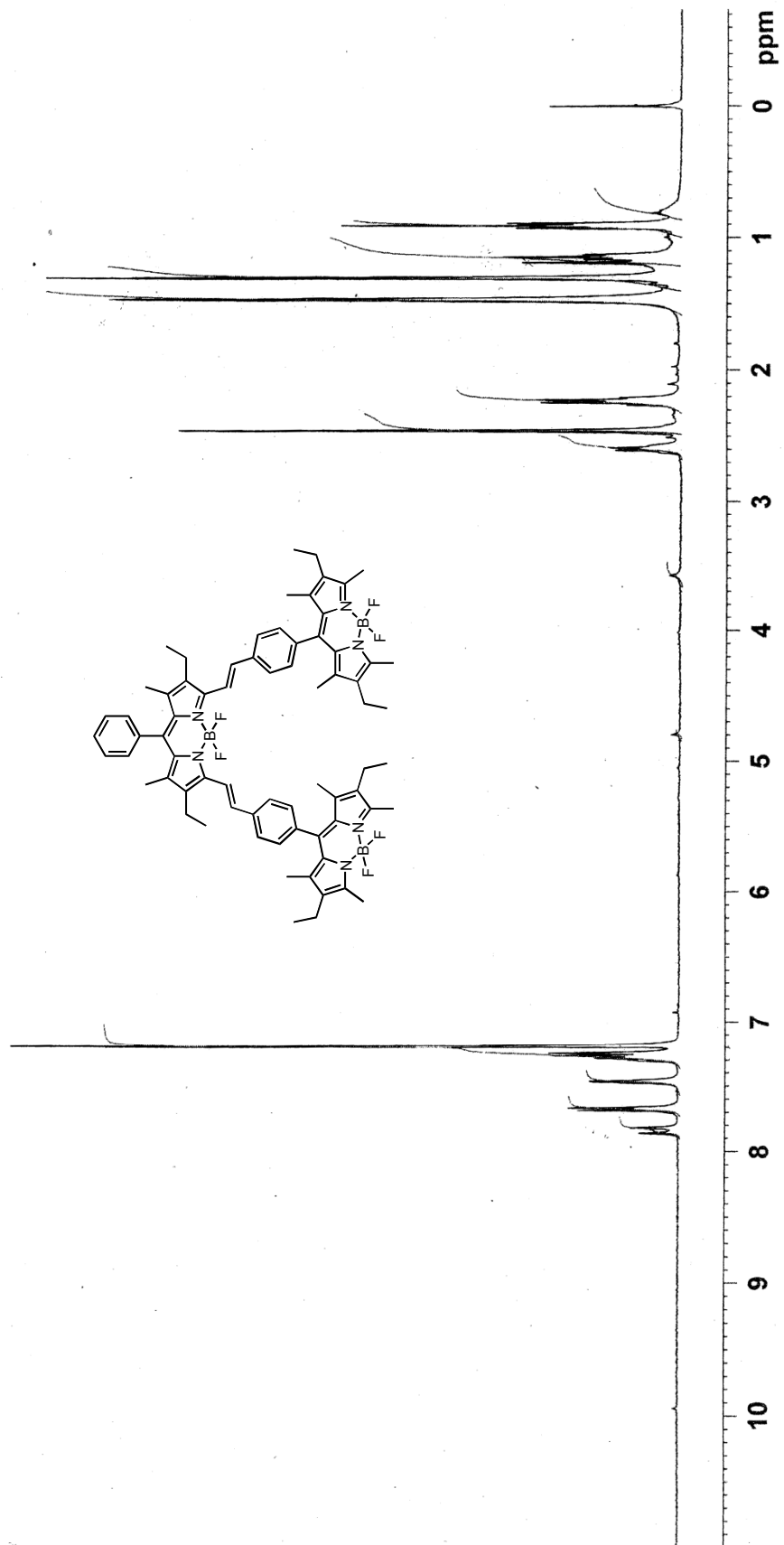


Figure 64. ¹H NMR spectrum of compound 46

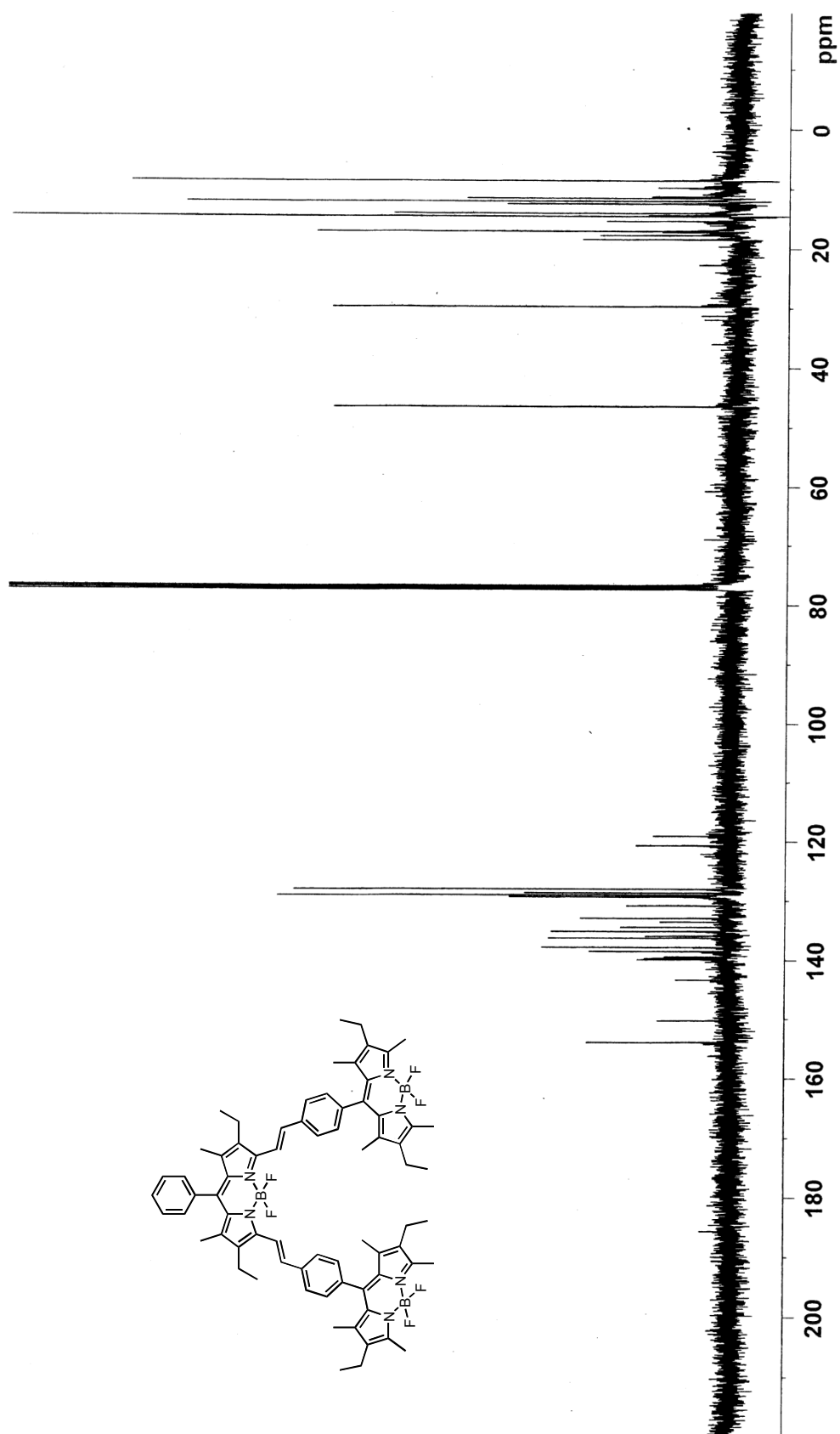


Figure 65. ^{13}C NMR spectrum of compound 46

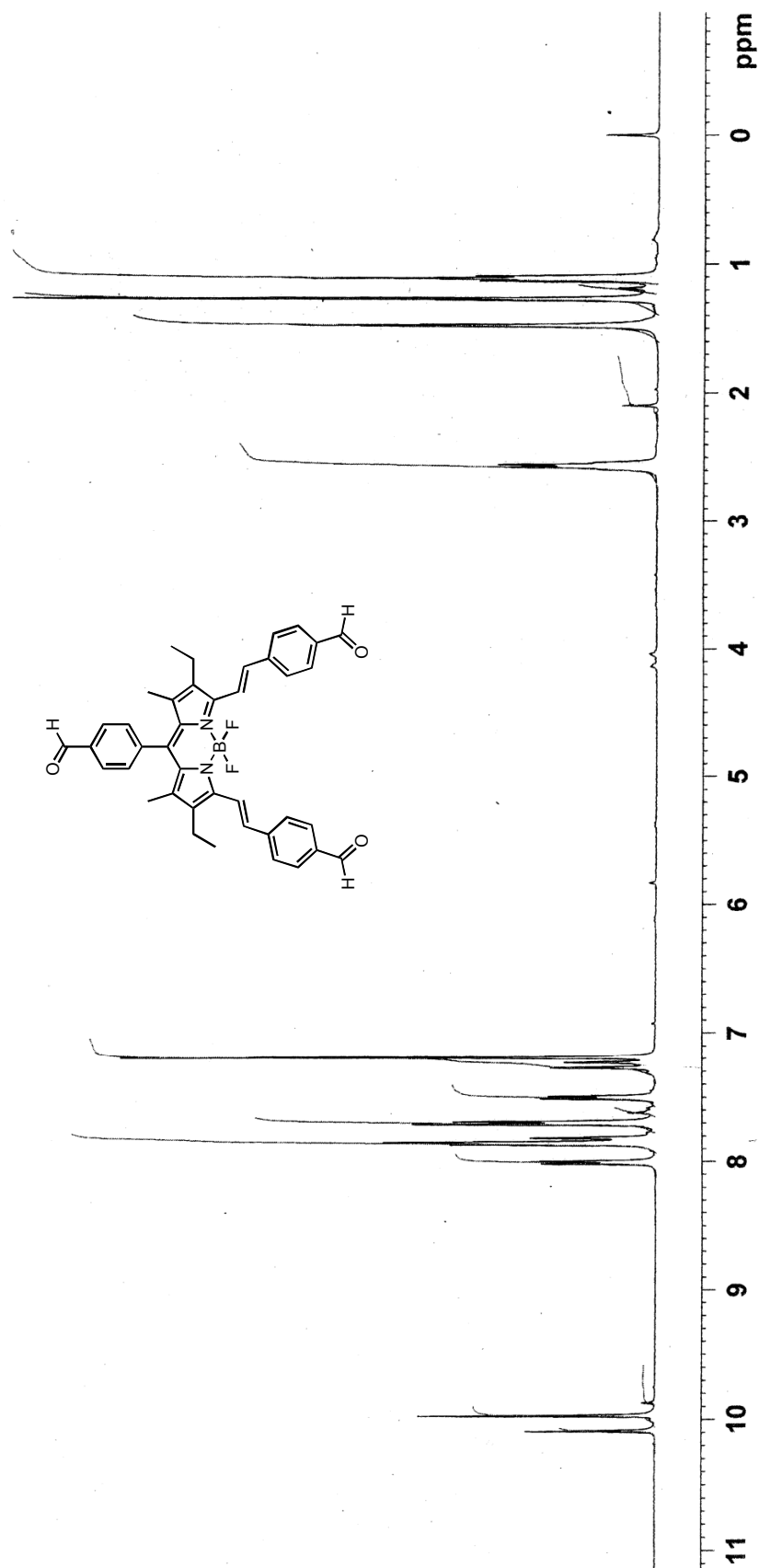


Figure 66. ¹H NMR spectrum of compound 47

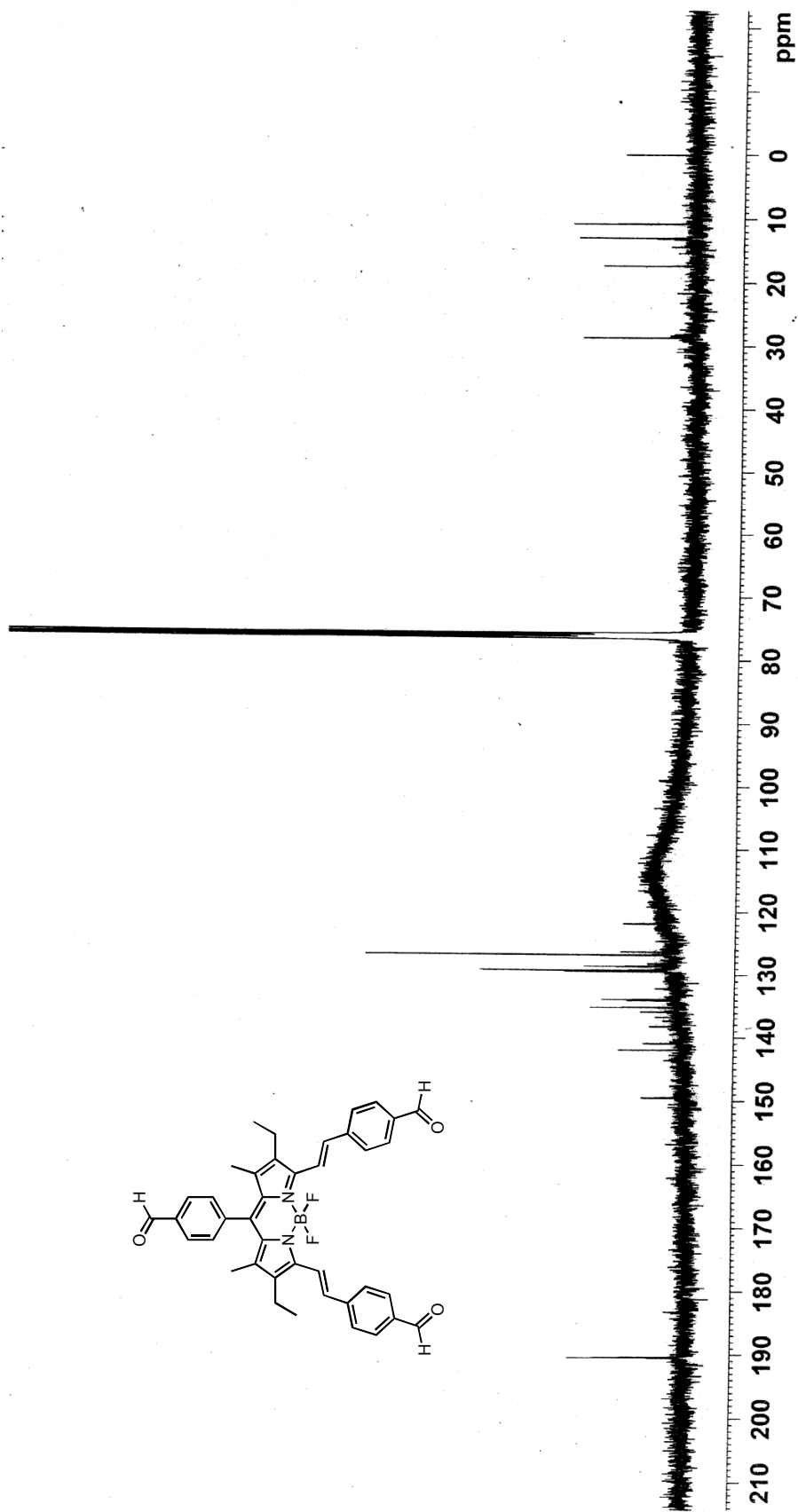


Figure 67. ^{13}C NMR spectrum of compound 47

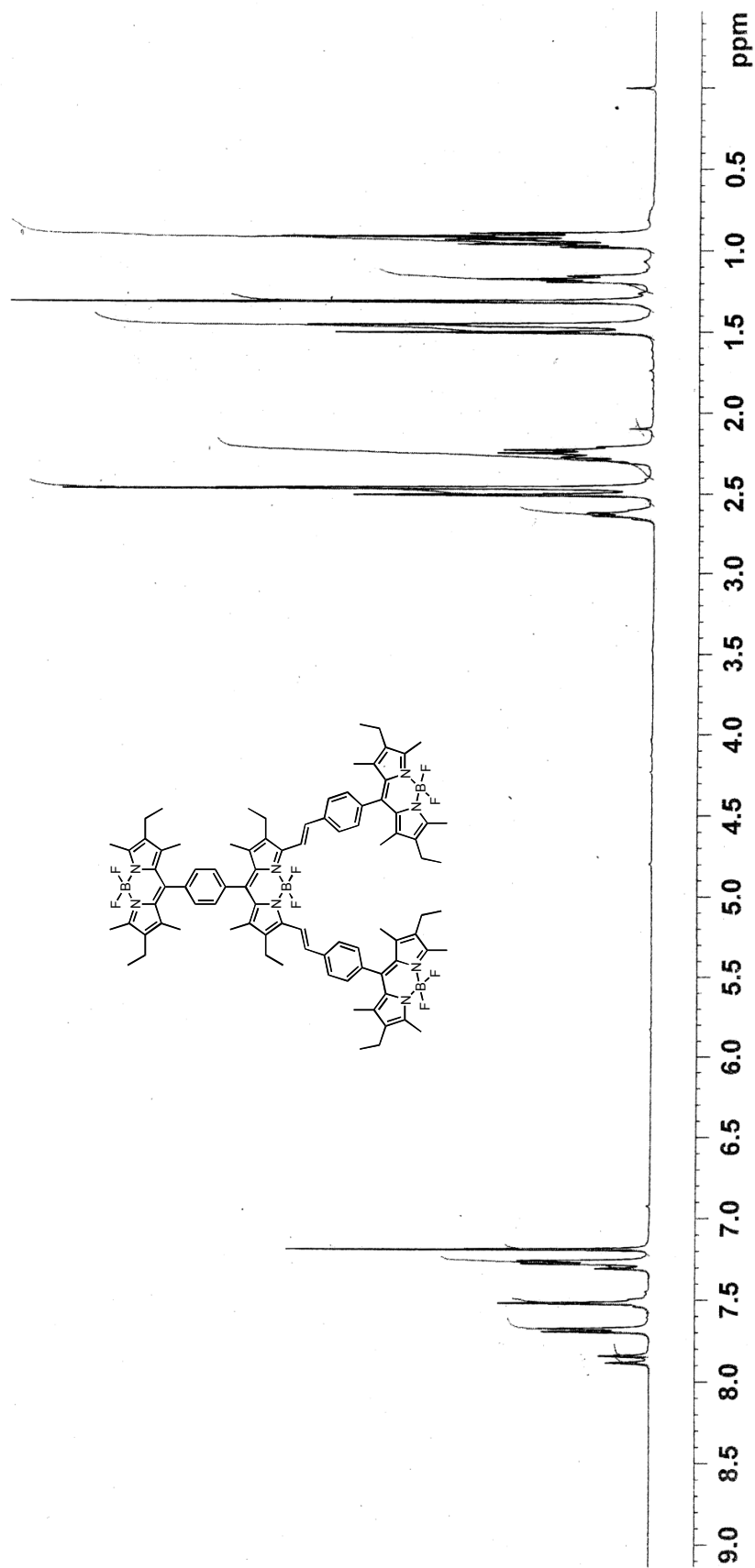


Figure 68. ¹H NMR spectrum of compound 48

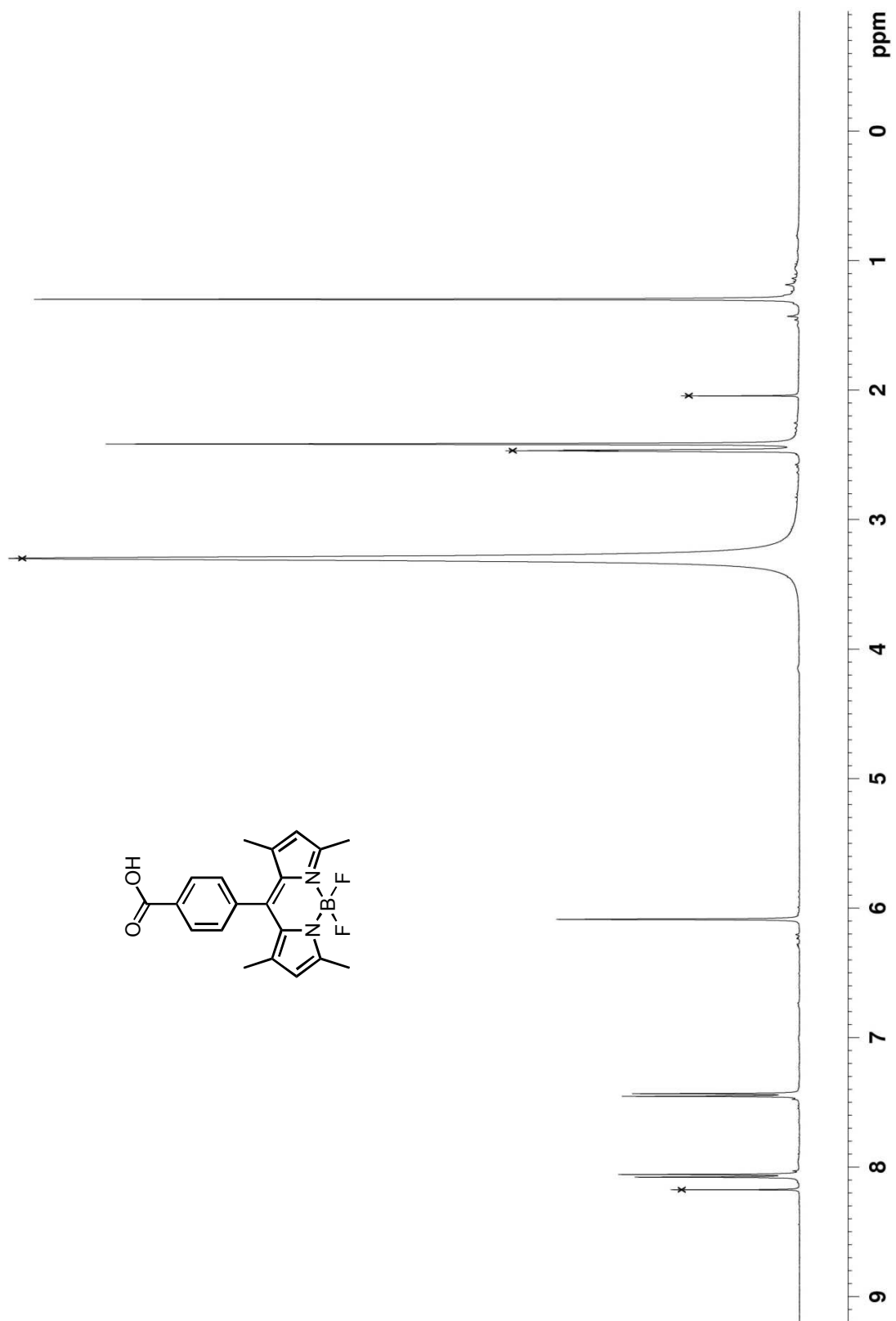


Figure 70. ¹H NMR spectrum of compound 49

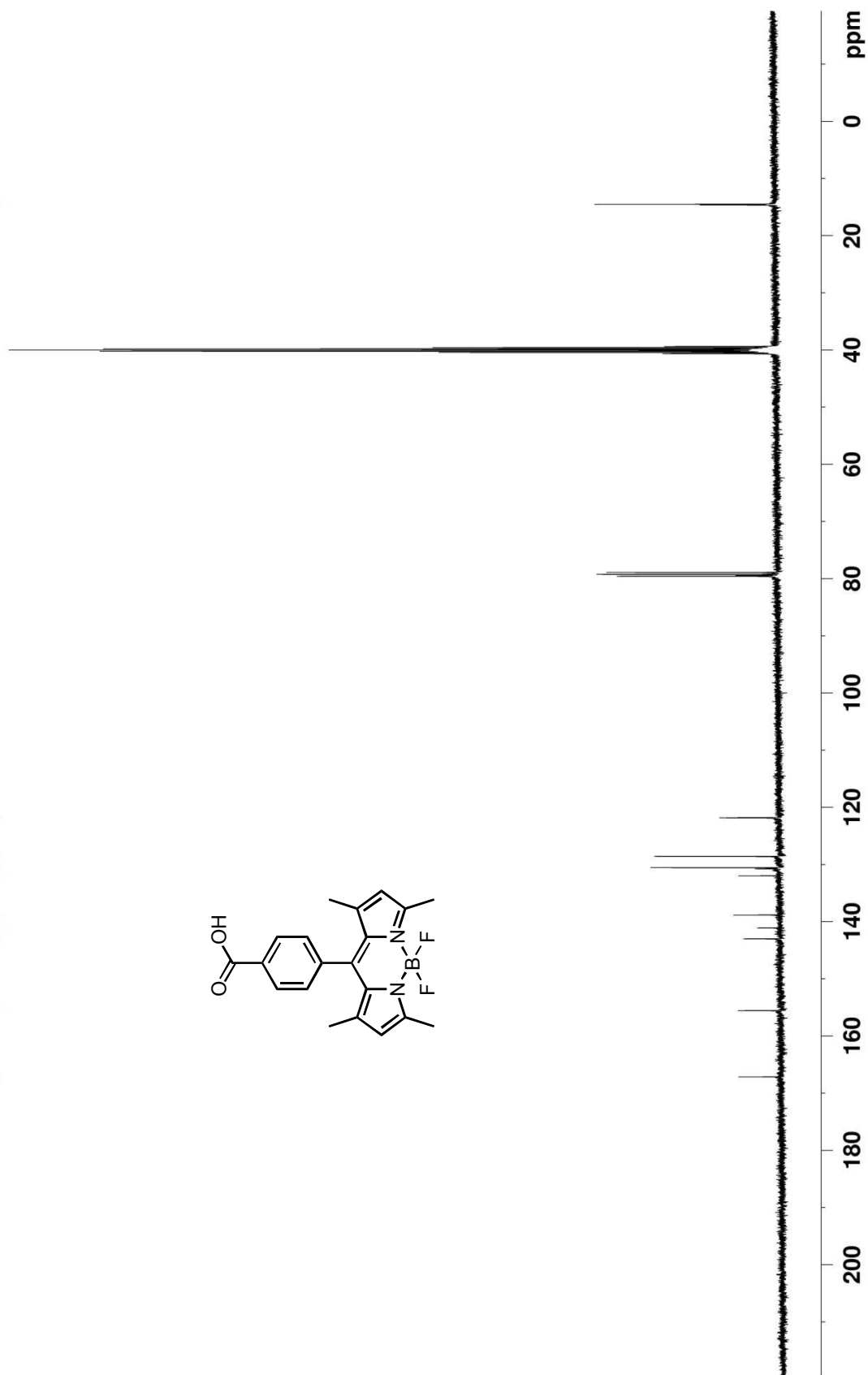


Figure 71. ^{13}C NMR spectrum of compound 49

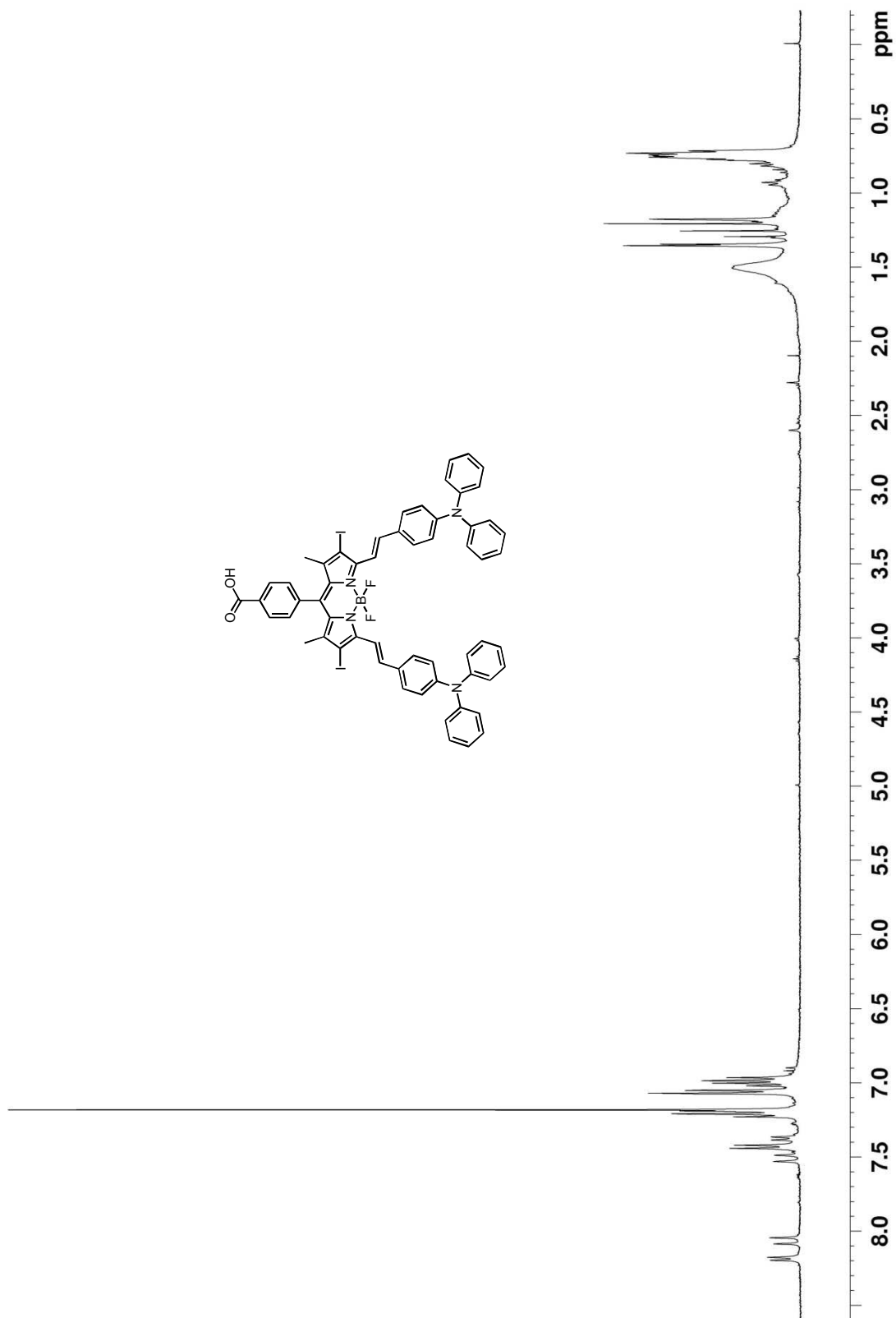


Figure 72. ¹H NMR spectrum of compound 52

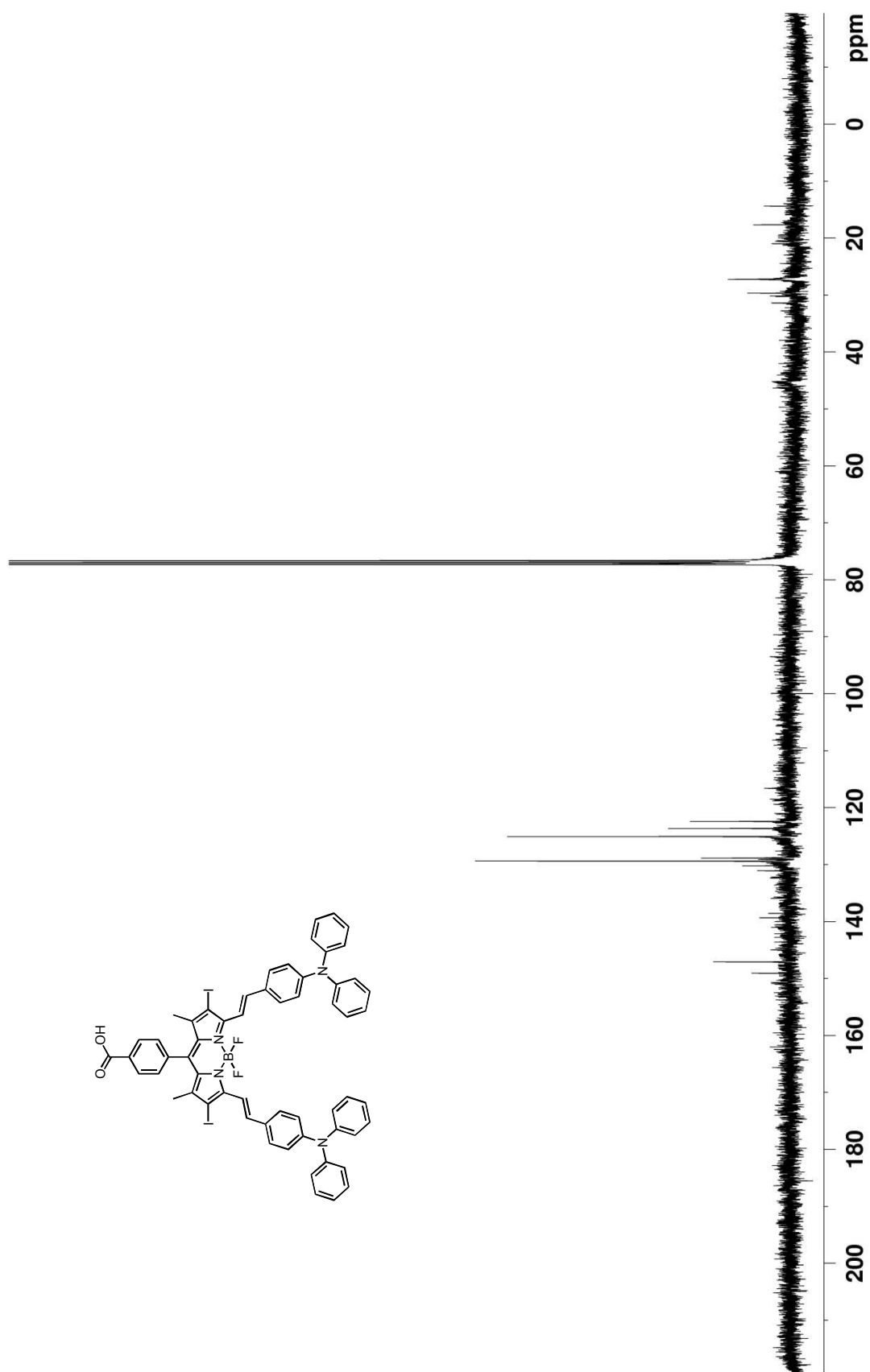


Figure 73. ^{13}C NMR spectrum of compound 52

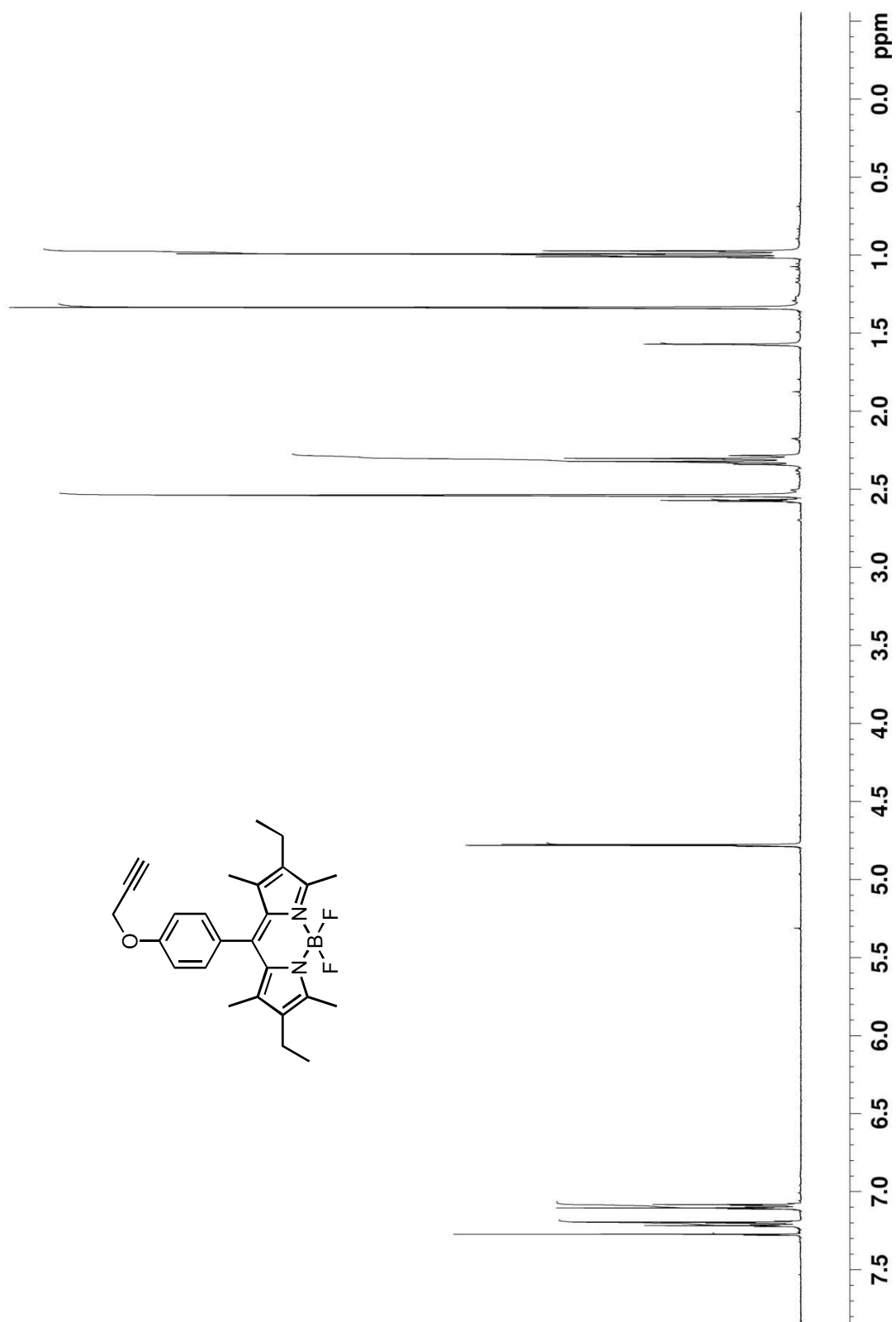


Figure 74. ¹H NMR spectrum of compound 54

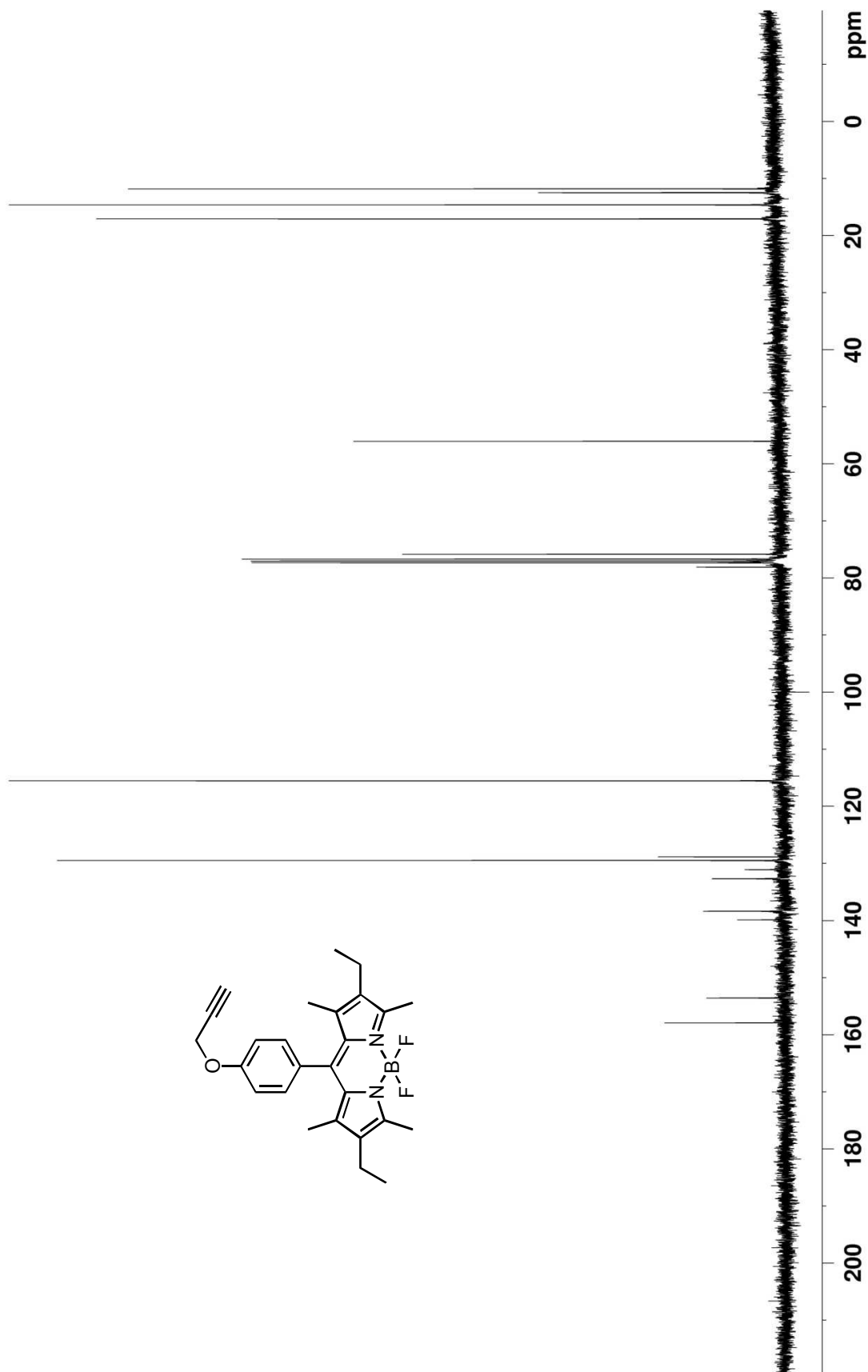


Figure 75. ^{13}C NMR spectrum of compound 54

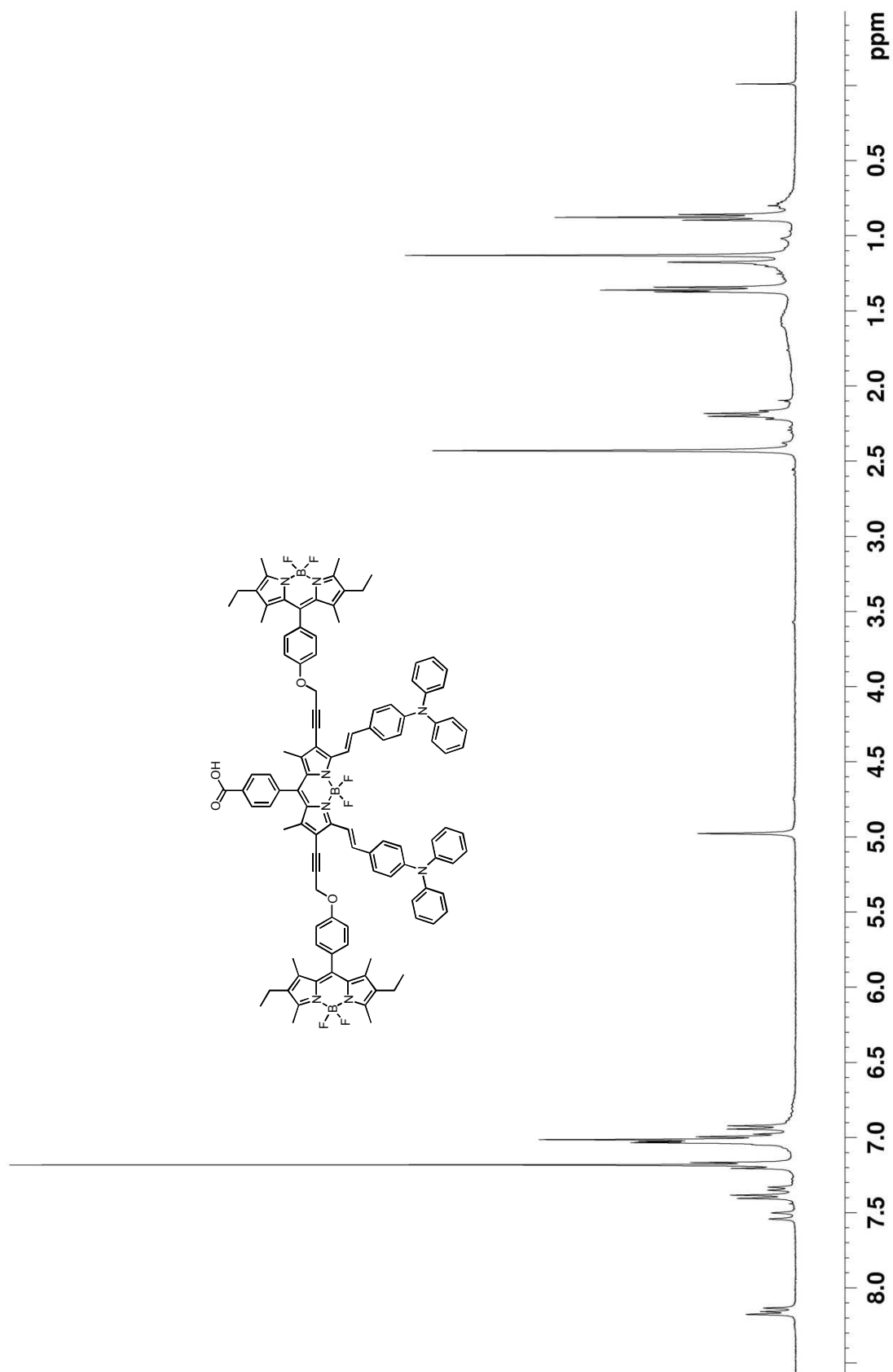


Figure 76. ¹H NMR spectrum of compound 55

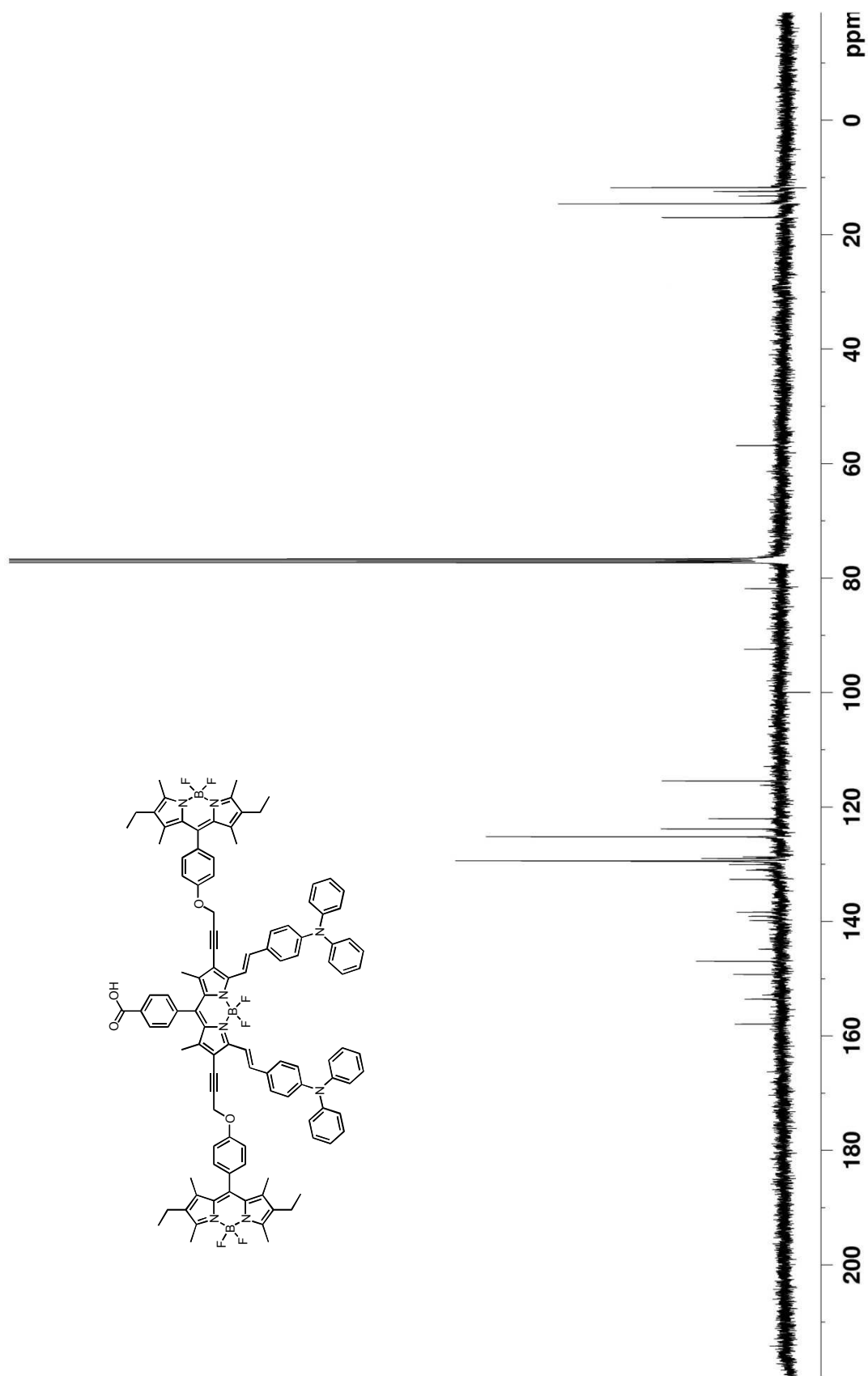


Figure 77. ^{13}C NMR spectrum of compound 55

APPENDIX B

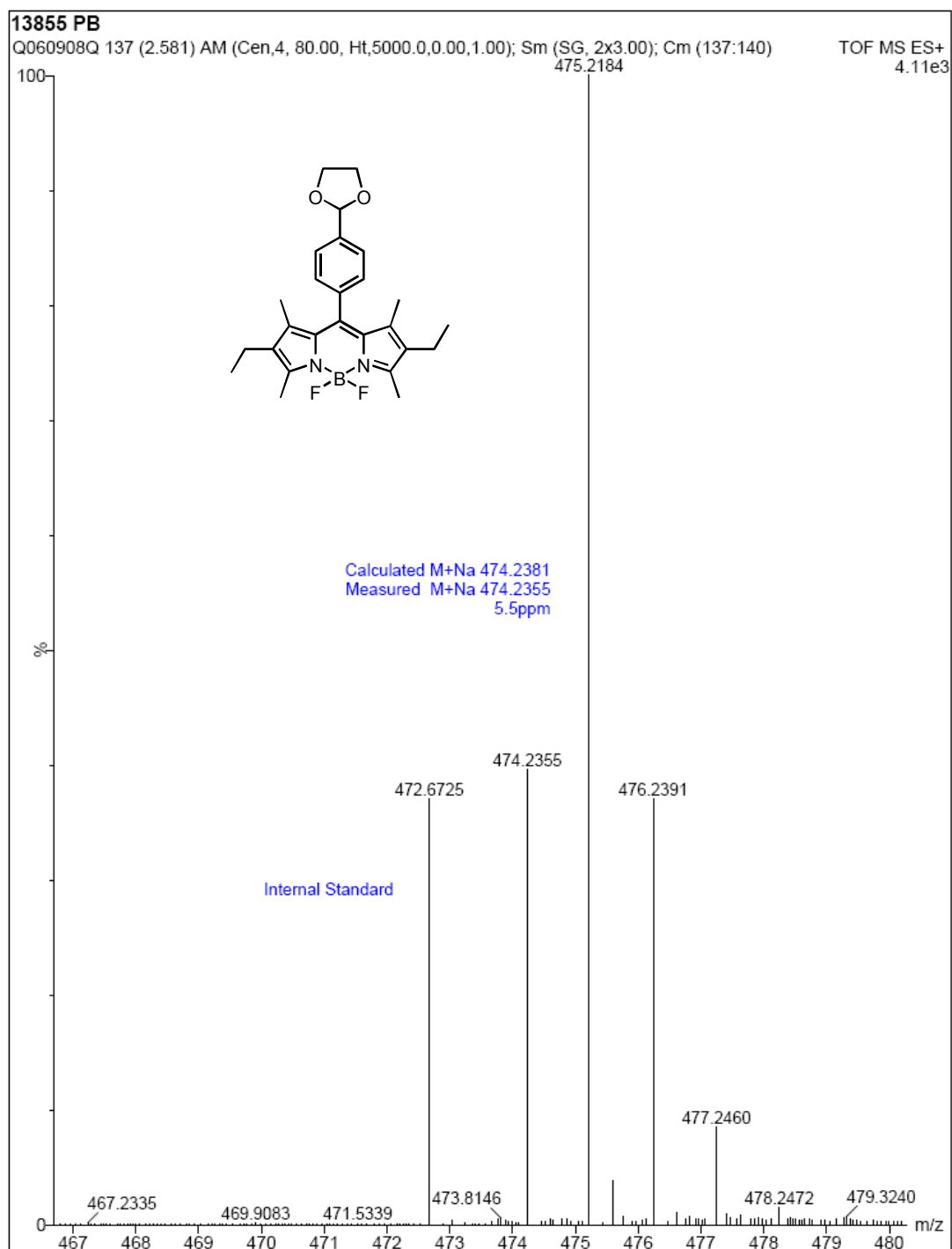


Figure 78. ESI-HRMS of compound 41

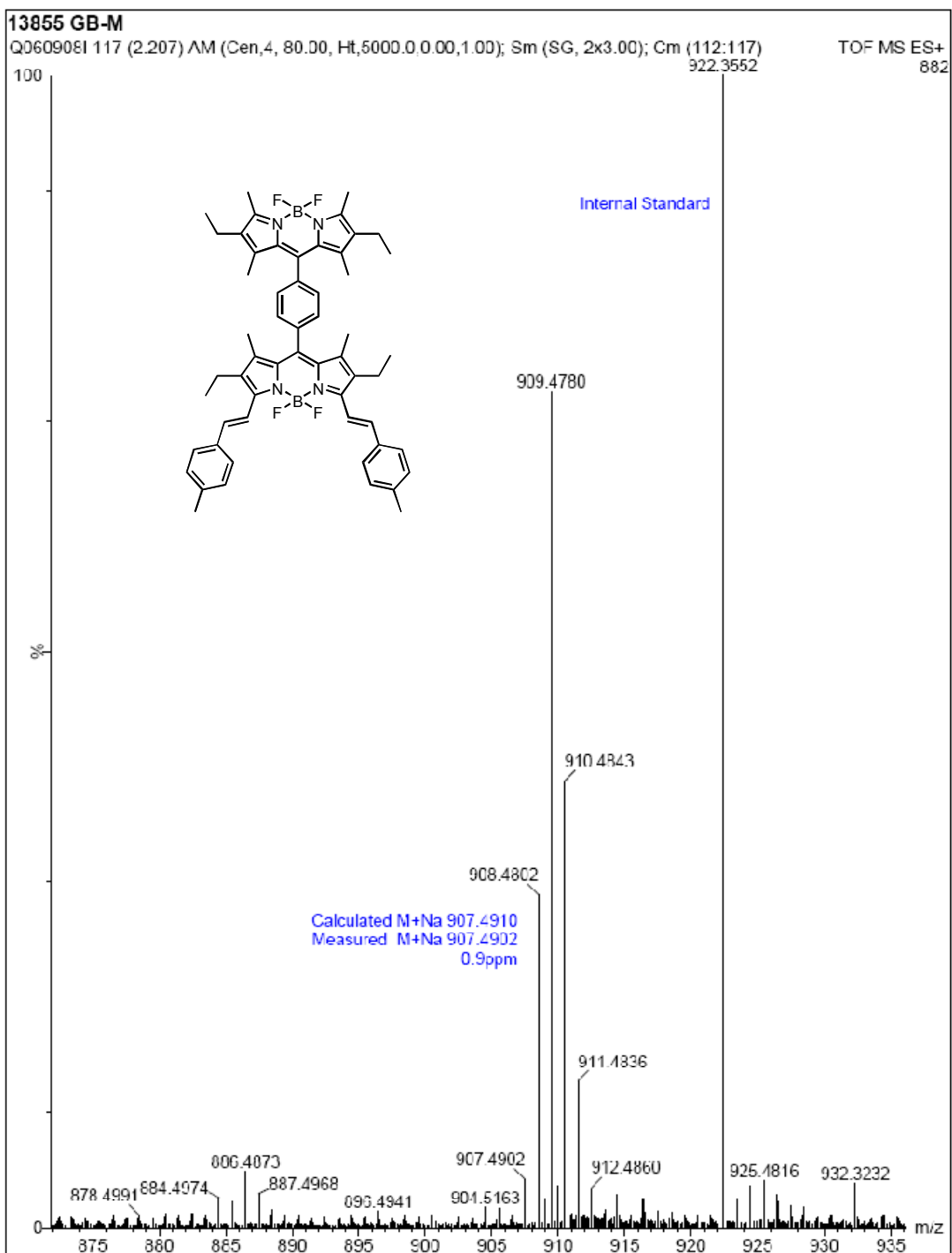


Figure 80. ESI-HRMS of compound 43

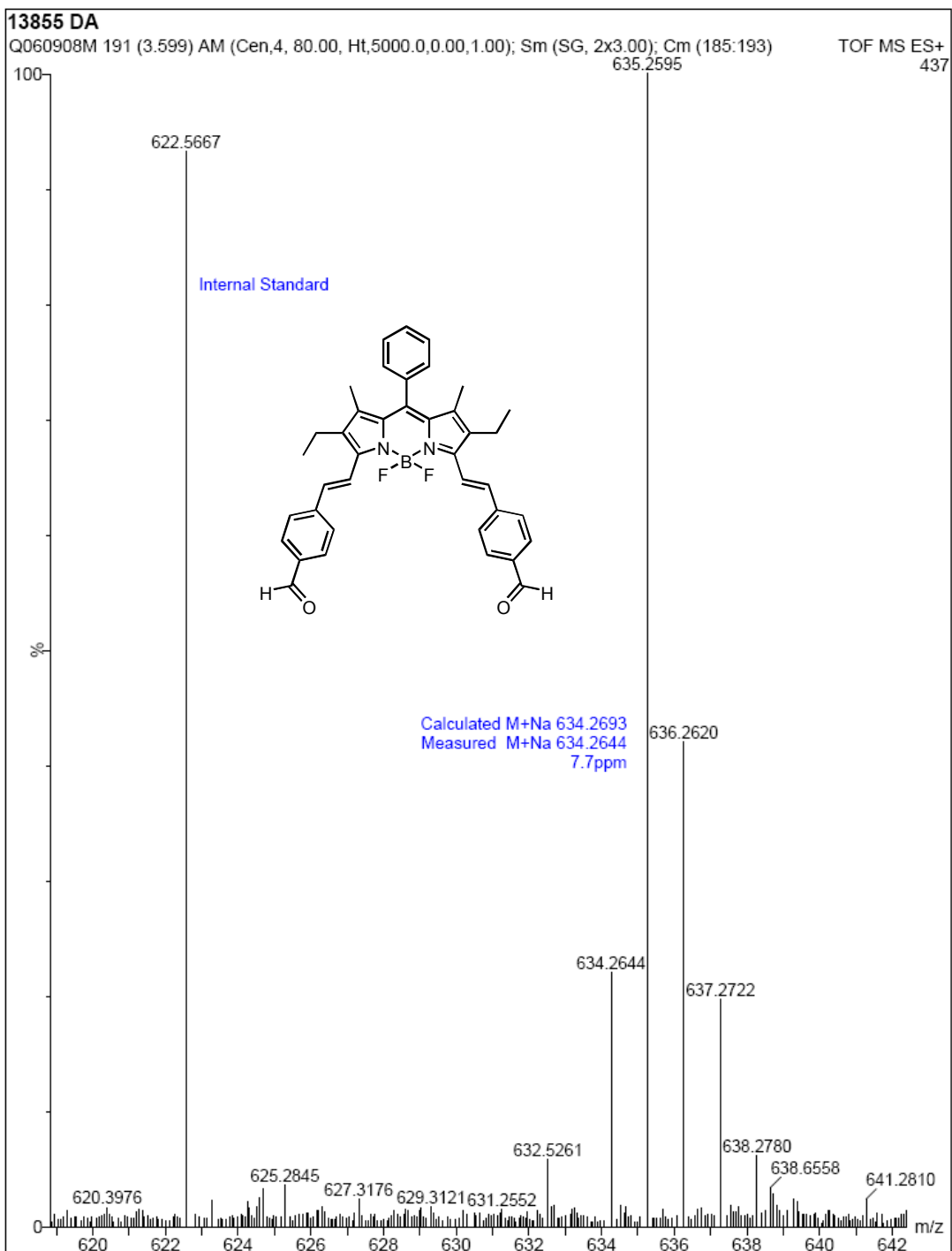


Figure 81. ESI-HRMS of compound 45

m/z	SN	Quality Fac.	Res.	Intens.	Area
1139.686	96.2	1.292	7796	58.00	9
1140.684	960.1	19359	7569	579.00	101
1141.684	2024.6	58697	6790	1221.00	241
1142.680	1237.0	22182	6865	746.00	142
1143.680	326.7	4605	7623	197.00	33
1158.663	36.5	366	8314	22.00	3
1159.641	492.5	9467	7359	297.00	50
1160.639	1051.3	22970	6210	634.00	130
1161.647	635.1	11278	6899	383.00	68
1162.622	140.9	1897	6717	85.00	14

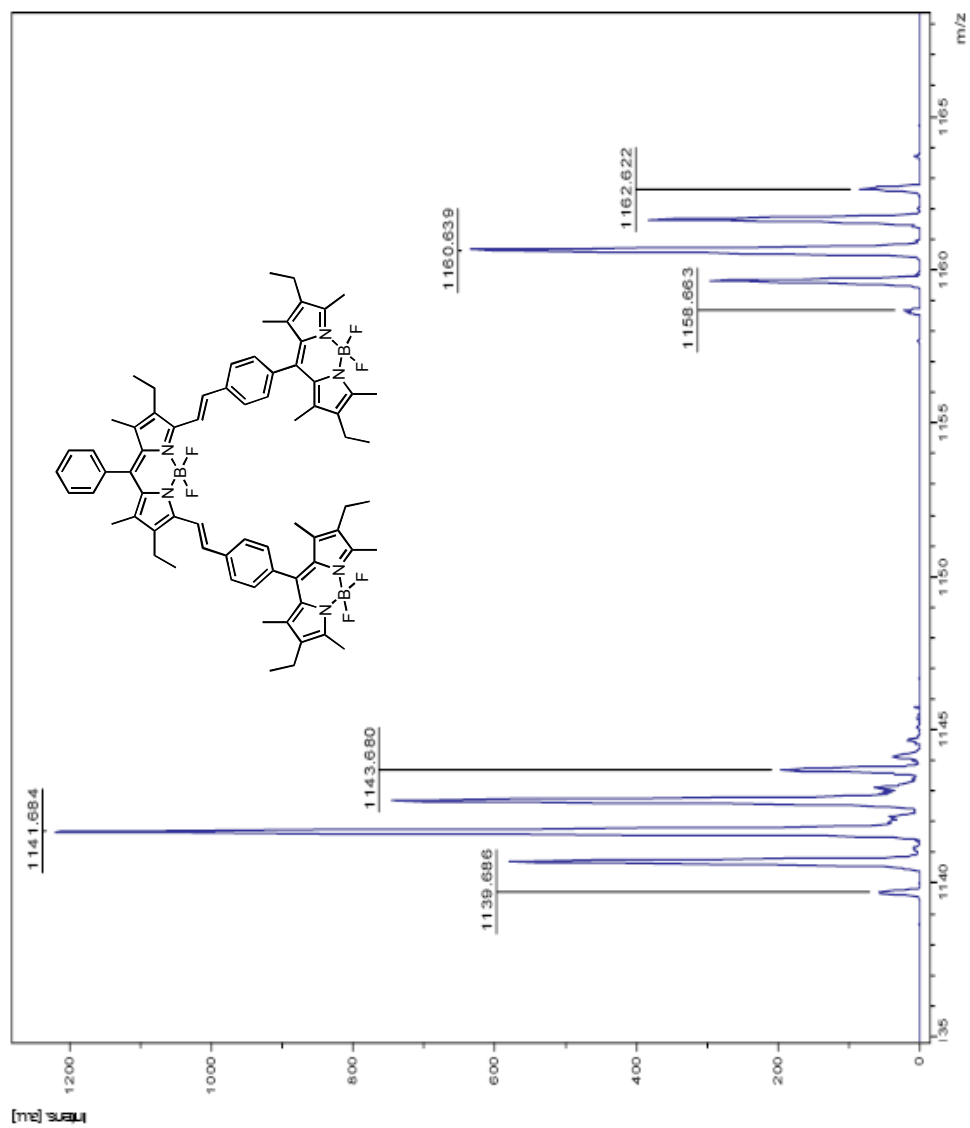


Figure 82. MALDI-MS of compound 46

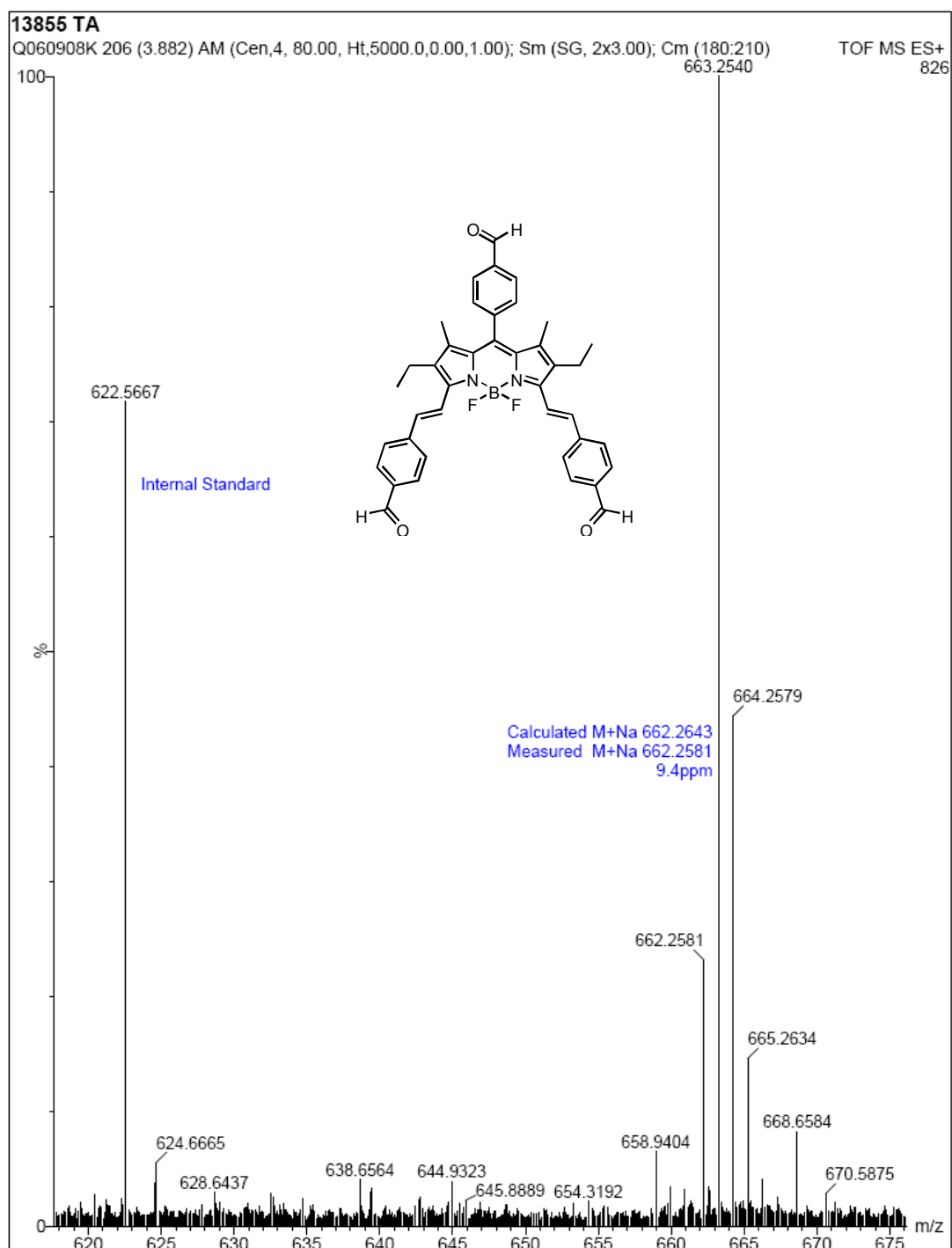


Figure 83. ESI-HRMS of compound 47

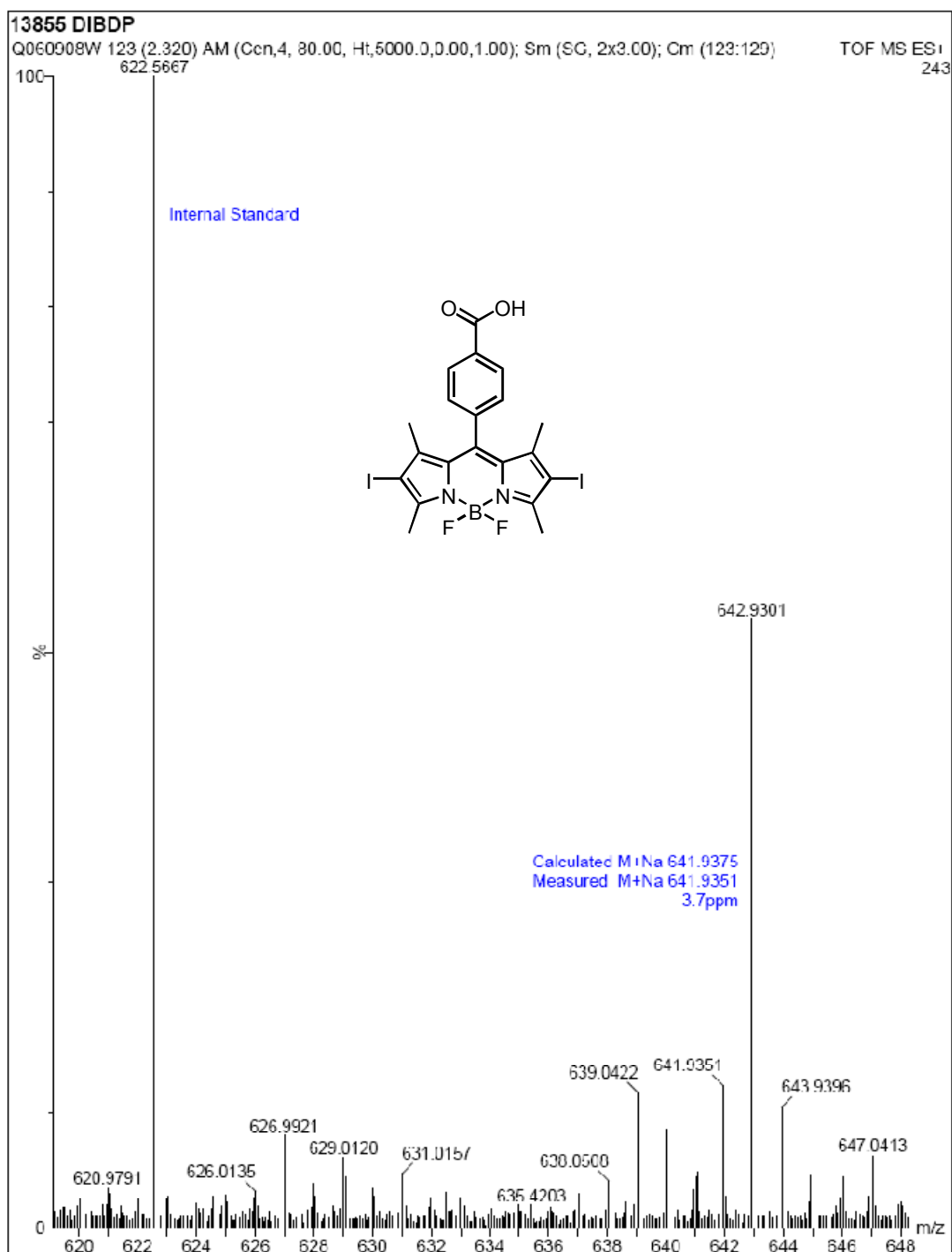


Figure 85. ESI-HRMS of compound 50

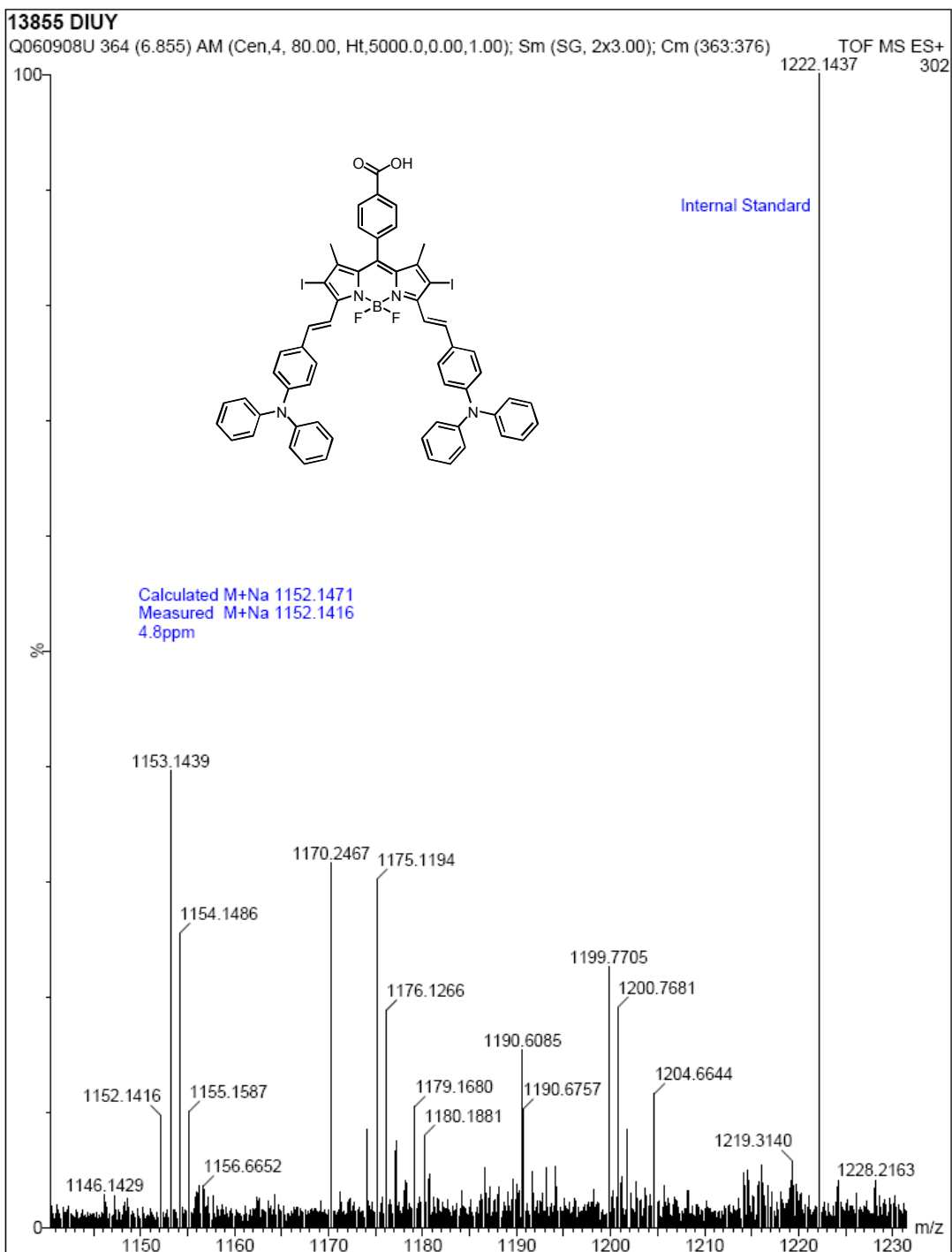


Figure 86. ESI-HRMS of compound **52**

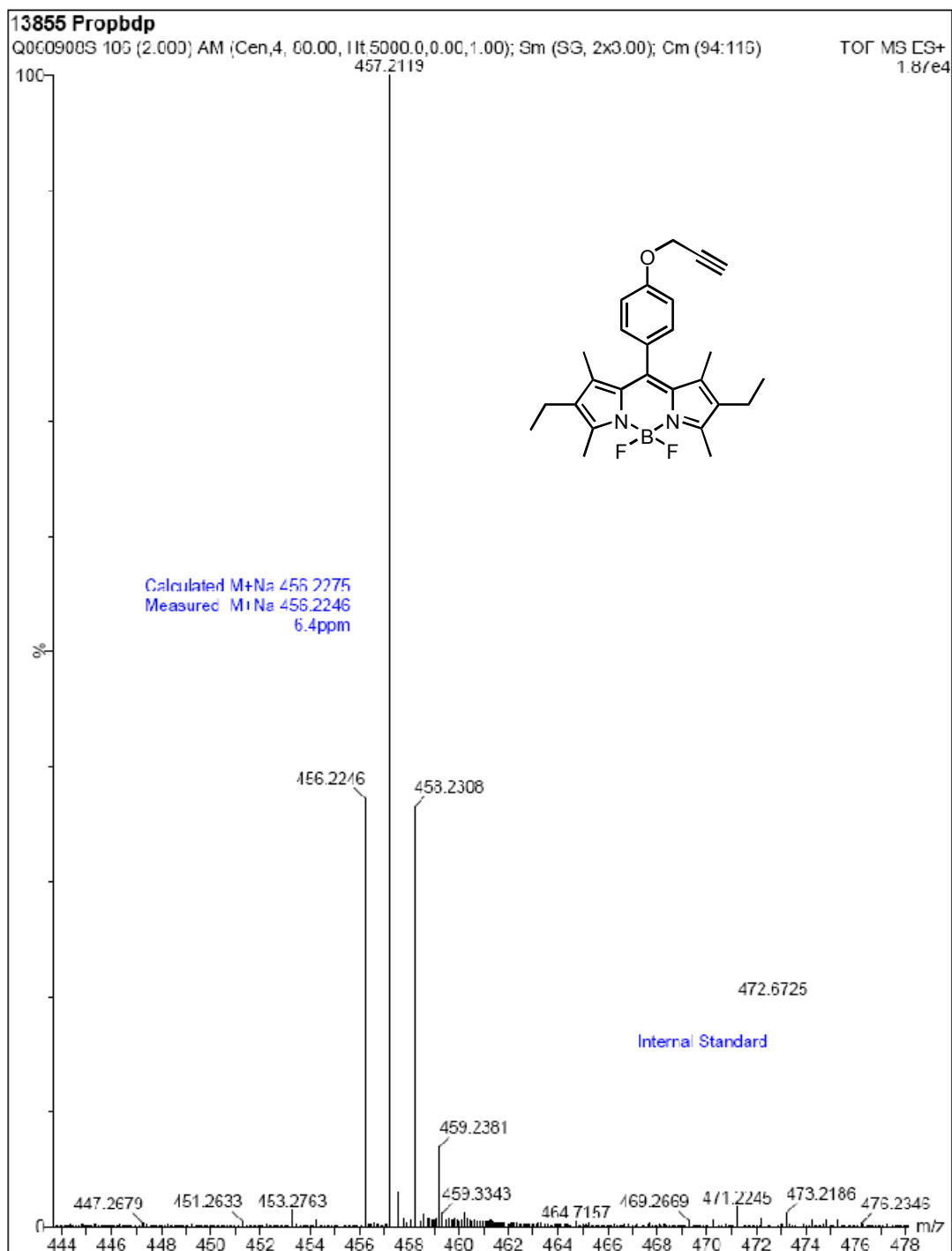


Figure 87. ESI-HRMS of compound 54

m/z	SN	Quality	Fac.	Res.	Intens.	Area
1722.005	16.8	354	13016	24.00	3	
1741.178	17.6	432	9386	18.00	3	

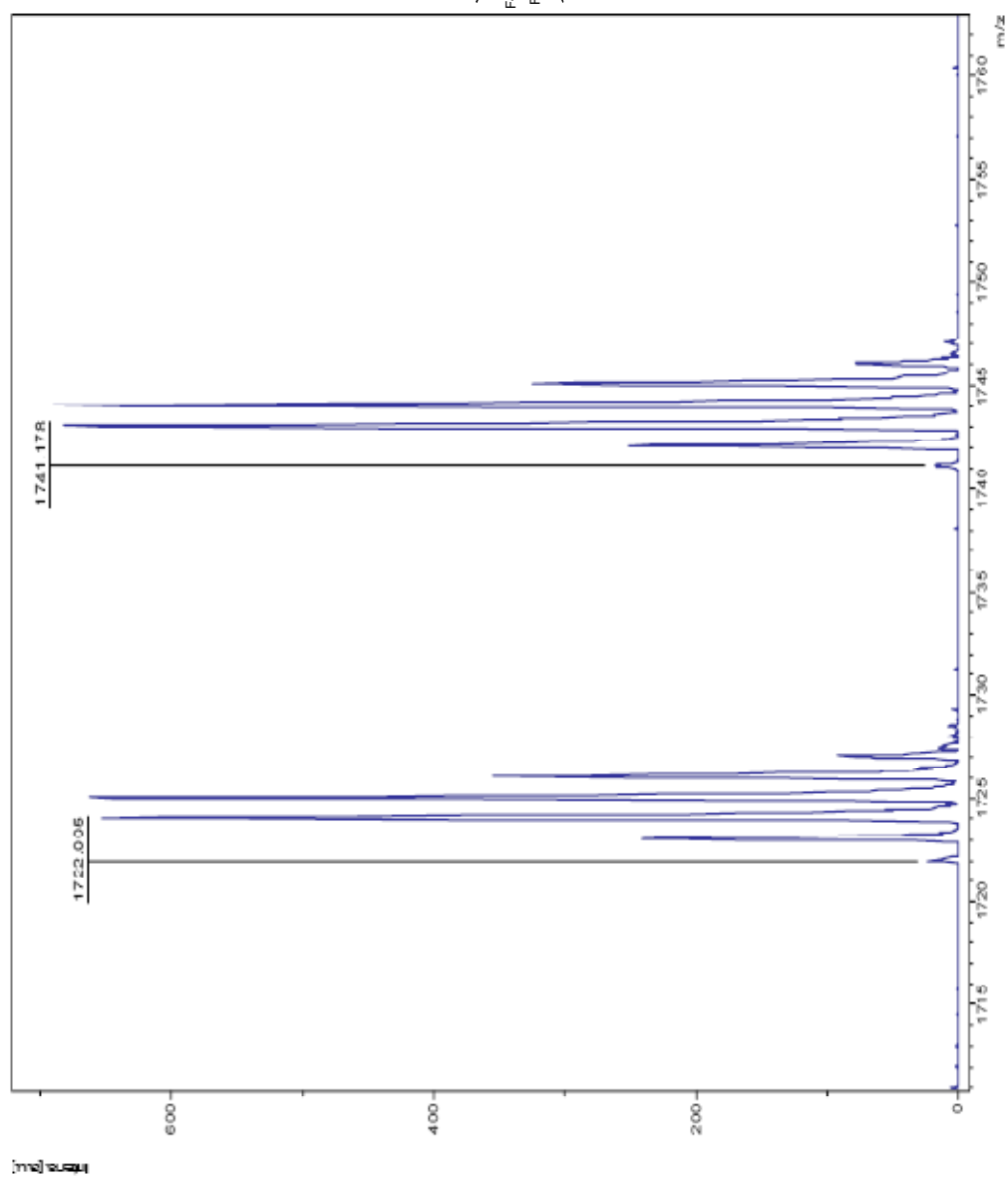
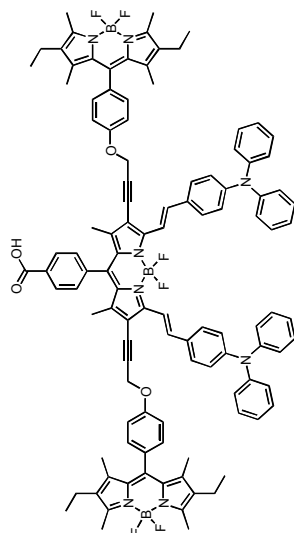


Figure 88. MALDI-MS of compound 55